[redacted]

MIT-Q-73-003

MASSACHUSETTS INSTITUTE OF TECHNOLOGY

Ocean Engineering

Cambridge, Massachusetts 02139

[redacted]

MIT-9-73-003

MASSACHUSETTS INSTITUTE OF TECHNOLOGY
DEPARTMENT OF OCEAN ENGINEERING
CAMBRIDGE, MASS. 02139

INTERIM REPORT
on
FUNDAMENTAL RESEARCH ON UNDERWATER WELDING

by

Alan J. Brown
Russell T. Brown
and
Koichi Masubuchi

Prepared on February 15, 1973

Acknowledgment

This study has been conducted as a part of the M.I.T. Sea Grant Program, supported by the Office of Sea Grant, National Oceanic and Atmospheric Administration, Department of Commerce.

The report covers the work from July 1, 1971 to June 30, 1972. The Welding Research Council and Ishikawajima Harima Heavy Industries, Ltd., have provided matching funds to the current program from July 1, 1972 to June 30, 1973.

A final report will be prepared to cover all phases of this study upon completion of the study which is expected to be June 30, 1974.

Summary

This is an interim report of the research program entitled "Fundamental Research on Underwater Welding." The program from July 1, 1971 to June 30, 1972 covered the following phases:

Phase 1: Survey of fundamental information on underwater welding and cutting

Phase 2: A study of heat flow during underwater welding

This report covers results obtained in Phases 1 and 2.

Part 1 of this report presents the progress of this research program.

Part 2 is the state-of-the-art of the technical aspects of underwater welding.

Part 3 discusses mechanisms of heat transfer during underwater welding.

Table of Contents

PART 1

Progress Report

on

FUNDAMENTAL RESEARCH ON UNDERWATER WELDING

by

Koichi Masubuchi

Introduction

There has been an increasing national and international interest in ocean engineering. Structural design, materials, and welding fabrication represent important areas of ocean engineering, as do underwater welding and cutting. However, present techniques for underwater welding and cutting are far from complete, and they have limited applications such as salvaging. There is a strong need for developing reliable techniques for underwater welding and cutting.

A portion of the welding industry has recognized the importance of this subject and has made some effort to develop new techniques for welding and cutting. The problem, however, is an almost complete lack of fundamental information on underwater welding and cutting. No sysematic study has been reported on the fundamentals of what occurs during underwater welding and cutting. It is very important for the ocean engineering and welding industries to generate fundamental information on underwater welding and cutting. Such information should be useful for further developing improved joining and cutting techniques.

The objective of this study is to conduct fundamental research on underwater welding and cutting. However, we consider this study as a necessary step toward developing improved underwater fabrication techniques. Although the primary objective of this study is to better understand mechanisms of underwater welding, efforts have been made to generate information which could lead to improved welding processes.

M.I.T.'s Past Efforts on Underwater Welding

This section summarizes briefly M.I.T.'s past efforts on research on underwater welding which forms the basis for this research program.

Massachusetts Institute of Technology has long been active in research and education in marine technology. The Department of Naval Architecture and Marine Engineering, which was founded in 1889, was the oldest and the largest marine engineering school in the United States. To meet the demand for qualified engineers in ocean engineering, the department was reorganized in 1971 to become the Department of Ocean Engineering.

M.I.T.'s active involvement in research on underwater welding and cutting began in 1968 when Professor Koichi Masubuchi, who had been engaged in welding research over 20 years, joined the Faculty.

In 1970, Professor Masubuchi published a textbook entitled Materials for Ocean Engineering which contains as its appendix, a state-of-the-art report on underwater cutting and welding[1]. This textbook was prepared under a program supported by the National Sea Grant Office.* This appendix was condensed from a comprehensive report prepared by Battelle Memorial Institute in 1968 for the Naval Ship Systems Command[2]. This report describes

---

* Under this program, the M.I.T. Press published four more textbooks covering various subjects related to ocean engineering, which include ocean engineering structures, vehicle design, stability and motion, and law and public policy. Efforts are continued for publishing more text-' books.

various underwater welding and cutting processes.

This textbook drew the attention of a number of students. Two theses were prepared, under the supervision of Professor Masubuchi, during the 1970/71 academic year. Lt. James A. Staub of the U.S. Navy, who received a Master's degree in June 1971, wrote a thesis which deals with computer analysis of heat flow during underwater welding[3]. The initial analytical model developed by Staub assumes that water keeps contact with the metal surface. It was later found, however, that analytically determined cooling rates are greater than those shown by experimental data. In other words, an actual weld cools more slowly than the initial analytical model predicted.

Mr. Alan J. Brown, who received a Bachelor's degree in June 1971, studied the underwater welding arc by use of high-speed cinematography[4]. He studied how an underwater welding arc is surrounded by bubbles created by the intense heat of the arc. It explains why experimentally determined cooling rates are slower than the analytical values. Due to the bubbles near the arc, the metal near the arc does not maintain a direct contact with surrounding water.

Summarizing the studies by Staub and Brown, a paper was presented at the 1972 Offshore Technology Conference[5].

State-of-the-Art of the Technical Aspects of Underwater Welding

Results of the Phase 1 study are summarized in the state-of-the-art report presented in Part 2 of this interim report. This report emphasizes "technical aspects of underwater welding" rather than "review of underwater welding and cutting." It emphasizes what we know about various technical problems related to underwater welding rather than underwater welding and cutting processes which are available today.

For those who are interested in reviewing underwater welding and cutting processes, the Battelle state-of-the-art report[2], of which condensed report is included in Masubuchi's textbook[1], is recommended.

It is worth mentioning that most of the articles referred to in the M.I.T. review of technical aspects of underwater welding are very new. The distribution of years of publication of the 26 articles referred to is as follows:

1972	5	
1971	8	15
1970	2	
1969	3	
1968	1	4
1967	0	
1966	1	
1965	2	4
1964	1	
1962	2	
1961	0	3
1960	1	
Total	26	

Thirteen out of 26 articles were published during the last two years. Nineteen articles were published since 1968 when the Battelle report was prepared.

Regarding the countries where these articles were published, they are from:

USA	12
USSR	9
Japan	6

These statistics may simply mean that we have a good access to publications from these countries.* However, it may also indicate that major current technical activities in underwater welding are taking place in these three countries. In view of the fact that most of the 26 articles were published very recently, it is quite possible that a number of research activities were initiated rather recently in various countries, including the United Kingdom, Germany, and France, but they have not yet been published or made easily accessible to people in the U.S.A.

Although the Phase 1 survey originally intended to cover both underwater welding and cutting, no new article has been found on underwater cutting which is worthy of being included in the state-of-the-art report. Consequently, the report presented in Part 2 covers underwater welding only.

The above statistics indicate that there is a sudden surge in the world technical community in the interest in underwater welding. It is noticed that there has been a significant rise in the technical level of articles published. Many articles published recently are much more technical than old articles which tended to simply describe

---

* This literature survey was conducted to find out what is already known on underwater welding so that M.I.T. studies in later phases can be directed intelligently by avoiding possible duplications and making use of information which has been generated already. No special effort was made to cover as many articles as possible published in various countries.

processes and applications. Efforts are apparently being made in various parts of the world to generate technical information useful for the development of new, improved underwater welding processes. These statistical results show that the funding by the National Sea Grant Office of this M.I.T. research is not only appropriate, but also, timely.

Although information presented in Part 2 of this report is far from complete, it should be useful to engineers who are engaged in or interested in underwater welding. To the best of our knowledge, this report is the only publication which reviews technical information on underwater welding.

Mechanisms of Heat Transfer During Underwater Welding

Results of the Phase 2 study are described in Part 3 of this report.

Compared to arc welding in an ordinary atmosphere, arc welding underwater involves the following phenomena:

1. Due to the quenching effect of water, a weldment cools rapidly, resulting in a hard and brittle weld.
2. Bubbles are formed due to the intense heat of the welding arc and the weld metal may become very porous.
3. Hydrogen in the bubbles and the surrounding water may cause hydrogen-induced cracking.

It is expected that high-strength steels are more difficult to weld than low-carbon steel, because steels with higher strengths generally have higher hardenability and they are more sensitive to hydrogen cracking.

The Phase 2 study was aimed at investigating the first subject: heat flow during welding. Mechanisms of bubble formation also were studied, because the presence of bubbles has profound effects on heat flow. The presence of bubbles also has significant effects on mechanisms of metal transfer in arc welding underwater (Phase 3).

Approaches Taken

When one thinks seriously about how to analyze heat flow during underwater arc welding, he will soon realize that the problem is extremely complex, as follows:

1. Wide temperature range in small areas. Temperatures near the arc are extremely high, temperatures in the molten weld metal are above the melting temperature, and yet, temperatures of regions of the base plate only a few inches away from the arc remain virtually unchanged.

2. Rapid temperature change. Temperatures in the weld metal and the heat affected zone change very rapidly.

3. Unsteady, mixed boiling mechanisms. Water near the welding arc and the weld zone boils due to high temperatures. Since the temperature gradient is steep geometrically and temperatures change rapidly, various types of boiling occur in a mixed manner and boiling mechanisms are unsteady.

Heat flow during arc welding in air has been studied by a number of investigators, since Rosenthal[6,7] developed a mathematical analysis in the 1930's. The heat supplied by the a c to the plate is lost primarily in two ways: the loss to the plate by conduction and the loss to the environment by radiation and convection (to a limited extent). In the case of joining large plates in air, the heat loss to the plate is much greater than that to the environment.

In the case of underwater arc welding, however, the major portion of the heat is lost to the water environment by boiling, radiation, and convection. What makes mechanisms of the heat flow complex is the fact that various types of boiling heat loss need to be considered.

Mechanisms of boiling heat transfer have been studied to some extent. However, most of studies conducted so far

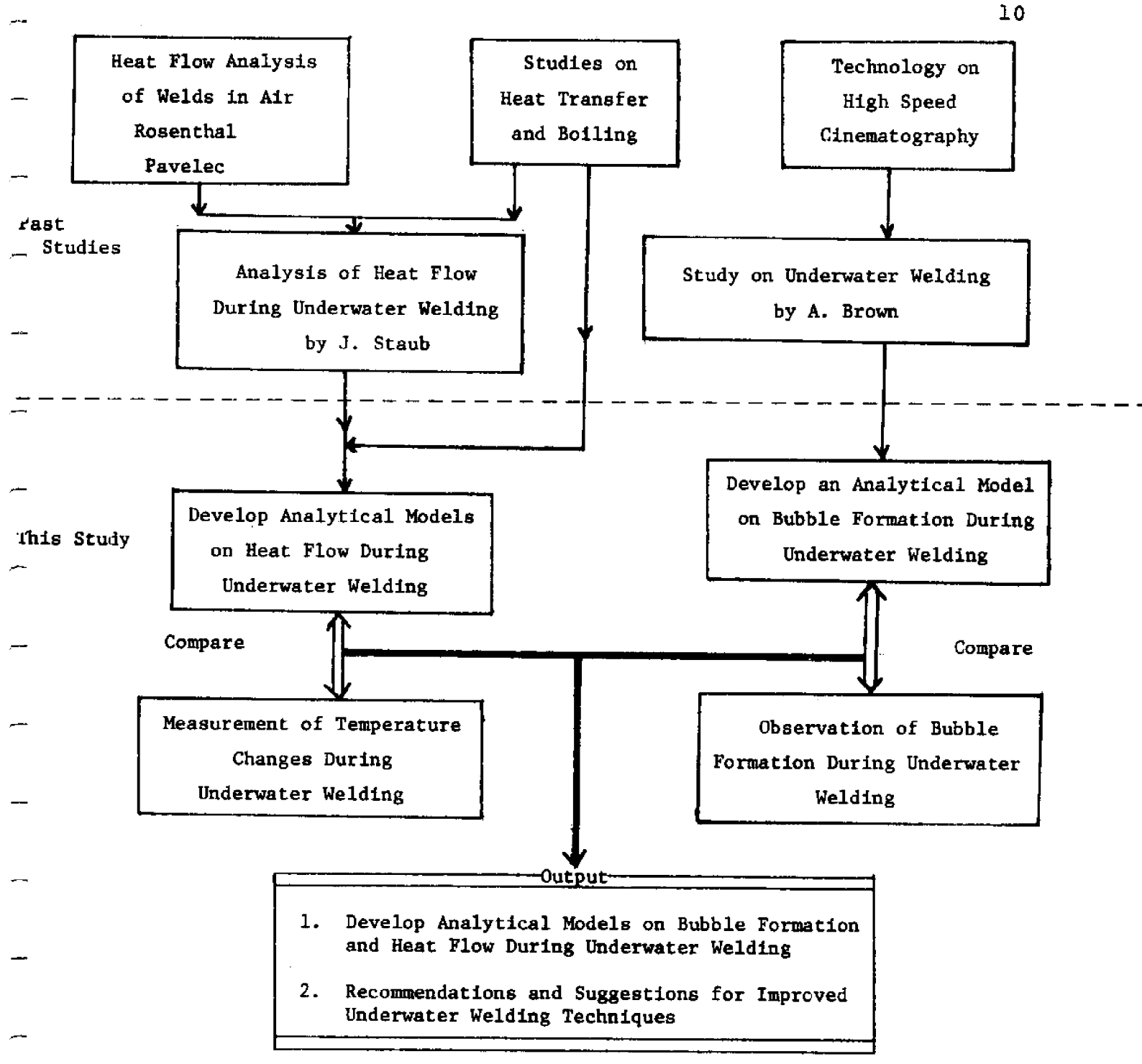

FIGURE 1 Various Efforts Involved in the Phase 1 Study

deal with steady-state heat transfer such as that in water around boiler tubes.

Figure 1 illustrates various efforts made in this study and their relationships. Analytical efforts were made to develop two models: a model for heat flow and a model for bubble formation.

The analysis of heat flow conducted in this study is essentially an extension of Staub's earlier work at M.I.T. Staub[3] started to work from Pavelec's study at the University of Wisconsin[8]. Pavelec developed a computer program which predicted temperature distributions for surface welding using gas metal-arc process. Staub modified this program and Pavelec's technique and applied them to the underwater shielded metal-arc process. Staub's work stands as the first in this area. However, his over-rapid cooling predictions indicated that something was left unaccounted for.

In this study, conducted primarily by Alan J. Brown, efforts were made to include effects of bubbles on heat flow. He studied basic differential equations describing various types of boiling---nucleate boiling, transition boiling, film boiling, etc., and developed several possible madels describing heat flow during underwater welding. Professor W. M. Rohsenow, an expert in heat flow, provided significant contributions in developing these models.

The analysis of bubble formation was conducted utilizing experimental results obtained in Brown's earlier work at M.I.T.[4] An analytical model was developed based upon Davidson's work[9] on bubble formation from an orifice.

Experiments were also conducted to verify analytical models. Bubbles were observed by use of a high speed camera, while temperature changes were measured by thermo-

couples. Experiments were conducted on the following three processes: 1. shielded metal-arc, 2. gas metal-arc, and 3. shielded metal-arc with a shroud.

The idea of using a "shroud" or a dome over the arc and weld puddle was originated by E. A. Silva at the University of California[10,11]. This device uses the gas formed during welding to displace water from the vicinity of the arc. In this study at M.I.T., a cinematographic study was made to examine how a shroud affect bubble formation near the welding arc.

Results.

Results obtained in the Phase 2 study are summarized as follows:

1. The analytical model on bubble formation proved to be quite satisfactory. Good agreements were obtained between analytical predictions and experimental results on bubble size, bread-up frequency, etc., as shown in Figures 5-3 through 5-6 and Tables 5-1 and 5-2 of Part 3.

2. Analytical models on heat flow, however, were not as accurate as expected. Figures 7-1 through 7-10 of Part e show measured and calculated temperature changes.

3. The shielded metal arc process is not very effective underwater because of the limited shielding offered by its dynamic bubble. Using multi-pass methods could increase the reliability of this process, and thus take advantage of its relatively simple and unencumbered application.

4. The shroud process is limited by the gas production at the arc, and the shielding shroud does not provide a positive, stable barrier. A larger shroud with an external gas supply could make this an efficient process.

5. Probably most unexpected of all was the poor performance observed using the gas metal-arc process. The shielding gas was not impinging to the plate, but was just bubbling up ineffectively. Higher flow rates or combination with a shroud-type device could greatly improve the process.

In closing, although the inadequacy of the boiling model limited the accuracy of the predicted temperature distributions, a greater understanding of the interactions between the boiling, spread heat, and "above the plate" phenomena has been derived.

Most important, the knowledge obtained using high-speed cinematography to study "above the plate" phenomena has suggested a number of alternatives for future development of underwater welding techniques.

References

(1) Masubuchi, K., Materials for Ocean Engineering, M.I.T. Press, May, 1970.

(2) Vagi, J. J., Mishler, H. W., and Randall, M. D., "Underwater Cutting and Welding State-of-the-Art," a report to the Naval Ship Systems Command from Battelle Memorial Institute Columbus Laboratories, 1968.

(3) Staub, J. A., "Temperature Distribution in Thin Plates Welded Underwater," Naval Engineer's Thesis, M.I.T., 1971.

(4) Brown, A. J., "Methods of Research in Underwater Welding," B. S. Thesis, M.I.T., 1971.

(5) Brown, A., Staub, J. A., and Masubuchi, K., "Fundamental Study of Underwater Welding," Paper No. OTC 1621, 1972 Offshore Technology Conference, Houston, Texas.

(6) Rosenthal, D., and Schmerber, R., "Thermal Study of Arc Welding," Welding Journal 17(4), Supplement 2-8 (1938).

(7) Rosenthal, D., "Mathematical Theory of Heat Distribution During Welding and Cutting," Welding Journal, 20(5), Supplement 220-s to 234-s (1941).

(8) Pavelec, V., "Temperature Histories in Thin Steel Plate Welded With TIG," Ph.D. Thesis, University of Wisconsin, 1968.

(9) Davidson, J. F., "Bubble Formation at an Orifice in an Inviscid Liquid," Institute of Chemical Engineers, Vol. 38, 1960.

(10) Silva, E. A., "An Investigation of Fusion Controlled Metallurgical Bonding in a Marine Environment," Ph.D. Thesis, University of California at Berkeley, 1971.

(11) Silva, E. A., "Shielded Metal Arc Welding Underwater with Iron Powder Electrodes," Welding Journal, 50(6), 406-415, (1971).

PART 2

Report
on

THE STATE-OF-THE-ART
OF THE
TECHNICAL ASPECTS OF UNDERWATER WELDING

by

Russell T. Brown

PREFACE

One of the curious things about doing a literature survey is that there are always points of information that appear to be in conflict. Certainly there are differences among the various investigators who have been partially reported in this paper concerning aspects of underwater welding. At times in this report, it may appear that an author is quoted as being the correct explanation of some phenomena. It needs to be mentioned that this is not necessarily the case. An author may be quoted simply because he offered the only available data on the subject. Where questions of this sort arise, the reader is warned to be cautious. The reader's personal knowledge may be in conflict and may in fact be the correct explanation to a given problem. It is hoped that questions will be raised as to the validity of some of the speculations contained in this report, and that this will be motivation for further study and research.

TABLE OF CONTENTS

The State of the Art of the Technical Aspects of Underwater Welding

Early in the 1900's, underwater arc welding was attempted commercially. These early trials involved bare wire or bare wire coated with varnish electrodes. During the First World War, underwater welding was used to make temporary underwater repairs on ships until they were able to be dry-docked and more permanently repaired. The success of these repairs was limited by the hardness and brittleness of these underwater welds. Covered electrodes were developed and waterproofed for underwater work about 1930. The drag or touch method of arc welding was soon developed and used in underwater welding. In this technique, the coating is made thick enough so that the electrode tip is held in contact with the workpiece and the arc burns in a melted cavity of the coating, protected by gases from the burning coating. Thus, the need for the diver-welder to hold a specified gap is eliminated, increasing the ease of underwater welding in undesirable conditions of visibility and turbidity. Iron powder electrode coatings were developed in 1946 by Van DerWilligen and proved very applicable to underwater welding. However, the iron powder electrodes received a bad review from the Navy by recording in their Underwater Cutting and Welding Manual (U.S.N., 1953) that only E6013 electrodes be used underwater. Since then, the techniques and the results of underwater welds have remained fairly constant, producing weld quality in terms of tensile strength of only 80% of open air welds and, in terms of ductility, less than 50% of the quality of similar open air welds. Recently, iron powder electrodes have again been employed with favorable results in underwater welding.

The demands by an ever-growing ocean industry have had some impact on a return to the continuing development of the underwater welding processes. Without good, high quality fabrication methods, there is little doubt that little will be accomplished towards actually dominating the oceans. It is to aid in this systematic, perhaps slow, but nevertheless necessary quest for a better fundamental understanding of what is really going on in the phenomena of underwater welding that this state of the art report is being written. It may aid in the development of underwater welding by a team of engineers, researchers and industrial concerns without duplicating each others' work, nor wasting time, effort or creativity. If this report were concerned with environmental issues, this would be the baseline report--that is, the starting point from which to measure changes, either improvements or detrements. It carries the name "state of the art" and, in one sense, art is the encouragement of creative ideas between one with some expression of an idea to others who as yet have only the idea. Hopefully, this report carries all that has been communicated on underwater welding to date. It is also hoped that many more ideas will be encouraged to grow and to show up soon hereafter in some creative and imaginative solution to one of the areas that, due to lack of imagination, has been left unsolved.

Theoretically, there is no difference between conventional open air metal arc welding and underwater arc welding. But the aqueous environment presents the peculiar properties of the high cooling effect of water, a higher ambient pressure, and a surrounding gaseous atmosphere which may be 93% hydrogen due to the dissociation of water. And due to the problems associated with working underwater, the process is slow, hard to control, and, to some degree, dangerous. The low visibility associated with turbidity, or depth filtering out of light, the high conductivity of salt water, the solvent effect of water on typical electrode

coatings, the high cost of the needed support vessel, corrosion, positioning, accessibility, and diver physiology combine to create a formidable engineering problem. The solution will require a systems approach, encompassing the individual mechanisms that comprise the underwater welding phenomena. This report will proceed to look at some of those component operations or mechanisms and attempt to show the stage of development that each is in at the present time. It will consider the various bubble formation phenomena and the atmosphere in the bubbles. The arc will be studied together with the parameters that affect the arc. Metal transfer from the electode to the arc, and heat transfer from the puddle into the parent plate and eventually into the surrounding sink of water will be looked at. The results of these mechanisms in producing the final metallurgy of the weld and heat-effected zone will be considered. The effect of turbidity and generally low visibility conditions effect on determining the welding technique will be analyzed. Finally, some of the recent innovations in underwater welding using iron powder electrodes, GMA, multipass welding, and protective shrouds will be reported and to some degree compared in advantages, disadvantages, and metallurgical properties. The report will end with a partial list of possible areas for further work.

Before embarking on a discussion of these technical aspects of underwater welding, it seems important to mention two related, though perhaps non-technical areas--waterproofing and safety. Waterproofing is necessary to either keep the water out, or keep something else in. The electrode coatings fall apart when wet, and it has also been shown that wet electrode coating results in increased porosity in the welds. The other type of waterproofing is more properly called insulation. Salt water and the human body will readily serve as the conductors of elecricity if given a chance. The salt water will conduct the current away from the job

to be done, causing increased current usage and cost, while the human heart mechanism pretty much demands that we keep as little stray current running through the body as possible. It appears that there is a lot of need for common sense as well as "ivory tower" technology. The sea is one environment that is going to demand both of these sorts of knowledge from those who try and work in it.

The Bubble Phenomena

Perhaps the most observable effect of arc welding underwater is the large quantity of bubbles originating at the arc and nearby plate surfaces. The major portions of the bubbles result from dissociation of the water by the extreme heat of the arc. This produces a large amount of hydrogen and oxygen. Most of the oxygen reacts quickly with other combustible elements to produce CO and CO_2. This is what causes the coating material to burn. A small portion of the gas consists of metal vapor, and various mineral salts from the electrode covering. On a percentage basis, the gas is 67-82% H_2, 11-24% CO, 4-6% CO_2, and 3% is the remaining N_2, O_2 and metallic and mineral salt vapors (Silva, 1971).

The bubbles appear brownish in tint and burn with a flash upon ignition, suggesting a high H_2 content (Silva, 1971). Also, the quasi-static bubble surrounding the burning arc has a glowing blue color, while the bubbles on the way to the water surface do not. The source of the major portion of the bubbles appears to be the arc. The bubble is expanding rapidly, and as it reaches a critical diameter, part breaks off and floats away. The remaining portion immediately grows in size and breaks again. This process continues at a frequency of 14 to 16 bubbles per second in six inches of water (Brown,1972). High speed

motion picture study has also revealed that the upper portion of this separating bubble is nearly spherical in shape at breakaway. The remaining hemisphere always remains in contact with the plate and encloses the arc. Minimum diameter for this fixed hemisphere is .25 to .35 inches (Brown, 1972) in six inches of water. This diameter grows until it reaches a diameter of .40 to .60 inches at which point the breakaway of the upper sphere takes place (Silva, Dec. 1971). The total volume of gas being evolved is reported by different investigators to vary according to the electrode type used, but to be invariant with welding conditions. Brown (1972) reports E6013 to generate 40cc/sec. Silva (1971) reports a rate of 50cc/sec. for E6027 and 60cc/sec. for the E7024 electrode. Madatov (1965) reports rates of 33cc/sec. and 100cc/sec. for the two electrodes he employed.

Thus, while various electrode coverings produce more or less gas, the gas rates are constant at a constant depth, even with changes in voltage or current. This implies that the dissociation of water is directly related to the arc temperature which is a function only of the depth. It is postulated that gas rates increase with depth for a given electrode (Silva, 1971), although no actual pressure tests have been run. The bubble velocity after breakaway has been determined (Silva, 1971) to be 2.3 ft./sec.

There are two other bubble formation processes taking place. Large bubbles with diameters of .25-.34 inches continue to form along the welded bead for up to one minute after the bead has begun to cool. This implies that it takes that much time for the bead temperature to cool below 100°C. Even after these bubbles stop forming, a stable band of small bubbles is left lying on the plate for an inch on each side of the bead. These appear to be the last bubbles formed as the 100°C isotherm retreated towards the bead. They are not of sufficient size to displace the water layer

and remain attached in a similar fashion to bubbles formed in a glass of carbonated beverage. These bubbles have a diameter of about 1/16 inch and are referred to as band bubbles.

Madatov (1965) reports small fluctuations in the voltage and current across the arc to be a result of the bubble cycle. It is argued that the bubble size affects the current density by producing tiny charges in the cross-sectional area of the arc.

The Bubble Atmosphere

Gaseous products of combustion of the weld metal, the parent metal, the components of the electrode flux covering, and of dissociation of water, as well as water vapor continuously interact within the bubble environment. And the atmospheric components vary both with time and with location in the bubble. The degree of dissociation of water vapor is maximum at the interior of the bubble nearest the extreme temperatures of the arc and decreases radially towards the bubble-water interface. At the arc, the dissociated water vapor is ionized and this entire process is taking place at excess pressure which accounts for the rapidity of this reversible process (Madatov, 1972).

The high hydrogen content in the atmosphere is perhaps the most critical component. This produces, during the mechanism of metal transfer from the electrode tip to the weld puddle, an extreme danger of possible hydration and saturation with hydrogen. This danger will be examined in more detail later in this report.

This gaseous, dynamic atmosphere reacts with the molten metal as it is transferred across the medium from the electrode tip to the weld pool. Burn-off of certain of the constituents,

especially the reducing agents manganese and silicon, occurs and is dependent of the concentration of the individual metal components in the electrode, and in the electrode covering used. The burn-off process is not as affected by current and voltage in the underwater process as it is in open air welds (Madatov, 1972). Burn-off does appear to be directly dependent on the dwell time in the bubble of the metal being transferred.

So, a good handle on the degree to which metallurgical reactions are taking place is the reaction rate in the bubble atmosphere. This rate will increase with depth (pressure). It is a function of the weight/time and volume of drops/time and the frequency of drop formation and the lifetime of the drop from electrode tip to puddle (Madatov, 1972). This reaction rate is formulated after the method of Potap'evskii for open air welds.

$$C_\eta = \frac{\eta v T_d \rho}{w \rho_o}$$

η = drops/unit time
w = weight/unit time (grams)
ρ = excess pressure of arc
ρ_o = atmospheric pressure
v = volume of drop at the puddle
T_d = lifetime of the drop from formation to puddle

Table 1 gives some tabulated results of this parameter C_η for various welding conditions. The effect of the metal transfer mechanisms on the coefficient of reactivity can be clearly seen. This is empirical data, as the relationships between the metal transfer and the bubble atmosphere reactions are not known. It is still useful for comparing two welding processes and achieving an understanding at least of their relative rates of bubble atmosphere reactions.

TABLE 1

Rate of Metallurgical Reactions in Various Methods of Underwater Welding

Characteristics of Metal Transfer	Thin Wire Without CO_2, salt	Thin Wire Without CO_2, salt	Thin Wire Without CO_2, fresh	Thin Wire Without CO_2, fresh	Thin Wire With CO_2, fresh	EPS-52 Covered Electrode
Number of drops transferred in 1 second	12	12.2	9.7	16	23	44
Lifetime of drops, second	.1700	.121	.132	.1305	.0575	.0254
Average Weight of one drop, gram	.1670	.1100	.0804	.0804	.1100	.1100
Volume of one drop, mm^3	21.4	14.1	10.3	10.3	14.1	14.1
Coefficient of reactivity of the process, C_η	21.8	15.5	16.92	16.77	7.37	3.26
Voltage of Arc	39	42	36	40	39	39(SP)
Arc Current	240	250	250	250	240	240

Note: (1) Drop Transfer Throughout
(2) Lifetime of drop has largest apparent effect.

Reference (Madatov, 1972)

The Arc

In shielded metal-arc underwater welding, no A.C. current arcs are used due to safety considerations. So only D.C. current arcs are considered here. Also, it is pointed out that a metal arc is extremely complicated on a theoretical level and is not at all well understood. This section will overlook this and proceed to describe what has been reported about the underwater welding arc.

Straight polarity is almost exclusively chosen for underwater work because it results in less spatter while welding, a better appearing bead shape, and more regular welds.

Possibly the major difference of underwater welding regarding the arc is the excess pressure present. This pressure effect is produced by the water constricting the arc column. Determining how this pressure is acting on the arc column requires knowing the geometry of the basic arc. Madatov (1966) investigated the geometry of underwater arcs for both metal-arc and CO_2 thin wire welding. The basic shape found using a technique of X-ray cinematography was a cylinder for metal-arc welding and a truncated cone with its base on the work for thin wire welding. The diameter of arc is related to the current using an expression by T. I. Avilov (1960) of

$D = A\sqrt{I}$ where A = 0.11 as found by Madatov (1966)

Superimposed on the basic shape there are two types of compressions occuring on the arc. The cooling effect of the high hydrogen content bubble atmosphere couples with the pressure of the water column to compress the arc. The other effect is the constriction of the cathode spot caused by the geometric dimensions of the end of the electrode which prevent the free expansion of the cathode spot

with increasing welding current. These compression phenomena explain why the volt-amp curve is concave or rising (Figure 1).

Now as the arc is moved along a weld, energy is being lost even more rapidly due to increased cooling of the arc. This produces a steeper gradient in the volt-amp curve then in the case of a stationary arc (Figure 2). With some form of sheilding,this volt-amp curve is generally lower. This may be due to the fact that the sheilding partially prevents the water column from constricting the arc column (Hasui, et. al., 1972). These processes are both dependent on the arc length. The longer the arc the more cooling by the water and by the effect of hydrogen cooling or deionization.

From these relationships of current to voltage and arc length the arc field intensity can be determined (Avilov, 1960). This is given by the ratio between voltage increase and the arc length increase.

$E = \frac{dV}{dL}$ Figure 3 shows this relationship.

The field strength is seen to increase with the welding current. This distinguishes underwater welding from open air welding. This is explained by the effect of the hydrostatic pressure against the arc column causing the cross-sectional area increase of the arc to lag behind the welding current increase, producing a current density or field intensity increase. Av lov (1960) found current densities in underwater arc columns of 280 amp/sq.cm. which, for his welding conditions, was five to ten times the current density of an equivalent arc in open air conditions. This also means that to maintain the same arc conditions, the current will have to be increased by 10% per bar of additional pressure (Silva, 1971).

Figure 1 Moving Arc Characteristics

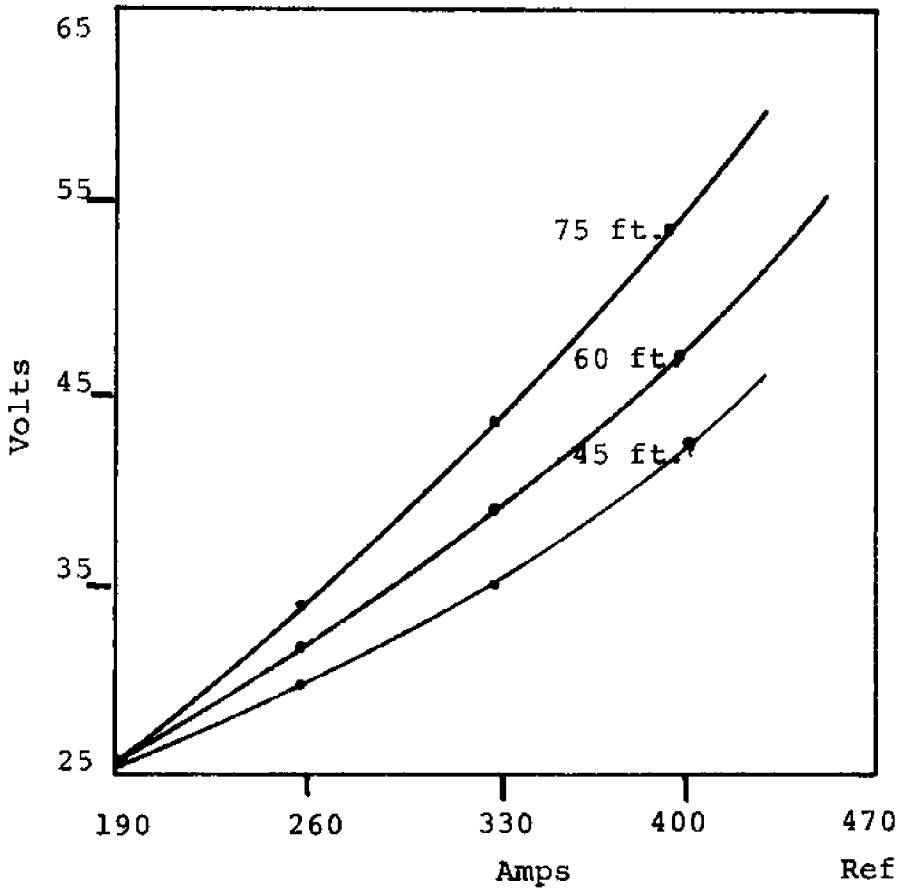

Reference (Avilov, 1960)

Figure 2 Moving Arc vs. Stationary Arc

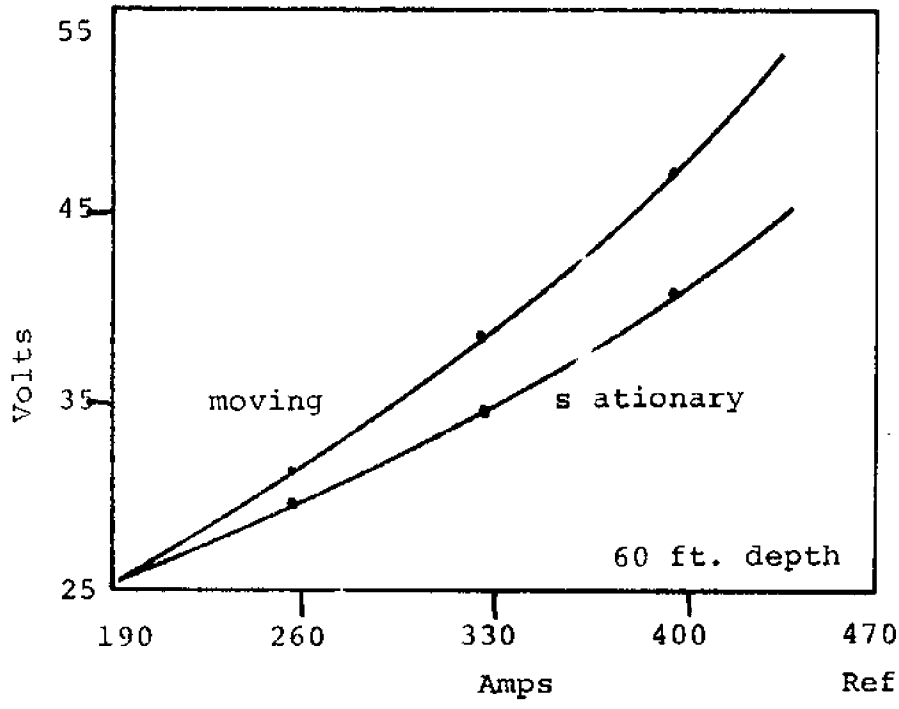

Reference (Avilov, 1960)

Figure 3 Field Strength Intensity

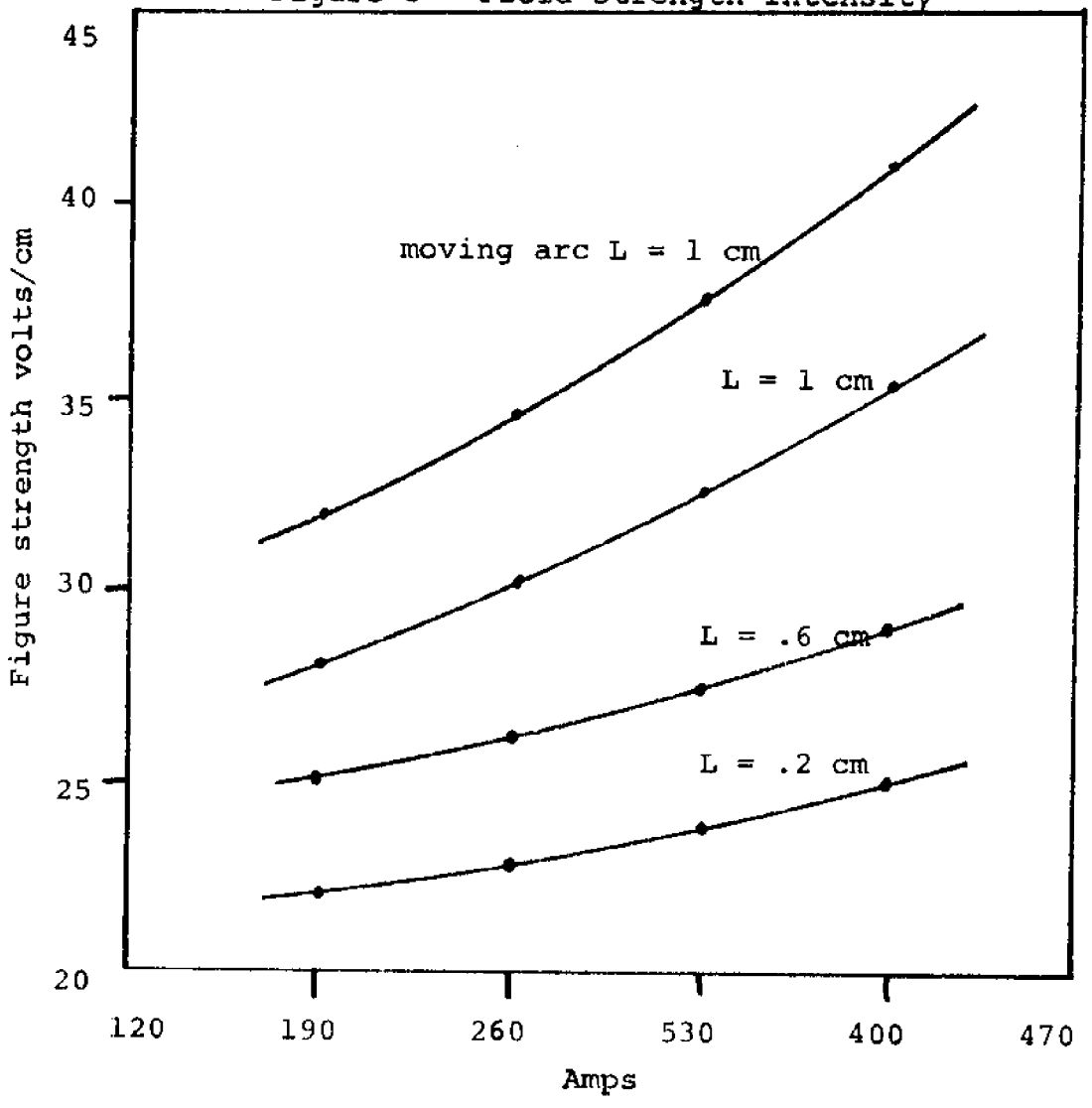

Note: Hydrostatic "lag" effect is greater with longer arc.

Reference (Avilov, 1960)

The higher current density of underwater arcs produces higher arc temperatures. Direct measurement of the interior arc temperatures is difficult. Madatov (1966) computed the theoretical temperatures using the Stefan-Boltzman law, realizing that the arc was not a perfect black body. Radiation occurs off the sides of the arc and the absorption coefficient was assumed to be the same as an arc burning in the air ($\alpha = .6$) then:

$$T^4 = \frac{E\ lac}{\alpha\ \tau\ F}$$

E = radiating power of arc and arc column

lac = arc length

α = coefficient of absorption

τ = Stefan-Boltzman constant

This was related to the following formula involving a factor that takes into consideration the welding conditions, and another factor that considers the welding depth or pressure. Then the temperatures of the arcs for these two parameters appear in Table 2,

$$T = C\ \ \xi^4\ \sqrt{I}$$

The ionization potential of both underwater CO_2 thin wire welding and metal-arc welding are quite high, suggesting the case of high hydrogen content in the arc bubble atmosphere (13.6v). It is found to be (Madatov, 1966) 12.0-12.4 volts for thin wire and 13-14 volts for stick electrodes. These levels of potential also suggest the possibility of CO_2 (14.3v), CO (14.1v) and some N_2 (14.5v).

A stability factor is defined by Madatov (1962) as the maximum current divided by the minimum current:

$$\frac{I\ max}{I\ min} = ;$$

For ordinary metal-arc underwater welding with D.C., the

TABLE 2

Temperature of arc column at different currents and depths

Welding Conditions			Temperature of arc column, °K	
Depth m	Current amp	Effective Diameter of Arc Column cm	Thin Wire Electrode	Rod Electrode
10	100	.202	8400*	9300
10	200	.205	9200*	10200
10	300	.210	9750	10700
10	400	.260	10150	11100
10	500	.317	10650	11500
20	300	----	10000	11000
40	300	----	10300	11300
60	300	----	10400	11500
80	300	----	10600	11700
100	300	----	10800	11800

*Note: Calculations based on assumption that arc column is a cylinder

Reference (Madatov, 1966)

stability factor was 1.61. For values near one, the arc is considered stable. For values >>1, the arc is considered unstable. One cause of fluctuations in the voltage and current occuring every .3 seconds or less has been attributed to the thick coating collapsing during arc welding (Silva, 1971). Different electrodes produce different levels of stability. Silva (1971) found E7024 more stable than E6027, while E6013 was unstable due to the thin coating it has. It also appears that in salt water, the metal-arc will become more stable due to the salt ions serving as charge carriers (Silva, 1971). This is evident in the change in sound of the arc from an erratic effervescence in freshwater to a smooth gurgling in salt water.

Finally, it is mentioned that depending on the quality of equipment used, there can be quite a current leakage in saltwater. This can have quite an effect on changing what actually happens at the arc compared to what is thought to happen, based on the power source meters. Silva (1971) found it could be as high as 65-110 amps at the open circuit voltage of 83-99 volts.

Metal Transfer

There are three basic modes of metal transfer in welding arcs. The first is globular or drop transfer, where the metal is transferred in large drops that travel slowly to the work piece. Spray transfer is where the metal is transferred in many fine particles that travel at a higher rate. The third is short circuit transfer, where direct metal-to-metal contact and transfer occur. These modes may sometimes occur in combination, or during a welding process the mode may undergo a transformation from one to another as the welding parameters are changed.

Theoretically, in metal-arc welding such a transition

should occur with changing pressure. The metal transfer might be expected to change from the spray mode to the globular mode as the underwater welding depth increased (Silva, 1971). For short arc lengths such as used in contact welding of 3/16 inches to 1/4 inches, this transition should not occur until a depth of 130 to 260 feet. Without a shielding gas, this depth may be decreased. However in practice, using the touch method of underwater welding with covered metal-arc electrodes, the normal metal transfer is small droplets except when an occasional large drop forms and short circuits the arc (Madatov, 1972). Silva (1971) also found that even at shallow depths, metal-arc welding underwater involves the globular rather than the spray mode of metal transfer. The mechanism for this phenomena is not explained.

Madatov (1972) has done some investigation of metal-arc and thin wire underwater welding metal transfer. In thin wire welding, the drop does not transfer immediately to the weld puddle, but may have a dwell time in the bubble surrounding the arc that is equal to or greater than the time taken to form the drop on the electrode. This slow drop transfer is in conjunction with occasional short circuiting. An interesting observation is that without CO_2 shielding gas, the drops formed may be hollow at the time of formation and as they drop to the weld puddle, they interact with the bubble atmosphere and become more solid, thereby decreasing in volume.

The constricted arc produces a high arc core temperature in spite of the cooling effect of the hydrogen present in the bubble atmosphere. Thus, whereas the welding arc between two iron electrodes in air may have a temperature of between 5000°K and 6000°K, underwater the same arc may burn at a temperature of 7000°K and 9000°K for depths of under 10 meters (Madatov, 1970).

This produces fast melting rates of the metal at the weld pool which tends to produce a very large fluid puddle that would be difficult to control except that in welding underwater, the cooling property of the water seems to minimize or compensate for this effect.

Metal transfer is an area in which very little is known as of yet. There is some current research proceeding along these lines, although more is needed.

Heat Transfer

The heat transfer processes occuring during a welding process, together with the rates at which these processes occur have a direct effect on the resulting weld microstructure, the metal properties obtained, and the residual stress. Due to the water environment's high heat transfer properties and the phenomena of boiling, cooling rates in underwater welding processes are rapid and temperature gradients are steep. A big step in understanding surface welding heat transfer came in the late 30's with Rosenthal's work using a point source estimation of the welding arc. This approximation is valid away from the arc and has met with some success in surface welding work, but underwater, where welding temperatures may drop off to ambient at a distance of 1/2 inch, the method is of little use (Brown, et al., 1972). After transients have settled out, the moving arc is surrounded by a quasi-static temperature distribution which produces a corresponding quasi-static solid and liquid region in the plate. The liquid region is a small area directly around the source where heat transfer takes place via a complicated combination of convection, conduction, melting, and fusion. A numerical method for predicting the temperature distribution in thin plates using not a point source but the liquid weld pool as

the interior boundary condition was developed at the University of Wisconsin and adapted to underwater welding at M.I.T.

Keeping track of all the energy emitted by the welding arc is a difficult problem, which has not been completely solved even for the simplest of arcs. It now seems apparent that spread heat or a pre-heating, post-heating effect takes place even in an underwater environment. The nature of this heat distribution is yet to be solved (Brown, et al., 1972).

The greatest heat losses underwater are from boiling and radiation. Boiling is a complex heat transfer phenomena and is usually divided into several distinct regimes. Ideally, as the temperature of the plate increases above the saturation temperature, bubbles begin to form. The bubble formation stirs up the surrounding water and increases the heat transfer. During the transition phase of boiling, these bubbles begin to come together forming an unstable film which tends to reduce the heat transfer. Finally, at very high temperatures, a stable film forms which limits the bulk of the heat transfer to radiation. However, several factors in underwater welding interfere with this ideal progression of phenomena. First, the plate temperature is in constant change. The temperature goes shooting up through all these boiling regimes very rapidly and then cools down back through them again. Also, the areas involved are so small that no one mode of boiling can be established without both interfering and being interfered with. Finally, the large perturbations resulting from the arc bubble phenomena of a continuously pulsating bubble destroys any stable film boiling mechanism on the top of the plate. The other problem with this model is that the heat transfer is three dimensional and the bottom of the plate is undergoing significantly different heat transfer. Boiling there may well be film boiling as the bubbles are trapped against the plate.

FIGURE 4

Temperature History Curves

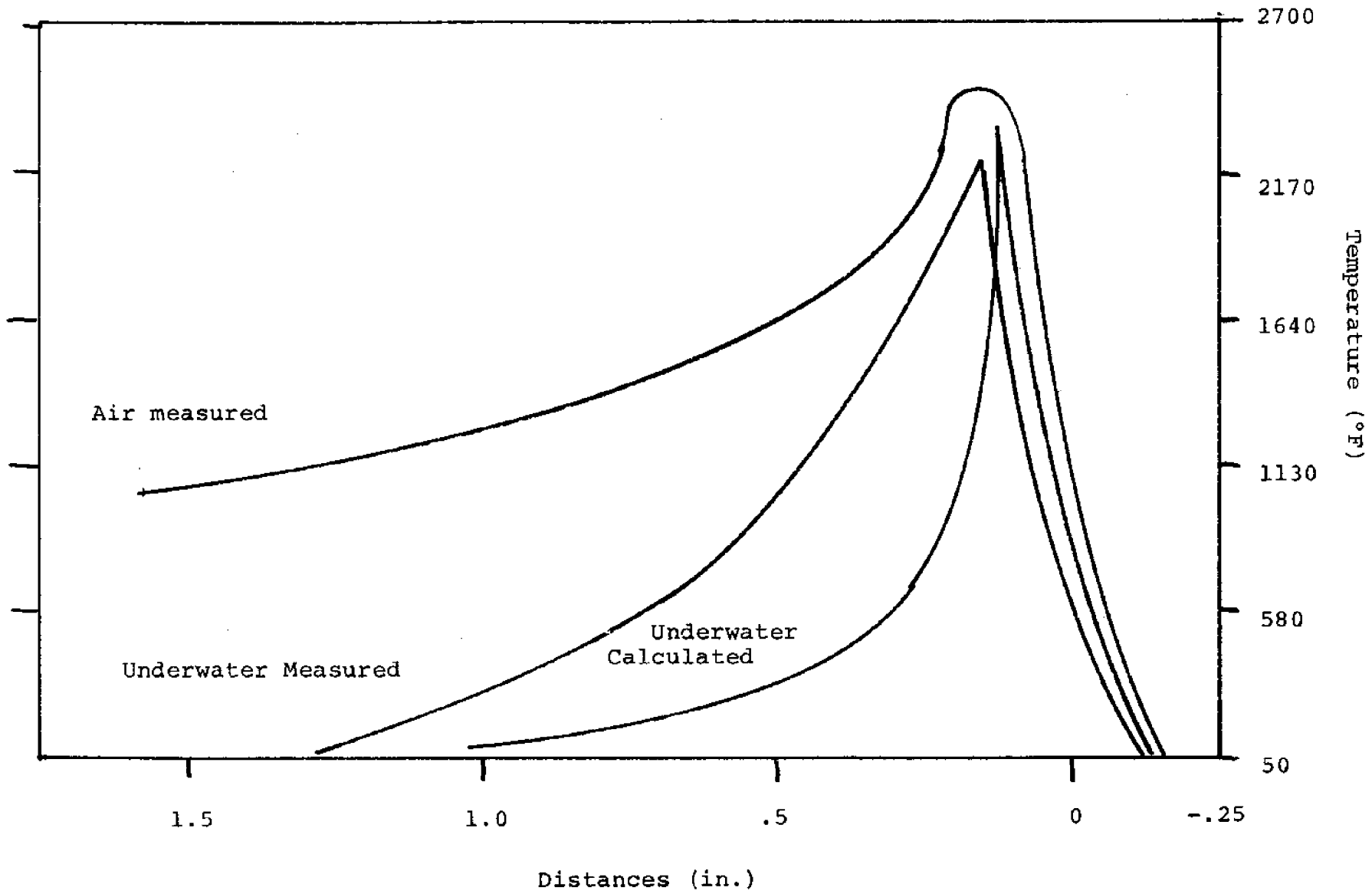

The bubble phenomena in the vicinity of the arc limits heat transfer in this area to radiation by forming a protective gas pocket over a portion of the plate. And the area of this region is changing at a frequency of ten to fifteen cycles per second. Clearly, this is an extremely complicated heat transfer problem. A purely analytical approach would be impossible, so analytic methods have been linked with empirical study to produce a numerical method of tackling this problem.

Results of these numerical attempts at duplicating what is found empirically are plotted in temperature history curves. Some such curves found for work done by Brown (1972) are shown in Figure 4.

Metallurgy

There are three major components to consider when discussing the weld metallurgy. Weld shape is the most obvious and easiest to observe. The weld properties of ductility, tensile strength, fracture toughness, and micro hardness are easily found using standard tests, but are often hard to directly correlate with welding conditions due to the often forgotten intermediate analysis of the actual weld metal, HAZ, and parent metal microstructure. While much has been reported on weld bead shape and the macroscopic weld properties, not very much has been studied on the root cause of these metal properties--the microstructure composition.

The weld penetration shape factor is defined as the width of the joint divided by the depth, or penetration, of the weld. Madatov (1969) reports a range for this parameter of .8 to 20. The optimum value is 1.2 to 1.3. Underwater welding makes deep penetration practically unattainable. Underwater covered arc welds have a shape

factor of between 2 and 6. Madatov (1969) studied both thin wire and covered electrode welding. For covered electrode welding, as the current is increased, the width of the weld increases and the penetration becomes more shallow, resulting in a shape factor that approaches 5. This is not generally the case in open air welding where an increase in the welding current will result in increased penetration. Thin wire welding produces slightly deeper penetration, but the trend is the same. In this case, using reverse polarity will give better penetration. There is an optimum voltage after which penetration does not increase. The shape factor for this voltage range (39-41 volts for unshielded thin wire) is below 3.5 (Madatov, 1969).

There are several extraneous factors which influence the weld shape. As salinity is increased from 0 to 41%, there is an increasing penetration and a slight width increase resulting in a shape factor change from 3.5 to 1.8. Thus, salinity has a favorable influence.

Madatov (1969) found that the weld shape factor and porosity were both less without CO_2 shielding of thin wire welding. Welding cable length increase results in higher resistance with a corresponding voltage and current drop. This results in reduced penetration and width and tends to produce a "humped" bead shape. As the pressure increases the bead penetration and width increase, but together they result in a reduced shape factor. At great depths, the current will have to be limited to 180-240 amps to prevent further concentration of heat. The welding nozzle angle has an effect on the bead shape. As the angle changes from a leading to a trailing angle, the bead becomes narrower and taller with decreased penetration. Finally, it is reported that thin wire welds in the vertical position produce a concave "countersunk" shape that has very good penetration.

The proportion of the weld that is electrode metal is also an interesting metallurgical parameter. It indicates

the amount of fusion taking place. Underwater, this value increases with increasing current to 60% due to the relatively low penetration as compared to the width of underwater welds (Madatov, 1969). The goal with the weld is to minimize these parameters. They are not independent and the optimum welding conditions will produce minimums in both. Another feature of underwater welding is the presence of undercut. This is attributed to the quenching action of the water and is not a function of welding speed or of machine settings, although Silva (1971) found that iron powder electrodes eliminated undercutting.

Although the microstructure of the metals in the vicinity of an underwater weld is not well studied, it is the factor behind any metal properties, and thus will be looked at next.

In broad terms, when considering mild steels, the microstructure can be described as fine pearlite grains outlined with ferrite. Using iron powder electrodes, Silva (1971) found the same fine pearlite grain surrounded by ferrite with some additional bainite and martensite at the fusion lines. Using E6013 much more martensite together with considerable porosity produced a structure suspected to have poor quality. The presence of both ferrite and martensite is not unusual in welded structures. the presence of many carbide precipitates in the HAZ provides evidence of carbon rejection due to the lower solubility of carbon in ferrite than in austenite. This rejection process can also provide the carbon necessary for martensite formation in low carbon steel. Brittle martensite is a logical source of poor quality, especially in hardness values. This precipitation process of martensite formation is enhanced by the fast quenching of the water. This fast quenching also produces fine grain sizes in the HAZ, slag entrapment, and porosity. Slag entrapment underwater is less of a problem because the slag is buoyant and tends to float. Porosity has been investigated

quite extensively by Masumoto, et al. (1972) and is unavoidable in some cases. The major components of the pores were found to be 70% H_2, 10% CO, and 20% other gases. This whole area of weld microstructure is so sketchy that no conclusions can be drawn from data except that martensite has an effect on increasing the hardness.

The one area of microstructure that has been investigated is the problem of hydrogen in the weld. Martensite and hydrogen are both associated with underbead cracking. The hydrogen dissociated from water in the bubble atmosphere diffuses into the weld puddle. Rapid quenching prevents its being able to escape. Thus it becomes trapped in the recrystalizing metal. When it is trapped in the highly stressed martensite regions, the small hydrogen bubbles coalesce into cracks. This can be critical. This sort of an embrittlement process is dependent on the history of the metal, the amount of hydrogen, the type of material, service loading, thermal cycle, etc. Underbead cracking is not the only phenomena associated with hydrogen content. Flakes on the fracture surface, fisheyes (bright spots with cracks at the center), and delayed cracking are also attributed to hydrogen. There seems to be no simple correlation between hydrogen content and mechanical properties of the weld. Degradation of weld has been observed with less than a 3 ppm hydrogen content (Silva, 1971). Generally, weld metals may contain from 1 to 50 ppm. Using neutron radiography, Silva (1971) found 3 to 4 times the hydrogen content in underwater welds reported in the literature. Again, insufficient data prevents any conclusive explanation of the effects of hydrogen in the weld metal microstructure.

An area that has been a little better reported is the final macroscopic metal properties as a result of an underwater weld. Historically, it is reported that an underwater weld will result in only 80% of the tensile strength and 50% of the ductility of a similar weld made in

air. This is not very encouraging. This has been improved using iron powder electrodes, thin wire welding, multipass techniques, and plasma arc welding as well as shrouds and other protective or shielding devices.

Standard Charpy impact testing was done by Silva (1971) on covered arc underwater and open air welds. For electrodes E7024 and E6027, the impact tests at 0°C (a good test for ocean specimens) showed 75% and 60% of an open air weld notch toughness. However, the E6027 showed less variation and is recommended as being more reliable than E7024.

Ductility in underwater welding is better using covered arc iron powder electrodes than when using a thin wire semi-automatic process. However, it is nowhere near open air quality as shown by Silva (1971), reporting only 20% ductility for covered arc welds.

Hardness values in the HAZ are the real indicators of possible failure from cracking. These values have been more widely studied and reported. The highest hardness values repeatedly occur along the fusion line which of course corresponds to the HAZ. For E7024 electrodes, Silva (1971) reports the hardness for an open air weld to be 192 kg/mm^2 while a similar weld underwater results in a hardness value of 412 kg/mm^2. Similarly for the E6027 electrode, underwater welding increases the hardness from 204 to 452 kg/mm^2. E6013 electrodes gave a maximum hardness of 415 kg/mm^2, but the hard region was considerably broader. Figure 5 shows some of these hardness charts.

Again, this whole area of metallurgy in underwater welding is critical and the nature of the weld microstructure should be investigated further.

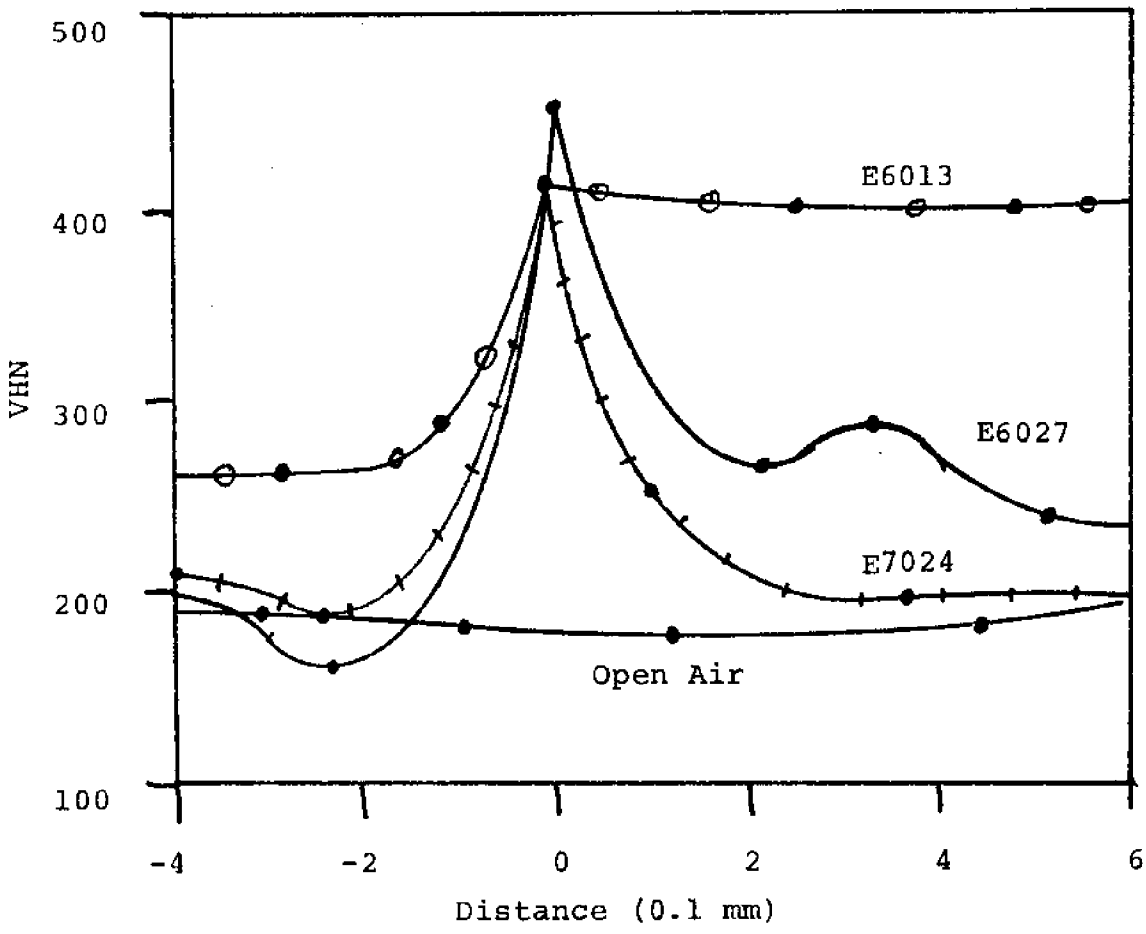

FIGURE 5

Microhardness Charts

Reference (Silva, 1971)

Turbidity

Poor visibility associated with a brown cloudy turbidity has been a major problem in practical underwater welding work. Underwater visibility is already a problem without additional turbidity from the weld itself. This has forced some welds to be made by touch, others to be made using the drag or touch method, and in more technical investigations, has motivated investigators to use X-ray photography to view the hidden arc. This cloudiness is independent of bubble activity. A slow moving brown cloud forms at the arc and gradually spreads out through the water. In a closed test tank, the problem can be critical.

In the past, it has been thought that this cloud was a fine suspension of iron oxides. However, Silva (1971) reports that separation did not occur after using either settling tests, glass wool filter, 2-3μ pore size filter paper, sodium ion exchange columns, or centrifuges. Next, using a spectronic colorimeter, the particle size was determined to be extremely small. An iron compound was suspected as the cause of the cloud due to the nature of the welding process. The pH of the water was determined and it was found that the welding water had a pH of 7.3, slightly above the freshwater pH of 7.1. Silva (1971) has hypothesized the cause to be the formation of ferrous hydroxide, $Fe(OH)_2$, a strong base, and then the oxidization of this to hydrous ferric oxide, $Fe_2O_3 \cdot xH_2O$, which turns from a green to a reddish brown. Confirmation of this hypothesis was sought using X-ray diffraction studies, but they were inconclusive. It was determined however, that the turbidity was not simply powdered electrode coating. The only other evidence supporting this hypothesis is the fact that adding a weak acid to a turbid sample resulted in immediate clearing of the sample.

Touch or Drag Welding

Because of the problems associated with underwater visibility and the stability of a diver underwater in a near weightless situation, it is desirable to use the touch or drag method of welding with covered arc electrodes.

The most apparent change in welding technique that takes place in changing from the ordinary manual method is that the electrode is held at a 60° to 70° leading angle. And rather than carefully holding the electrode a short arc length away from the plate, the diver-welder now exerts a constant pressure of about one pound (Silva, 1971) to the electrode against the plate. This dragging technique is possible without shorting the arc because of the coating that burns slightly slower than the electrode metal itself. The electrode coating used for this underwater welding process is iron powder.

The iron powder electrode coating used in such an arrangement must maintain a constant arc length as it is dragged along, it must not disintegrate during the welding, and the slag being formed must not flow ahead of the electrode. Silva (1971) recommends E6027 as being even better than E7024, another iron powder electrode. Madatov (1962) selected EPO-55 iron powder electrodes. Some sort of water-proofing needs to be added to the iron powder electrodes to keep them from disintegrating underwater. Almost everything from wax to paint has been used with varying degrees of success.

The welds produced using iron powder electrodes with the touch or drag method were more principally composed of parent metal. Normal covered arc welding produces welds with 80% filler metal. However, using the touch method only 30% to 40% of the weld is filler metal. This simultaneously results in 35% to 50% less consumption of the weld electrode (Madatov, 1962).

The protective cone in which the arc burns has a good effect on the arc stability. Using k, the stability factor previously mentioned, it is seen that horizontal touch welding with DC current reduces the factor (which indicates increasing stability) from 1.61 to 1.45. And using AC current (although this is not recommended for underwater use) k was reduced from 1.86 to 1.37 (Madatov, 1962). Similarly for vertical welding positions, the stability was 33% better with DC current and 22% better for AC current. This stability results in more uniform penetration, with the weld bead finely rippled and nicely shaped in the horizontal and in the vertical positions, although it retains the characteristic concave bead in the vertical position (Madatov, 1962). The penetration using a reduced voltage due to the shortened arc length of 25 to 30 volts at 280 to 300 amps was 3/16". Spatter was minimal and the slag was easily detached. Table 3 gives some other welding conditions for the iron powder electrode using the touch technique.

The type of metal transfer in touch welding is small droplet transfer except for an occasional large drop that short-circuits the arc gap. The resulting metallurgical structure is fairly sound. The usual pearlitic-ferritic structure with characteristic grain growth in the HAZ was noted (Madatov, 1962). Ductility was improved, although it was not comparable to that of open air welds. Tensile strength was reported by Madatov (1962) to be 80% to 100% of the parent metal and Silva (1971) reported it to be 100%. Both report improvement over manual arc welding techniques.

The ease with which the touch method gives sound underwater welds should be emphasized in light of the often poor welding conditions and the fact that divers are not often skilled welders. This situation is to be avoided, but it may be necessary under certain circumstances.

The drawbacks of using iron powder touch arc welding are: 1) that the iron powder electrodes oxidize readily and

TABLE 3

Iron Powder Touch Welding Characteristics

Thickness of Metal, mm	Electrode Diameter, mm	Arc Voltage	Welding Current, A			
			Welding in Flat Position		Welding in Vertical Position	
			Butt	Lap or tee	Butt	Lap or tee
5-6	4	25-30	240-260	260-280	250-270	280-300
8-10	4	25-30	260-280	280-300	280-300	300-320
8-10	5	25-30	300-320	320-340	---	---

should be kept hermetically sealed, and 2) that due to the deep penetration, plates with a thickness below 3/16" cannot be welded without burning through. Beyond these drawbacks, it is a superior method.

Shrouded Metal-Arc

Because of the extremely steep temperature gradients in underwater welding, even the iron powder touch welding technique does not eliminate weld degradation, especially in its brittle properties. The drastic quenching in underwater welding produces bainite and martensite formations at the fusion line, fine grain size in the HAZ, slag entrapment and porosity, and the possibility of hydrogen embrittlement.

One answer to the above problems is to use the gas formed during the welding process to displace water from the immediate vicinity of the weld pool. Another answer is to build a complete enclosure around the area to be welded. This is referred to as "dry" underwater welding. The advantages of a shroud, which is a device to displace a limited volume of water, over a dry welding technique are that there is no limitation on the size of the joint to be welded, no external shielding gas needed, and a minimum of diving encumbrances are needed. Around the arc vicinity where the natural bubble phenomena is occuring, the weld atmosphere is changed from a dynamic water gas interface into a quasi-static gas atmosphere. The disadvantages of such a scheme is that the gas atmosphere has a high hydrogen content, allowing for the possibility of hydrogen embrittlement, and the plate itself is still in contact with the water resulting in a high cooling rate. And as might be suspected, the mechanical properties are found to be intermediate between an open air and an open water weld.

In actual operation, the size of the shroud is critical.

An equilibrium must be maintained between gas formation and loss. Too much gas will tend to bounce the shroud off the workpiece. Too little gas will be ineffective in displacing the water and nothing will be gained.

Silva (1971) met with some success using a 1 1/2" hemisphere. The shroud eliminated undercut and produced a better bead shape. Changing the number of ports through which gas could escape resulted in different qualities of welds. This exemplified the equilibrium situation that is required.

Tensile strengths matched those of similar welds made in open air for both E6027 and E7024 electrodes. Impact tests at 0°C were 76% and 70% of the open air values for E7024 and E6027 respectively. However, the E6027 gave more uniform values and is therefore perhaps more reliable. The weld bead appeared more flattenened and had a width/penetration ratio of 4.1-5.4 which was close to the 4.2-5.4 range observed for open air welds (Silva, 1971). The brittleness of the weld was improved using the shroud. The hardness was decreased by 27% from the open water values. This was correlated with a 35% band width decrease of the martensite region in the HAZ.

Although the shroud has not proven to be the complete answer to the problems associated with underwater welding, it is another improvement leading towards a possible complete answer.

Multipass Underwater Welding

Until recently it was recommended that underwater welds not be multipass in nature. However, Chicago Bridge and Iron Company have been successful in producing sound underwater multipass welds (Grubbs, et al., 1972). Visibility

may be the major reason multipass welds were not recommended; indeed, visibility is necessary to place the beads correctly. Assuming visibility problems are minimized, the quality of the weld is then dependent to a large degree on the welder-diver. Thus, good welders were trained to become good divers, rather than the other way around. Based on tests using various standard electrodes underwater, E6013 electrodes were selected. This is quite a significant difference from the iron powder electrodes used in the underwater drag technique. The drag technique may be used during multipass welds.

Welds made on plates showed porosity but no other defects. Penetration and fusion were good. These results have not been expected when attempting to weld high carbon-equivalent plates. This type of plate is normally subject to severe hydrogen induced underbead cracking in the HAZ. The carbon-equivalent, CE, is defined as:

$$CE = C + \frac{Mn}{6} + \frac{C_r + M_o + V}{5} + \frac{Ni + C_u}{15}$$

It was found that when welding underwater, the rapid quenching magnified the hydrogen problem by retarding the diffusion rate of the hydrogen, and trapping it in the weldment. Austenitic electrodes are known to often be able to decrease this hydrogen cracking problem by storing large quantities of hydrogen in the weld metal, keeping the hydrogen away from the crack-sensitive HAZ. It was found that a carbon equivalent of .40 was the transition point between crack-free welds and underbead cracking when using the mild steel E6013 electrodes. Austenitic electrodes should be used when the carbon equivalent exceeds .40. This corresponded to maximum hardness zones in the welds. The hardest HAZ values without cracking were Vickers 30kg 408. The softest with cracking were 439. Thus, the transition at CE = .40 corresponds to

TABLE 4

Multipass Welding Properties

	UTS (ksi)	Yield (ksi)	% elong. in 2"	% reduction in Area
Sample #1	67.2	61.9	7	5.8
Sample #2	61.2	51.7	8	9.6
AWS Standar E 6013	67	55	17	---

4a. Properties of Underwater Weld Using Electrodes in Flat Position. 12' depth.

Reference (Grubbs, Seth, 1972)

Temperature °F	Charpy V-notch Impact Energy Ft/lbs	
	Dry	Underwater
70	59	24
30	46	22
0	28	17
-30	25	10

4b. Charpy V-notch Tests

Reference (Grubbs, Seth, 1972)

a welded hardness of Vickers 30kg 420.

Notch toughness impact energy values were only 50% of open air values. Porosity in the welds is thought to be the result of wet electrode coatings. A method of waterproofing the coating may reduce this problem. The E 6013 electrodes were successfully welded in all positions. The austenitic electrodes are much more difficult to control underwater, but it has been possible to weld in all positions. Table 4 summarizes the physical properties obtained with the E 6013 electrodes underwater.

Underwater GMA

Madatov and others have tried gas shielded thin wire welding underwater and have found it generally to have no advantage over non-shielded methods. Brown (1972) found that the shielding gas forms bubbles at the tip of the electrode rather than shielding the arc. Madatov (1969) found that using CO_2 shielding, a gas flow rate of 920-1480 l/hr. was optimum. The weld shape factor was found to be 2.6-3.5 which is satisfactory. The CO_2 has a slight cooling effect on the arc causing a slight increase in penetration. But Madatov concludes that the weld is better when made without CO_2 shielding. The proportion of weld metal and the shape factor are lower without shielding. CO_2 shielding may also increase the porosity and cause a haze around the arc zone. GMA is being used successfully in various sorts of underwater dry welding techniques.

Underwater Plasma Arc Process

According to the developers of an underwater plasma arc welding process, there are several reasons for considering

it for underwater applications (Hasui, et al., 1972). The plasma arc process provides a stable arc, good fusion due to the highly concentrated energy in the plasma, good directional properties, an easily automated or mechanized potential, as well as a source of illumination for the diver-welder.

Hasui, et al., (1972) have done some experimentation on the stability of the arc using a shielding gas (argon) and a shielding liquid, water glass ($Na_2O \cdot 2SiO_2$), as well as in an unshielded situation. They found that using the plasma jet of shielding material the plasma arc was very stable for spacing variations of several millimeters provided the flow rate of plasma gas was at least 2 l/min.

The current voltage characteristics are not really understood, but the arc voltage is generally lower with shielding. This may be because the shielding prevents the water column from constricting the plasma column (Figure 6). Without a shielding jet, the arc is unstable. Argon shielding provides no resistance to the surrounding water movement and can be deformed badly. Use of water glass in the shielding jet stabilizes this effect. Also the Na present in the water glass provides additional stabilizing effects.

Because the heat transfer in a process has direct effects on the resulting weld quality, any variation within a process must be evaluated. The shielding material used in the plasma jet changes the cooling rate of the welded structure. Water glass provides the slowest cooling rate. The water glass is covering a portion of plate being welded and has an insulating effect, which prevents rapid cooling. A slower cooling rate results in a better weld quality, but this insulating effect is dependent on the flow rate and the viscosity. Argon provides little insulation for the cooling weld. Figure 7 shows the thermal histories at the bond for the three possible variations: water glass shielding, argon shielding, and unshielded. As might be expected, the water glass shielding produces the best quality welds but the quality

FIGURE 6

Electrical Characteristics of Plasma Arc Underwater

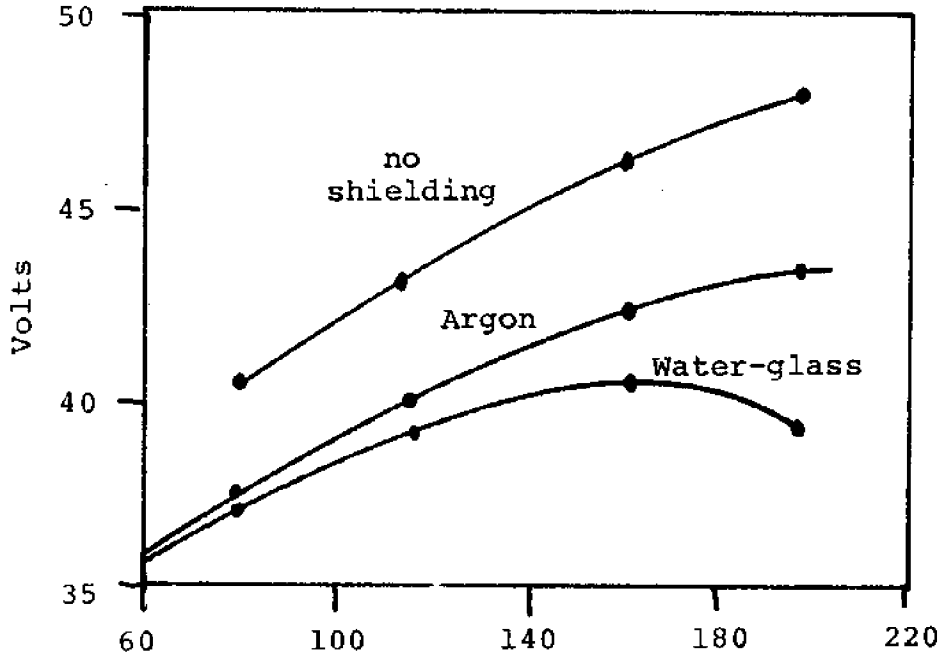

FIGURE 7

Thermal Histories at Bond

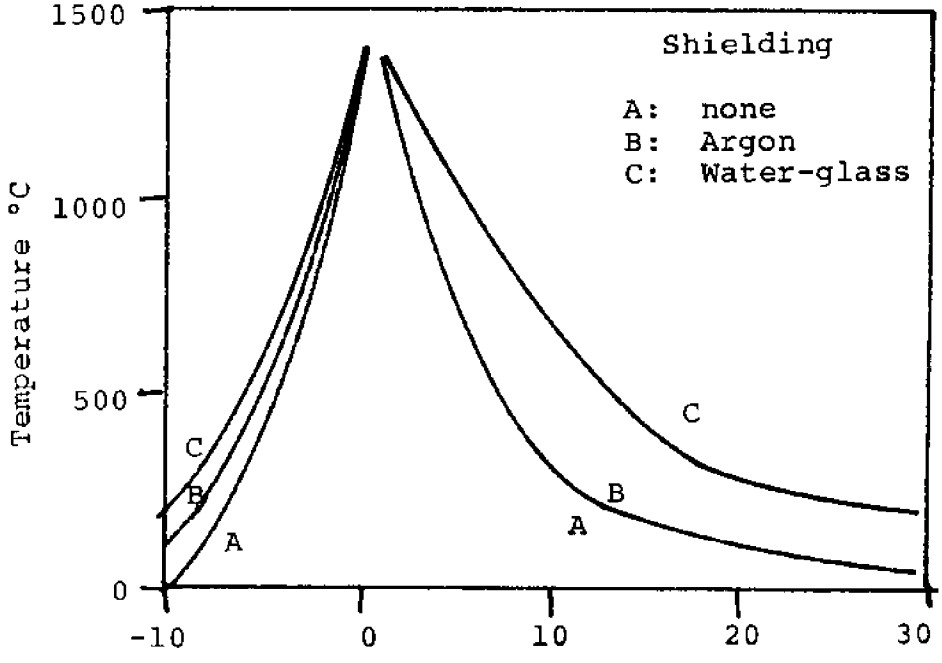

Reference (Hasui, 1972)

is then dependent on the flow rate and viscosity of the water glass used. Figure 8 shows the range of these variables that appear to produce good welds. From this data, a viscosity coeffeicient of 60 and a flow rate of .6 l/min. was chosen for the remainder of the experiments (Hasui, et al., 1972).

Metallurgical tests showed that all weld metal had a joint efficiency of 100%. Ductility was much increased for water glass shielding as evidenced by the doubling of the crack initiation angle. Two pass welding in both the unshielded and the water glass shielded processes increased the crack initiation angle by 50%-60%. Single pass water glass shielded welds had 80% of the base metal notch toughness based on the Charpy impact test at 15°C. Double-pass shielded welds had 100% notch toughness. Unshielded single-pass welds had only 40% notch toughness, while the double-pass welds were about the same. Here it appears that while the tempering effect of the second pass bead on the first has a positive effect, the main factor preserving a good notch toughness is the slower cooling rate initiated by the water glass shielding. Table 5 contains these results in tabulated form (Hasui, et al., 1972).

Vickers microhardness tests were run on these same four welds. Figure 9 shows the results graphically (Hasui, et al., 1972). In all cases, as is normally expected, the heat affected zones had the highest hardness. For single-pass welds with water glass shielding, the maximum value was H_V 330. Without shielding, the value was H_V 390. In both cases, the double-pass weld lowered the hardness in the first bead to H_V 190 and H_V 290 respectively. In the case of hardness, the double-pass tempering effect is more important than the water glass shielding, although it too has a beneficial effect. It can be seen from this that water glass shielding together with double or multipass welding techniques will be most effective in producing superior weld quality.

The microstructure of the water glass shielding method of single-pass welds were described (Hasui, et al., 1972).

FIGURE 8

Shielding Liquid Effect on Weld Quality

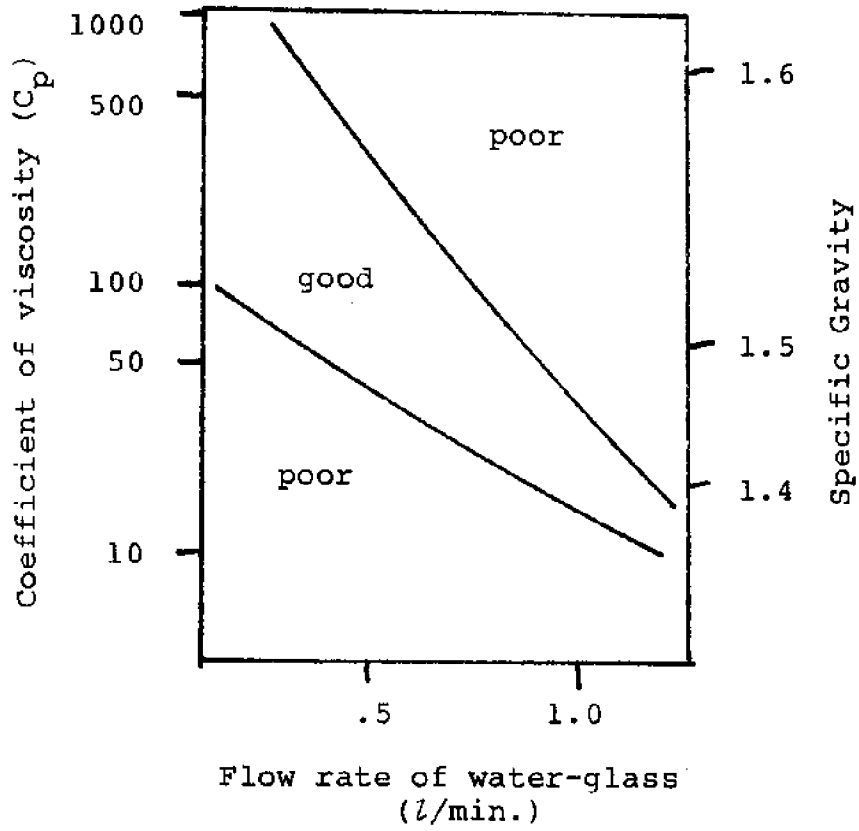

Plasma gas: 2 ℓ/min.
Arc Current: 150 amp.
Torch to metal spacing: 6 mm.
Welding Speed: 10 cm/min.

Reference (Hasui, 1972)

TABLE 5

Macroscopic Properties of Plasma Arc Welds

Shielding	Passes	Current	Voltage	Yield (kg/mm^2)	% elongation	UTS (kg/mm^2)
Water Glass	Single	190	40	46.1	23	57.8
Water Glass	Double	150	42	47.2	25	53.0
None	Single	140	45	44.6	23	57.4
None	Double	130	44	45.9	24	56.7
Base Metal				45.2		49.6

	Crack Initiation Angle (°)	Impact Value (kg/cm^2)
Water Glass	46.8	4.4
Water Glass	78.4	5.7
None	26.8	2.2
None	52.5	1.8
Base Metal		5.6

FIGURE 9

Microhardness of Plasma Arc Underwater Welding

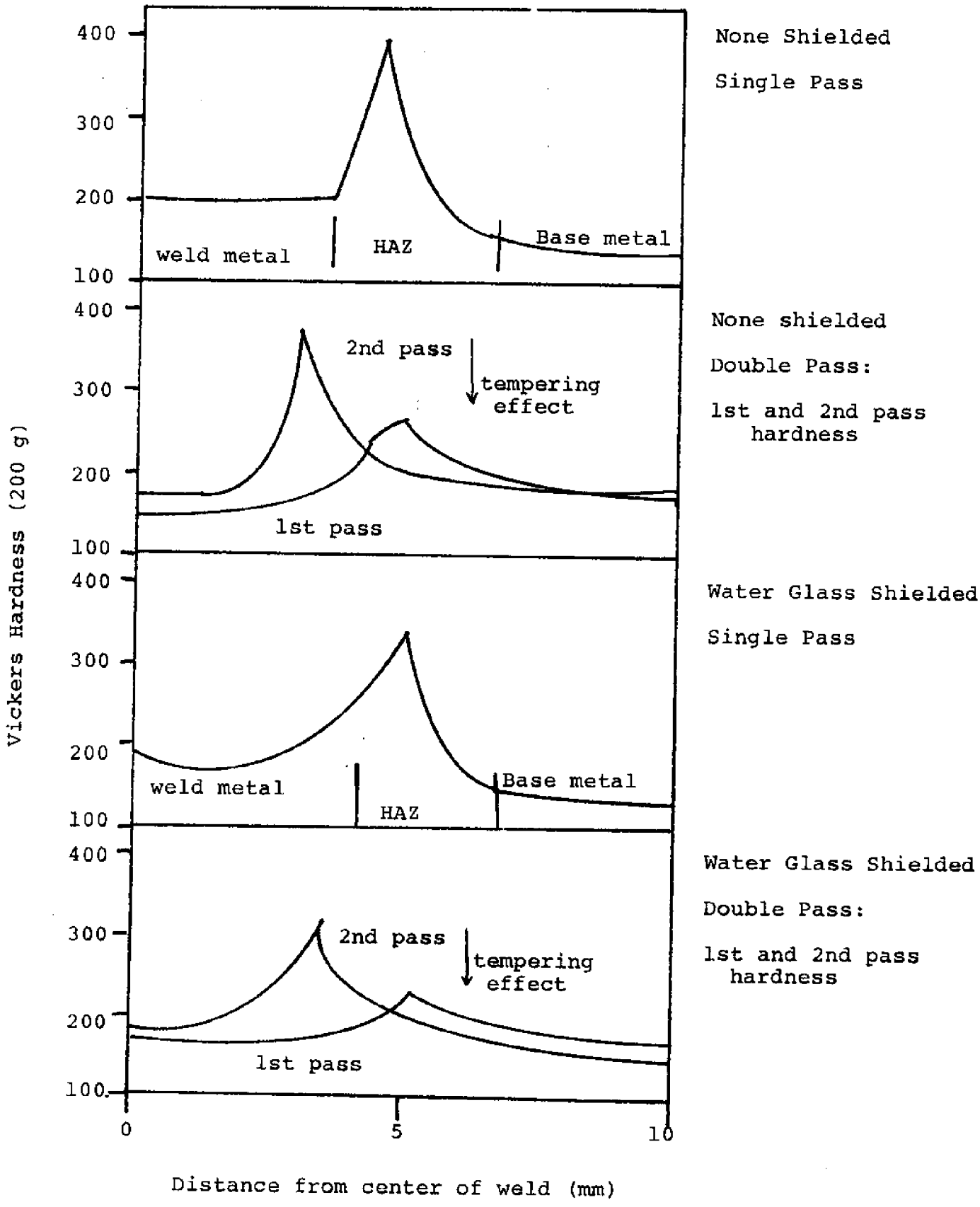

The weld metal contained ferrite precipitate at the grain boundaries. The inside of the grains contained bainite and pearlite. The base metal contained a coarse ferrite network with martensite, bainite and a little pearlite inside the grains. The heat affected zone structure varied with distance. At 0.5 mm from the bond, there was a coarse structure of martensite, bainite, pearlite and ferrite at the grain boundary. At a distance of 2.0 mm from the bond, the grain size becomes a fine ferrite network with some pearlite inside the grains. At the 3.5 mm distance, the grains were a fine network of ferrite and pearlite. At 4.6 mm, the grains were ferrite with spheroidized pearlite. Beyond this distance, the metal was like the base metal with a nerwork of uniform ferrite and pearlite outside the grains already described. This same structure was found for the argon shielding and unshielded cases, although the HAZ was narrower in these cases.

With the second pass in a double-pass weld, the grain size becomes finer by the reheating. More ferrite and pearlite form in the weld metal with much more forming in the HAZ. This sort of structure is much improved over that originally formed which explains the improved metal properties achieved using the double-pass method. Table 6 contains a summary of the heat transfer and metal properties using unshielded, argon shielded, and water glass shielded methods.

TABLE 6

Comparison of Shielding

Characteristics	No Shielding	Argon Shielding	Water Glass Shielding
Concentration of heat	strong	weak	medium
Fluctuation of heated spot (anode spot)	small	great	medium
Bead width	narrow	wide	medium
Penetration	deep	shallow	medium
Insulating effect to base metal	poor	poor	good
Heat input (joule/cm)	4.2×10^4	3.9×10^4	3.8×10^4
Cooling rate at 500°C °/sec	100	96	44
Joint efficiency - %	116	126	117
Notch toughness (% of base plate)	39	---	78

1) Some thought and effort should be given to the effect of depth (or increasing pressure) on the underwater welding processes. Gas evolution rates, voltage and current relationships, metal transfer, etc., should all be considered as possible functions of depth.

2) The effect of natural and induced turbidity in the underwater environment remains a problem in any underwater welding attempt. The mechanism behind, as well as the composition of covered-arc electrode induced turbidity ought to be determined. Practical, clever engineering solutions should then be initiated to remove this particular hindrance to underwater welding efforts.

3) Whereas basic heat flow models are available for general underwater welding, specific processes ought to be compared. Empirical corrections to the heat model may become necessary. A better explanation and description needs to be formulated for the turbid, not-steady boiling phenomena taking place in the immediate vicinity of the welding arc.

4) The possibilities and effects of tempering underwater weld regions needs further study. Several investigators hint that this may prove to be of practical value in improving the mechanical weld properties. Multipass techniques, as well as forms of post heat treatment should be studied. Again, the fundamental effects on the microstructure must be considered before jumping into a study of mechanical property improvements. In this area of improving the weld microstructure, more thought and study ought to be given to various forms of shielding the weld from the water. In addition to "dry" welding techniques, water-glass shielding and shroud shielding ought to be more fully investigated.

5) Weld defects such as porosity need to be linked back with a fundamental mechanism. Wet electrode eovering has been suggested as the cause of porosity. Other defects such as lack of fusion, lack of penetration, and undercutting need to be understood to be the results of a more fundamental process.

6) Imaginative innovations such as a shroud attachment to covered arc electrode welding need to be assessed in all positions of welding, again with an emphasis on how this addition influenced the basic underwater welding processes and mechanisms.

7) A better understanding is needed in the area of matching weld metal to parent metal. Metallurgical reasons for a metal's weldability need to be investigated. Underwater welding feasibility for metals other than mild carbon steels ought to be obtained.

8) Various combinations of shielding, shrouds, multipass techniques, etc., ought to be investigated, keeping in mind that when working in the underwater environment, the simplest tools are the best. The general area of underwater welding equipment appears underdeveloped.

9) Basic research ought to be continued to evaluate hydrogen-induced failures, corrosion-stress failures, and other poorly understood failure mechanisms that are particularly critical in the underwater environment.

It is hoped that the scope of these specific suggestions will not limit thoughts in the area of underwater welding. Proper solution to the varied problems that face this area of fabrication will not come from any one source at any one time. It is hoped that this summary of the

state of affairs in technical research in underwater welding will prove helpful in understanding underwater welding phenomena.

> "And I set my mind to seek and explore by wisdom concerning all that has been done under heaven. It is a grievous task which God has given to the sons of men to be afflicted with."
>
> -Ecclesiastes 1:13

Bibliography

Avilov, T. I. "Properties of Underwater Arcs," Welding Production, 1960, Vol. 7, No. 2, pp.30-33.

Brown, A. J. "Methods of Research in Underwater Welding," Undergraduate thesis, M.I.T. Ocean Engineering Department, 1971.

Brown, Staub, Masubuchi, "Fundamental Study of Underwater Welding," Offshore Technology Conference (OTC), 1972, Vol. 2, No. 1621, pp. 55-64.

Elliss, J. B. "Arc Welding in the Ocean: A Diver-Welder Shares His Experience," Metal Construction and British Welding Journal, March, 1969, pp. 151-154.

Grubbs, Seth, "Multipass All Position 'Wet' Welding--A New Underwater Tool," OTC, 1972, Vol. 2, No. 1620, pp. 41-54.

Hasui, Inomata, "Plasma Underwater Welding," Journal Japan Welding Society, July, 1971, Vol. 40, No. 7, pp. 622-31.

Hasui, Fukushima, Kinugawa, "Development of Underwater Plasma Welding Process," Second International Ocean Development Conference, October 5-7, 1972, Tokyo, Vol. 2, pp. 1007-1036.

Hydrotech Services Co. "Hydroweld--The New Underwater Welding Development from Hydrotech that Meets the API 1104 Code," 1972, Company Literature.

Madatov, N. M. "Special Features of Underwater Touch Welding," Automatic Welding, 1962, Vol. 15, No. 9, pp. 52-55.

_____. "Underwater Welding Electrodes With Coatings Containing Iron Powder," Welding Production, 1962, No. 8, p. 25.

_____. "The Properties of the Bubble of Steam and Gas Around the Arc in Underwater Welding," Automatic Welding, 1965, Vol. 18, No. 12, pp. 25-29.

_____. "Energy Characteristics of the Underwater Welding Arc," Welding Production, 1966, No. 3, pp. 11-14.

_____. "Shape Relationships for Underwater Welding," Welding Production, March, 1969, Vol. 16, No. 3, pp. 18-23.

_____. "Underwater Ship Repair," Naval Ship Systems Command, Washington, D.C., 1970.

_____. "Influence of the Parameters of the Underwater Welding Process on the Intensity of Metallurgical Reactions," Welding Research Abroad, March, 1972, p. 63.

Madatov, Dorhodya, Kostenko, "High Speed X-ray Cinematography of the Underwater Welding Arc," Welding Production, September, 1965, Vol. 12, No. 9, pp. 72-73.

Masumoto, Nakashima, Kondo, Matsuda, "Study on Underwater Welding," Report 1, Journal Japan Welding Society, July, 1971, Vol. 40, No. 7, pp. 683-93.

Masumoto, et al. "Study on Underwater Welding," Report 2, Journal Japan Welding Society, August, 1971, Vol. 40, No. 8, pp. 748-754.

Mishler, Randall, "Underwater Joining and Cutting--Present and Future," OTC, 1970, Vol. II, p. 235.

Savich, I. M. "Underwater Welding With Cored Electrode Wire," Welding Production, October 1969, Vol. 22, No. IV, p. 70.

Silva, E. A., Hazlett, "Shielded Metal-Arc Welding Underwater with Iron Powder Electrodes," Welding Journal, June, 1971, p. 406.

Silva, E. A. "Gas Production and Turbidity During Underwater Shielded Metal Arc Welding with Iron Powder Electrodes," Naval Engineering Journal, December, 1971, p. 59.

_____. "An Investigation of Fusion Controlled Metallurgical Bonding in a Marine Environment," PhD. Dissertation, vc, Berkeley, 1971.

Staub, J. A. "Temperature Distribution in Thin Plate Welded Underwater," Master Thesis, M.I.T., Ocean Engineering Department, 1971.

Vagi, Mishler, Randall, "Report on Underwater Cutting and Welding--State of the Art," Battelle Memorial Institute, 1968.

Waugh, Eberlein, "Underwater Metallic Arc Welding," Welding Journal, October, 1964, pp. 531s-534s.

PART 3

MECHANISMS OF HEAT TRANSFER DURING UNDERWATER WELDING

by

Alan J. Brown

Part 3 is a revised edition of the M. S. Thesis by Alan Brown to be submitted to M.I.T. in June, 1973. This edition does not include Appendixes C and E and three photographs. A copy of the thesis can be purchased through the Engineering Library of M.I.T.

ACKNOWLEDGEMENTS

The author would like to thank Mr. Julius Ritter and all his staff at the Boston Naval Shipyard for all their assistance with the experimental portion of this thesis. Without their help this work could not have been possible.

Also, to be mentioned are Professors Rohsenow, Glicksman, and Griffith for their help with the boiling, radiation and bubble models.

Finally, I would like to thank Professor Koichi Masubuchi for his overall coordination of this effort.

TABLE OF CONTENTS

* Appendixes C and E are not included in this interim report

LIST OF FIGURES

* Figures 5-1, 5-9, and 5-11, which are photographs, are not included in this interim report

LIST OF TABLES

NOMENCLATURE

a	film thickness
A	contact area (cm^2)
b	bubble growth rate
c_p	specific heat (Btu/lbm. °F)
E	machine voltage (volts)
e	emissivity (Btu/hr-ft^2)
G	volume flow rate (cc/sec)
H_m	total heat content
h	bubble height (cm); enthalpy
I	machine current (amps)
K_o, K_1	Bessel functions
L	plate thickness (ft)
$\dot{m}$	mass flow rate (lbm/hr)
N	lumped welding parameter
p, B, a, b	pool correlation parameters
$\dot{Q}$	energy input frim machine (Btu/hr.)
P	pressure
$\dot{q}$	heat transfer rate (Btu/ft^2-hr)
R	bubble radius (cm.)
R_o	residual volume radius (cm.)
$\bar{R}$	universal gas constant
S	finite difference grid spacing
T	plate temperature
T_o	ambient temperature
T_{sat}	water saturation temperature
T_M	plate melting temperature
T_{sub}	subcooled temperature
t	time (sec)
V	welding speed

w	time independent x coordinate
x	distance in direction parallel to weld bead
X_o	characteristic length (ft)
X_{max}, Y_{max}	maximum length and width of weld pool
w_i	volume source term (Btu/ft^3-hr)
α	thermal diffusivity (ft^2/hr)
λ	average reciprocal diffusivity (hr/ft^2); wavelength
κ	thermal conductivity (Btu/hr.ft.°F)
ρ	density (lbm/ft^3)
τ	bubble period (sec.)
σ	surface tension (lbf/ft)
σ	Stefan-Boltzmann constant (Btu/ft^{2}hr°R^4)
η	deflection of film interface (cm); welding efficiency
*	indicates non-dimensionalized variable
$\overline{\text{bar}}$	indicates average

CHAPTER I

INTRODUCTION

Before any research effort is undertaken, there must be a need to justify it. The need for a reliable underwater welding process is generally recognized, but the need for basic research in this area is sometimes questioned. This author and others believe that decades of stagnation in this field can be traced to "poke in the dark" methods of process design and modification. All such attempts have been made with little or no true knowledge of the intricate mechanisms of heat transfer and chemistry occurring during underwater welding. For this reason the value of this research cannot be questioned. Before any progress can be made, a basic understanding of underwater welding processes must be obtained and this new knowledge applied to the rational development of a reliable process.

Chosen for analysis here are three basic processes which jointly possess many of the conceivable system characteristics one might encounter in any underwater joining process. All three processes are arc welding processes.

1.1 Background and History

Underwater welding has developed almost entirely from dry land processes and suffers greatly because of it. Dry land adaptation skips many fundamental design procedures, and thereby results in a system which is totally limited by various aspects of the underwater environment, rather than using them to its advantage.

Welding processes which have been used underwater include (ref. 1):

"Wet" Applications

1. shielded metal arc (SMA)
2. gas metal arc (GMA)

"Dry" Applications

1. gas metal arc (GMA)
2. gas tungsten arc (GTA)
3. shielded metal arc (SMA)

The application of these processes has been largely for ship, structure, and pipeline repair.

"Dry" welding underwater uses a chamber or bell to surround the joint, close out the water, and create an artificial environment in which the welding may be carried out. Great success has been achieved using this process, especially when welding regular shapes such as pipelines. This process is, however, limited to regular

shapes, as irregular forms require custom fabrication of the bell which causes great expense.

For more general underwater repairs and fabrication chambers are impractical and welding "in the wet" is desirable. The only other alternatives for such work are prefabrication and dry-docking, but complete prefabrication is not always possible, and dry-docking is costly. Only "wet" welding will be considered in this thesis.

The demands of World War I led to increased use of all types of welding. In 1917 the British Navy began using underwater arc welding to make temporary repairs on ships until they could be dry-docked. These repairs consisted mostly of welding over leaking rivets, and their success was limited in both strength and ductility.

When coated electrodes appeared on the scene in 1926, they were almost immediately brought underwater, but unfortunately the improvement due to these coatings was nowhere near that achieved in open-air applications. Since 1930 numerous coatings and coverings have been tried, but little progress has been made. (ref. 3)

The effectiveness of underwater "wet" welding at this time is best summed up by the standard U. S. Navy rule of thumb, "Underwater welds will generally yield 80 per cent the strength and 40 per cent the ductility of similar welds made in air." The reasons for this lack

of success lie in two basic categories:

1. Diver related problems
   a. Visibility
   b. Equipment encumberances
   c. Upsetting forces due to currents and vessel motions

2. Welding problems
   a. Enormous heat transfer rates due primarily to boiling and radiation
   b. Dissociation of H_2O at high temperatures into hydrogen and oxygen causing hydrogen embrittlement

Mechanisms of heat transfer during underwater welding are directly responsible for temperature distributions and cooling rates in the welded joints. These ultimately affect the metallurgy and residual stress distribution of the weldment and thus its overall quality.

1.2 Recent Research

Realizing the great value of a reliable underwater welding process, a number of researchers in Japan, the Soviet Union, and the United States finally began to do some basic research in this area.

The first to attack this problem were the Russians in the early 60's. (refs. 4,5,6,7,8,9) Madatov, in a series of articles, studied in depth many aspects of underwater welding. Although he laid little theoretical foundation for the phenomena he observed, his observations were many and precise. Among the topics he discusses are bead penetration and shape, effects of salinity and pressure, welding positions, properties of the steam and gas around the welding arc, energy characteristics of the arc, electrode coatings, and the use of iron powder electrodes underwater. Much of this work will be described and referred to throughout this text.

Dr. E. A. Silva at the University of California has also done extensive work in this field. (refs. 3,10, 11,12) He has considered the effect of various welding parameters on weld metallurgy, has looked at gas production, iron powder electrodes, deep ocean applications, and most important has developed a new process using a shroud in conjunction with the shielded metal arc process.

This shroud technique is considered in some detail in this text.

Finally came the work of Lt. James Staub here at M.I.T. (ref. 16) His research in the area of heat transfer and temperature distributions during underwater welding laid the groundwork for the further research presented here. His basic method was an application of Pavelec's research at the University of Wisconsin. (ref. 13,14,15) Pavelec developed a computer program which predicted temperature distributions for surface welding using GMA. Staub modified this program and Pavelec's technique and applied them to the underwater shielded metal arc process. Staub's work stands as the first in this area. His over-rapid cooling predictions indicated that something was left unaccounted for. (see figure 1-1) His conclusion predicted what this missing element might be. Staub states,

"A reevaluation of boiling during underwater welding must be conducted. It can be speculated that gases generated at the tip of the electrode could disrupt the boiling, shield the surface of the plate, and limit heat transfer in this region to radiation."

How right he was!

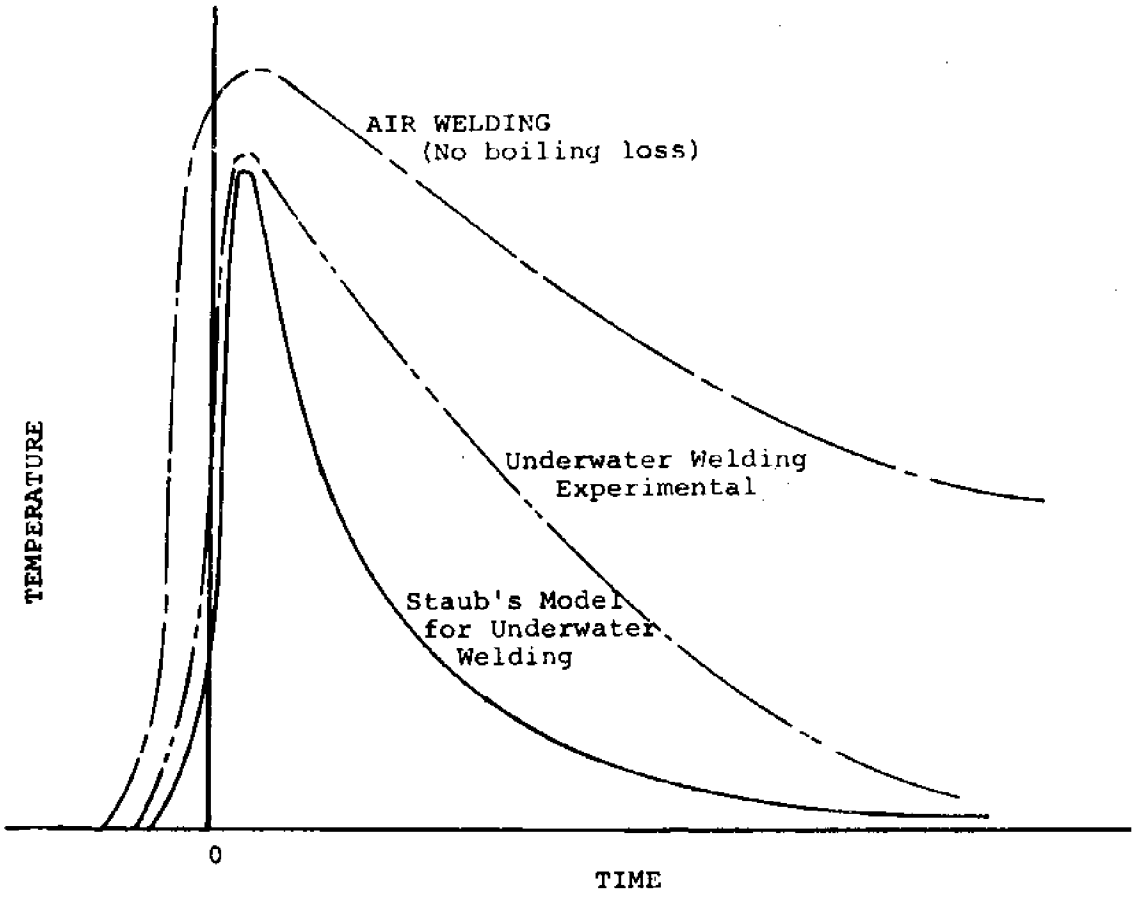

PREDICTED TEMPERATURE
VS. MEASURED TEMPERATURE

FIGURE 1-1

1.3 Organization and Goals of this Effort

The main goal of this thesis is to unravel once and for all the mystery around the various mechanisms involved in the underwater SMA process and at the same time to look at a sufficient cross section of other mechanisms so that a reliable process might be developed from the sum. This work was initially aimed at substantiating or disproving Staub's hypothesis, but has grown to an in depth look at three basic processes:

1. shielded metal arc (SMA)
2. gas metal arc (GMA)
3. SMA with a shroud

SMA, the most basic of these, displays the characteristic bubble growth phenomena left unmolested by any other goings on. The shroud attempts to hold the evolved gases in the vicinity of the arc and GMA adds the complication of impinging gases to the already present bubble growth. The intelligent combination of these mechanisms could produce a composite process of acceptable quality, but this can never be realized until each is understood in full.

The structure of this thesis is simple, the individual steps are not so simple:

1. Establish the identity and mathematical

description of each individual phenomena involved in the above processes.

2. Combine these into a single mathematical model to predict temperature distributions in plates welded underwater.

3. Measure these temperature distributions in actual underwater welding runs.

4. Compare these results to those predicted. Evaluate and modify the basic mechanism models in terms of this comparison.

Each step is crucial, but successful completion of each may someday lead to an improved underwater welding process. This is our ultimate goal.

CHAPTER II

THE PROCESSES

The three processes selected for analysis here were chosen to represent three unique types of "above the plate" phenomena in underwater arc welding:

1. dynamic bubble (SMA)
2. gas trapping (shroud)
3. impinging gas (GMA)

Before any research could begin on these, all current knowledge had to be gathered, evaluated, and understood.

2.1 Shielded Metal Arc Process

The process used in nearly 100% of all underwater "wet" welding in this country is the shielded metal arc process or stick electrode welding. The underwater process is very similar to that used on the surface. However, the effect of the surrounding water and of pressure at depth makes the implementation of this process quite unique.

An arc is formed between the tip of a consumable metal electrode and the grounded workpiece. Filler metal is provided by the melting electrode which is manipulated by a diver. (see figure 2-1) The arc is sustained in a

THE WELDING ARC

FIGURE 2-1

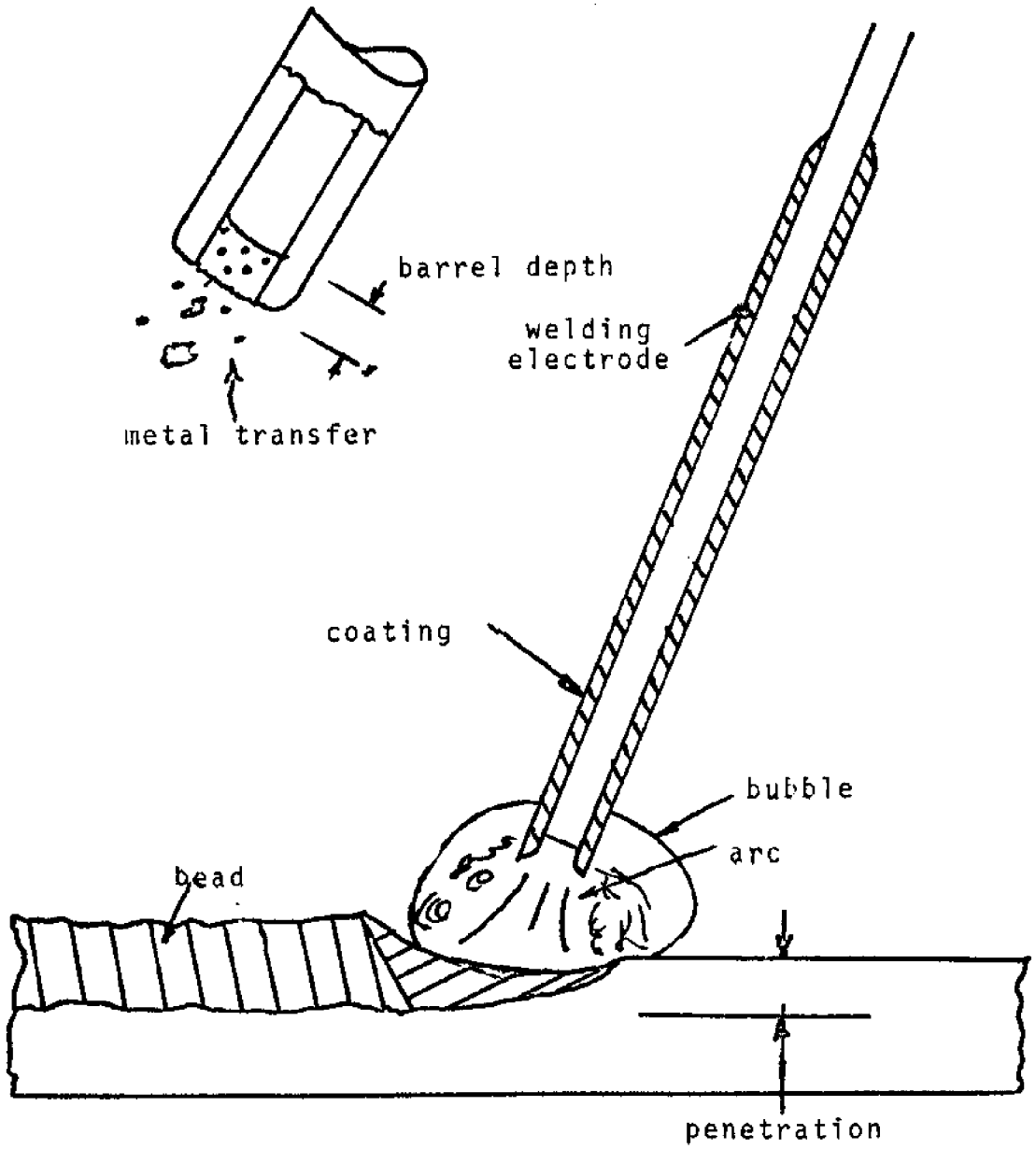

high temperature plasma which is surrounded by a gaseous bubble. Due to the abundance of H_2O and the high temperatures this gas may contain up to 92% dissociated hydrogen. (see table 2-1) Slow burning coatings on the electrodes allow a drag manipulation technique to be used.

The underwater arc is greatly affected by the surrounding water. The water's cooling action constricts the arc and increases the current density of the arc column. The volt-ampere characteristic of the arc is rising and is shown in figure 2-2. The constricting effect of pressure can also be seen in this graph. Most important, constriction raises the arc temperature as can be seen in figure 2-3. Due to this increase in temperature penetration is greater in underwater welding and will increase with pressure. This can become a problem.

Crucial to detailing the heat transfer for this process is understanding the bubble growth mechanism above the plate. A dynamic bubble is continuously growing and departing at the tip of the electrode due to the evolved gases. This bubble has been looked at by both Madatov and Silva, but neither proposes a suitable dynamic model for the process or gives a very detailed description. As this bubble is the solution to Staub's dilemma and very crucial to the heat transfer model, it had to be investigated further. This investigation is described in Chapter V.

TABLE 2-1 COMPOSITION OF GASES GENERATED BY WELDING WITH COVERED ELECTRODES

Gas Composition, Per Cent by Volume				
Carbon Monoxide (CO)	Carbon Dioxide (CO_2)	Hydrogen (H_2)	Oxygen (O_2)	Metal Vapor
15-25%	3-5%	70-92%	-	small amount

ref. 1

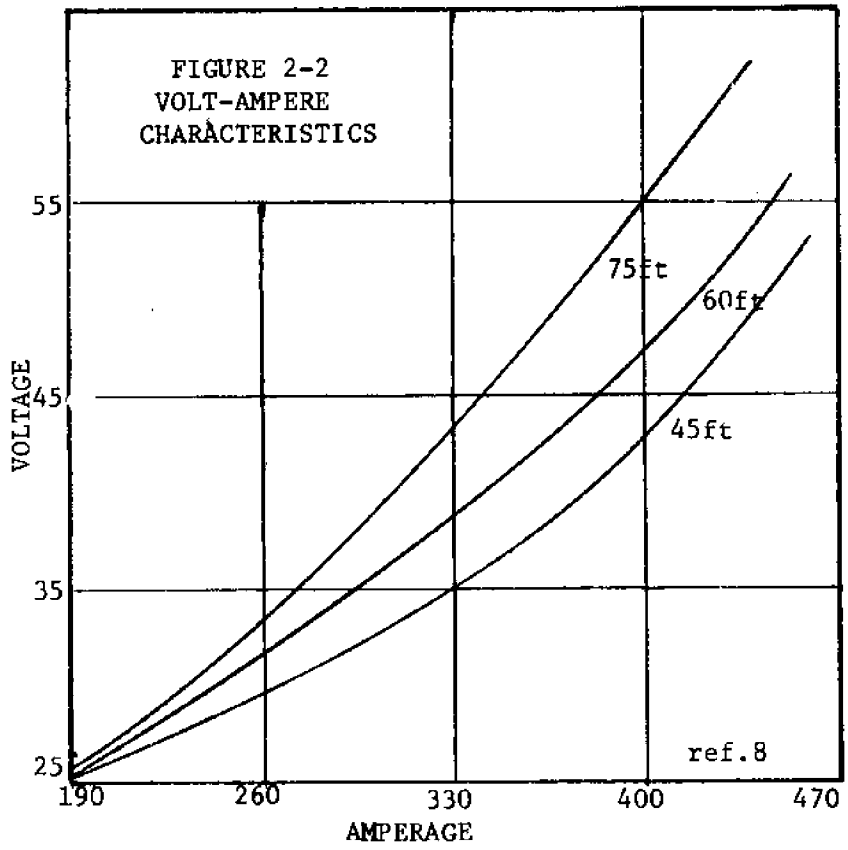

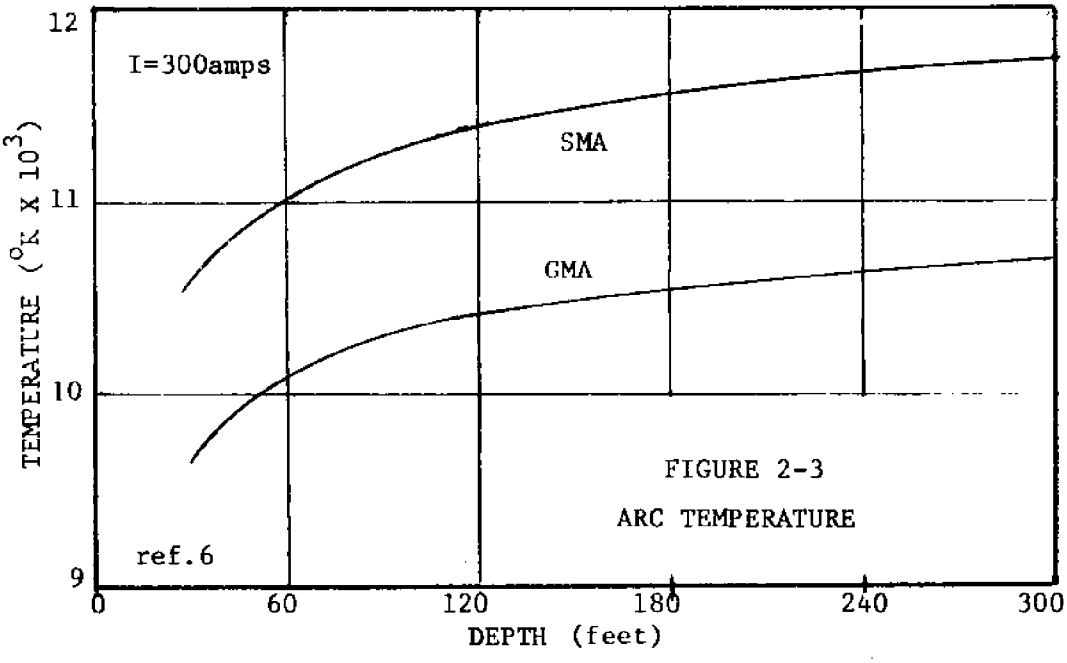

FIGURE 2-3

ARC TEMPERATURE

2.2 The Shroud Technique

E. A. Silva at the University of California has done extensive work in the field of underwater welding. (ref. 3) Among other things he substantiated the supremacy of iron powder electrodes over the standard 5/32 inch E6013 electrode used by the Navy. The Russians have acknowledged these electrodes for years, but the United States has been reluctant to accept them. More important, however, was his conception and testing of an underwater welding shroud. This device uses the gas formed during welding to displace water from the vicinity of the arc and consists simply of a dome or "shroud" over the arc and puddle. Although the mixture of gases in the shroud still contains hydrogen, at least the water to weld contact is reduced at the weld puddle. Silva reports improved strength, ductility and appearance with this process.

The shroud setup is shown in figure 2-4, and a detailed drawing in figure 2-5. The size and port arrangement of the shroud was determined through repeated trials. The shroud has four basic segments:

1. the dome or shroud body
2. the electrode passage
3. the port
4. the bead passage

Its effectiveness depends on a delicate balance of gas

THE SHROUD METHOD

FIGURE 2-4

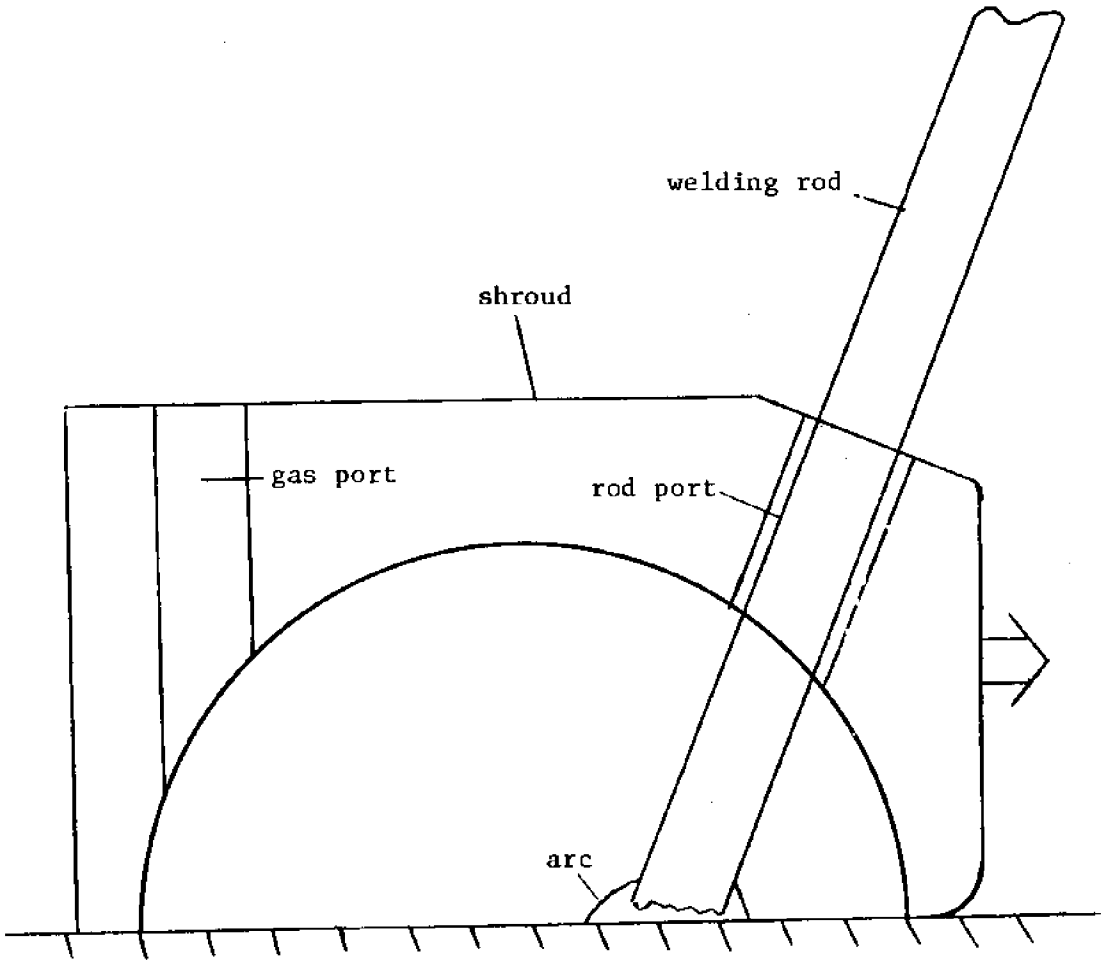

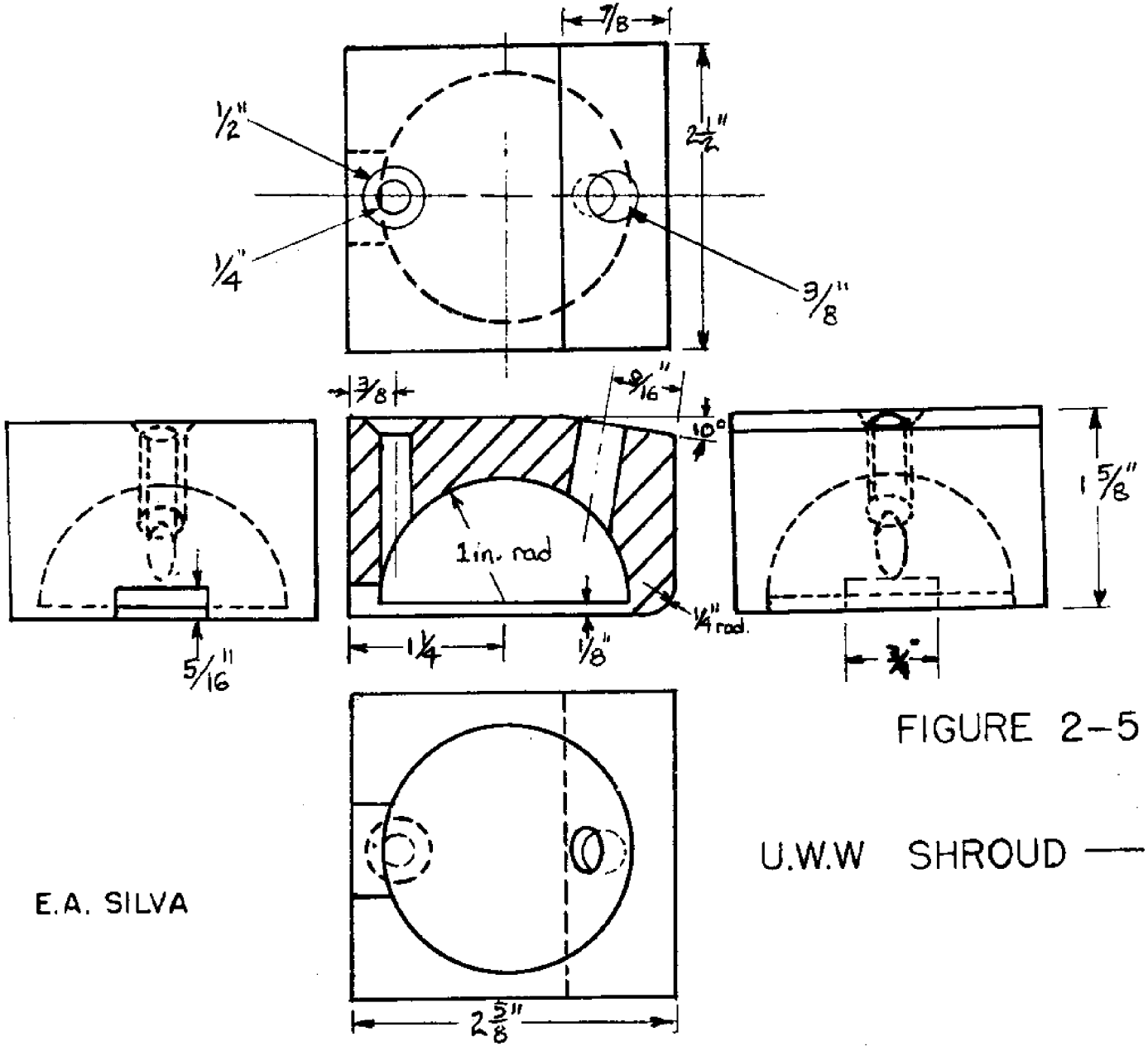

FIGURE 2-5

U.W.W SHROUD — DETAILED

E.A. SILVA

production and entrapment. Buoyancy is also critical as this device is simply dragged along with the electrode, and yet must remain level. The original shroud material was mild steel although a weighted acrylic shroud was used for experimentation.

This gas entrapment idea, possibly coupled with an external gas supply, (GMA) could be an answer to the underwater welding problem.

2.3 The Gas Metal Arc Process

Little is known about the application of GMA underwater, and it would seem that the Russians are the only ones who have made extensive use of it. (ref.1) A schematic of their process is shown in figure 2-6.

The basic principle of the underwater process goes one step beyond that in air. An arc is formed between the tip of a continuously fed filler wire and the grounded workpiece. Surrounding this wire is a tube or nozzle through which a shielding gas is driven. This gas impinges on the plate in the vicinity of the arc and molten pool. The purpose of the shielding gas in surface welding is to provide an inert gas environment for the molten metal, displace contaminating gases, and improve the quality of the weld. Underwater it is hoped that the

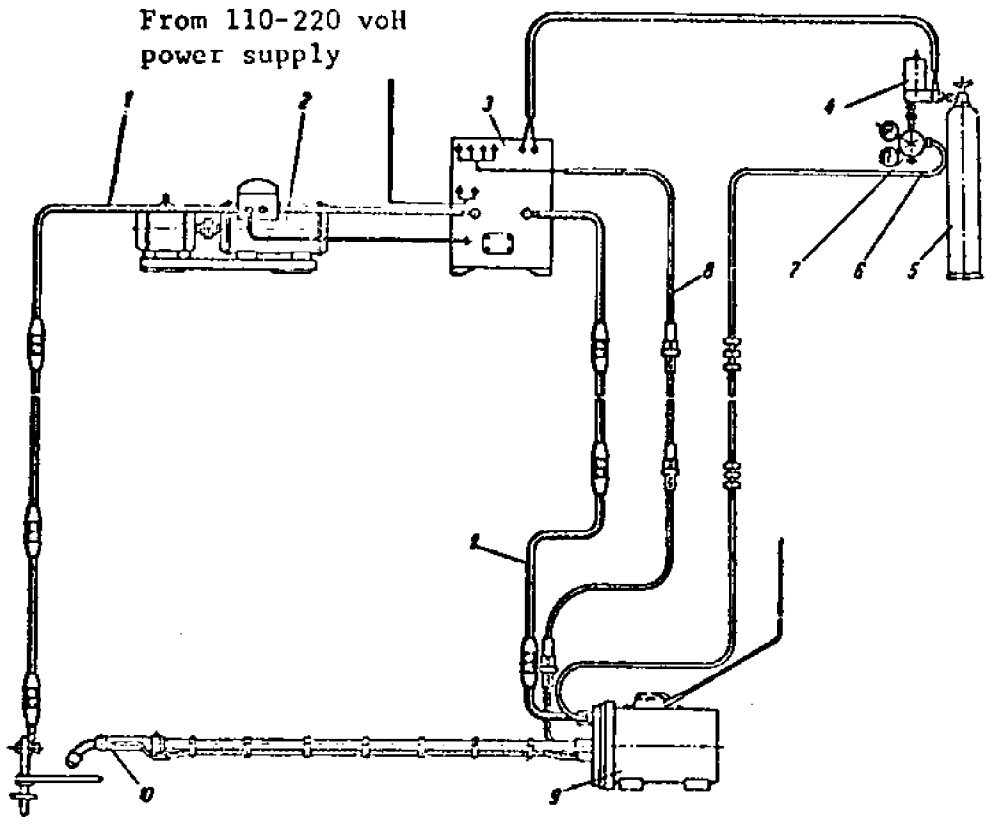

GAS METAL-ARC WELDING EQUIPMENT ARRANGEMENT FOR UNDERWATER WELDING

1. Welding cable
2. Power supply
3. Control unit
4. Heater and flow gage
5. Gas cylinder
6. Gas hose
7. Reducing valve
8. Welding cable
9. Gas reservoir and wire feed unit
10. Welding head.

ref.1

FIGURE 2-6

impinging gas would also displace water in the vicinity of the weld puddle. This would reduce the heat transfer in this area, slow the rapid cooling, and thereby improve the quality of the weld. This process has great potential, but will require extensive experimentation.

CHAPTER III

THE HEAT TRANSFER MODEL

Heat transfer during underwater welding involves a number of intricate mechanisms. Understanding these mechanisms is the key to understanding the processes themselves. Such an understanding can be evaluated in terms of the mathematical models of each mechanism by integrating these models into a single temperature predicting program and comparing results to those obtained empirically. The steps involved in such a procedure are as follows:

1. Set up the basic differential equation describing the conduction and energy conservation in the plate.

2. Identify and model all sources and losses of energy.

3. Mathematically define the boundary conditions on the differential equation.

4. Solve the differential equation numerically on the digital computer.

The general method used here follows that developed by Pavelec (refs. 13 and 14) for GTA (gas tungsten arc) welding and later applied by Staub (ref. 16) to underwater welding.

Due to the water environment encountered in

underwater welding, cooling is rapid and steep temperature gradients during welding are unavoidable. A great breakthrough in surface welding research came with Rosenthal's work in the late 30's on plate temperature distribution during welding. Rosenthal assumed that the welding arc was a point source of heat moving in a straight line. This approximation is valid away from the weld, but poor in close, making it of little use with underwater welding where temperatures may drop off to ambient at a distance of 1/2 inch from the weld centerline. Pavelec, however, uses Rosenthal's work to correlate molten pool shapes, and then uses the molten pool as the inner boundary condition on the energy equation. Solutions to this must be carried out numerically, but provide a distinct advantage in computing temperatures close to the arc.

Pavelec's and Staub's method will be used here.

3.1 The Basic Equation

The entire analysis to be presented here is based on the energy equation in two dimensions with source terms:

$$\frac{\partial}{\partial x}\left(K\frac{\partial T}{\partial x}\right) + \frac{\partial}{\partial y}\left(K\frac{\partial T}{\partial y}\right) + w_L = \rho C_p \frac{\partial T}{\partial t}$$

Using the method described in Appendix A yields the following non-dimensional, time independent form:

$$\frac{\partial^2 T^*}{\partial w^{*2}} + \frac{\partial^2 T^*}{\partial y^{*2}} + \frac{\partial \log K}{\partial T^*}\left[\left(\frac{\partial T^*}{\partial w^*}\right)^2 + \left(\frac{\partial T^*}{\partial y^*}\right)^2\right]$$

$$+ \frac{\dot{q} X_o^2}{K L (T_M - T_o)} = - \frac{V X_o}{\alpha}\left(\frac{\partial T^*}{\partial w^*}\right)$$

The physical significance of this time independence is that after transients have settled out, the moving arc is surrounded by a temperature distribution which remains constant with respect to the arc. (figure 3-1) This is termed a quasi-static temperature distribution. The third term on the left hand side represents sources and losses of energy while the other terms relate directly to conduction. The source and loss terms represent the varied and least understood mechanisms of an underwater welding process.

3.2 Heat Loss Terms

Keeping track of all the energy emitted by the welding arc is a difficult problem, one which even for surface welding has not been completely solved. The energy

QUASI-STATIC TEMPERATURE DISTRIBUTION

FIGURE 3-1

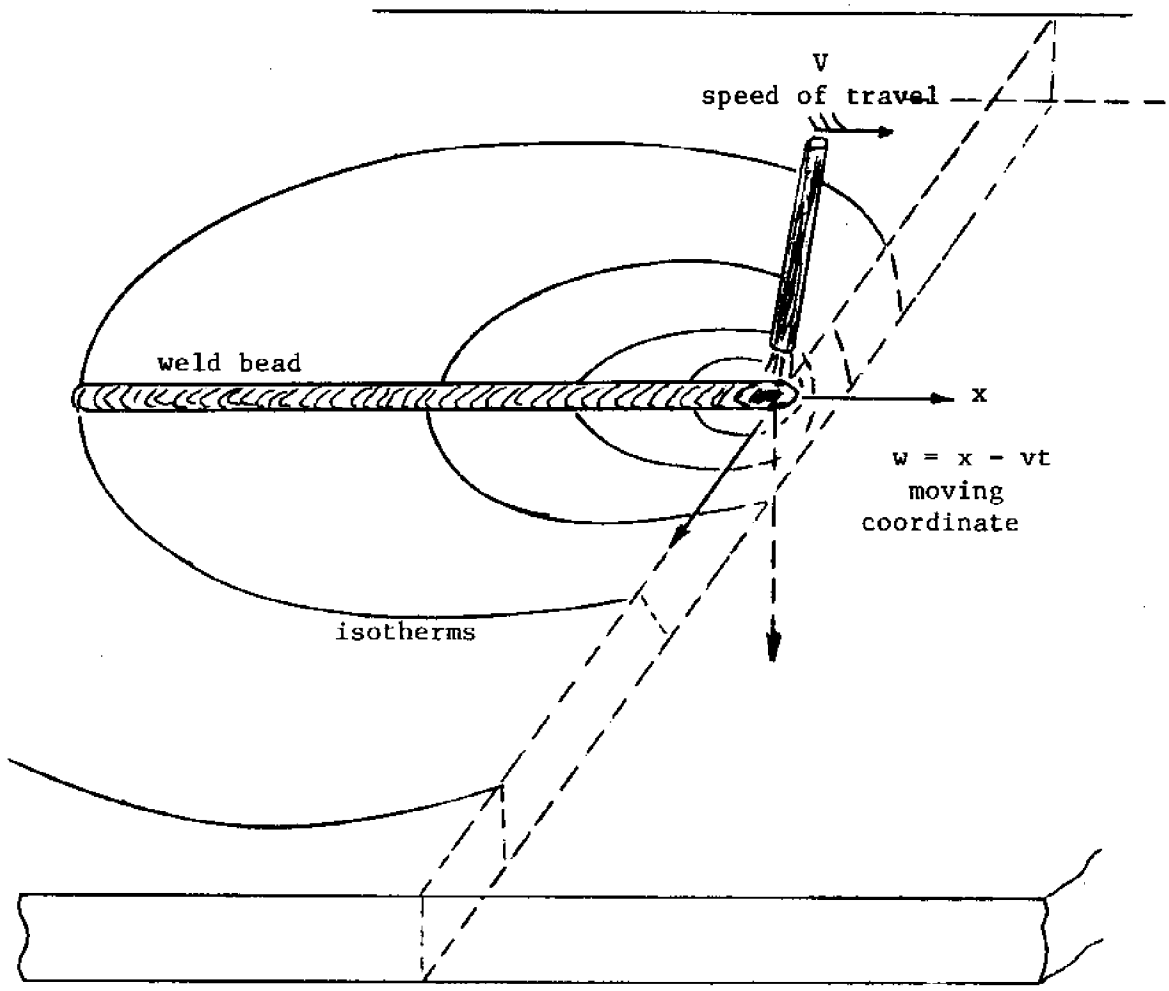

Table 3-1

Values of Physical Constants

At saturation temperature:

$\rho_L = 59.8$ lbm/ft^3

$\rho_v = .0372$ lbm/ft^3

$h_{fg} = 970.3$ Btu/lbm

$\sigma = 4.04 \times 10^{-3}$ lbf/ft

$g = 4.17 \times 10^8$ ft/hr^2

$\mu_v = .0314$ lbm/hr-ft

$Pr = 1.9$

$C_{sf} = .013$

$K_v = .0145$ Btu/hr-ft-^oF

$g_o = 4.17 \times 10^8$ lbm-ft/lbf-hr^2

$C_L = 1.005$ Btu/lbm^oR

$\mu_L = .72$ lbm/ft-hr

At ambient temperature:

$\rho_L = 62.3$ lbm/ft^3

$K_L = .327$ Btu/hr-ft^oF

$\alpha_L = 5.17 \times 10^{-3}$ ft^2/hr

$Pr_L = 6.4$

delivered to the molten pool by the electric arc may be on the order of 10^4 Btu/hr. This energy acts to pre-heat, melt, and post-heat the weld metal and is eventually dissipated in a number of ways.

The greatest heat losses during underwater welding are due to boiling and radiation. Prior to boiling the heat transfer is mainly due to convection. McAdams derived the following relation for top of the plate convection: (ref. 29)

$$\frac{h_c L}{K_L} = .14 \left(Gr_L \cdot Pr_L \right)^{1/3}$$

where

$$\frac{Gr_L}{L^3 \Delta T} = \frac{g \cdot \beta_L \cdot \rho_L^2}{\mu_L^2} = 4.4 \times 10^7$$

This yields for the heat transfer:

$$\dot{q}_{cTOP} = 32.1 \left(T - T_\infty \right)^{4/3} \frac{Btu}{ft^2\text{-}hr.}$$

For bottom of plate convection he recommends

$$\frac{h_c L}{K_L} = .27 \left(Gr_L \cdot Pr_L\right)^{1/4}$$

which yields

$$\dot{q}_{cBOT} = 12.2 \left(T - T_\infty\right)^{5/4} \frac{Btu.}{ft.^2 - hr.}$$

As temperatures continue to increase above the boiling point, convection heat transfer levels off and becomes negligible in comparison to boiling and radiation.

Much research has been done in the area of boiling heat transfer, and many semi-empirical equations have been developed for relating surface temperatures to heat transfer rates. This work has been conducted, for the most part, under ideal conditions with uniform surface temperatures or heat transfer rates in steady state. Underwater welding, however, involves extremely transient temperature distributions with steep gradients and takes place in sub-cooled water (below T_{SAT}). Prior to using

existing boiling models it is therefore necessary to determine their applicability.

Before discussing individual phenomena it is worthwhile to consider boiling as a whole. Heat transferred from the arc to the welded surface raises its temperature well above the saturation temperature. The degree of this superheat, as well as various parameters of the physical situation, determine the type of boiling which occurs. Boiling appears in a number of distinct regimes, each with its own characteristic phenomena and heat transfer rates. Heat transfer rates corresponding to the models derived here are shown in figure 3-2, with the various regimes as indicated. It is worthwhile to discuss each of these regimes in detail.

3.21 Nucleate Boiling

When the surface temperature sufficiently exceeds the saturation temperature of the liquid, vapor bubbles may begin to nucleate on or near this surface. In a sub-cooled liquid these bubbles will grow and collapse under the influence of various hydrodynamic and thermodynamic forces.

The heat transfer rate during nucleate boiling is very high and a number of mechanisms have been proposed

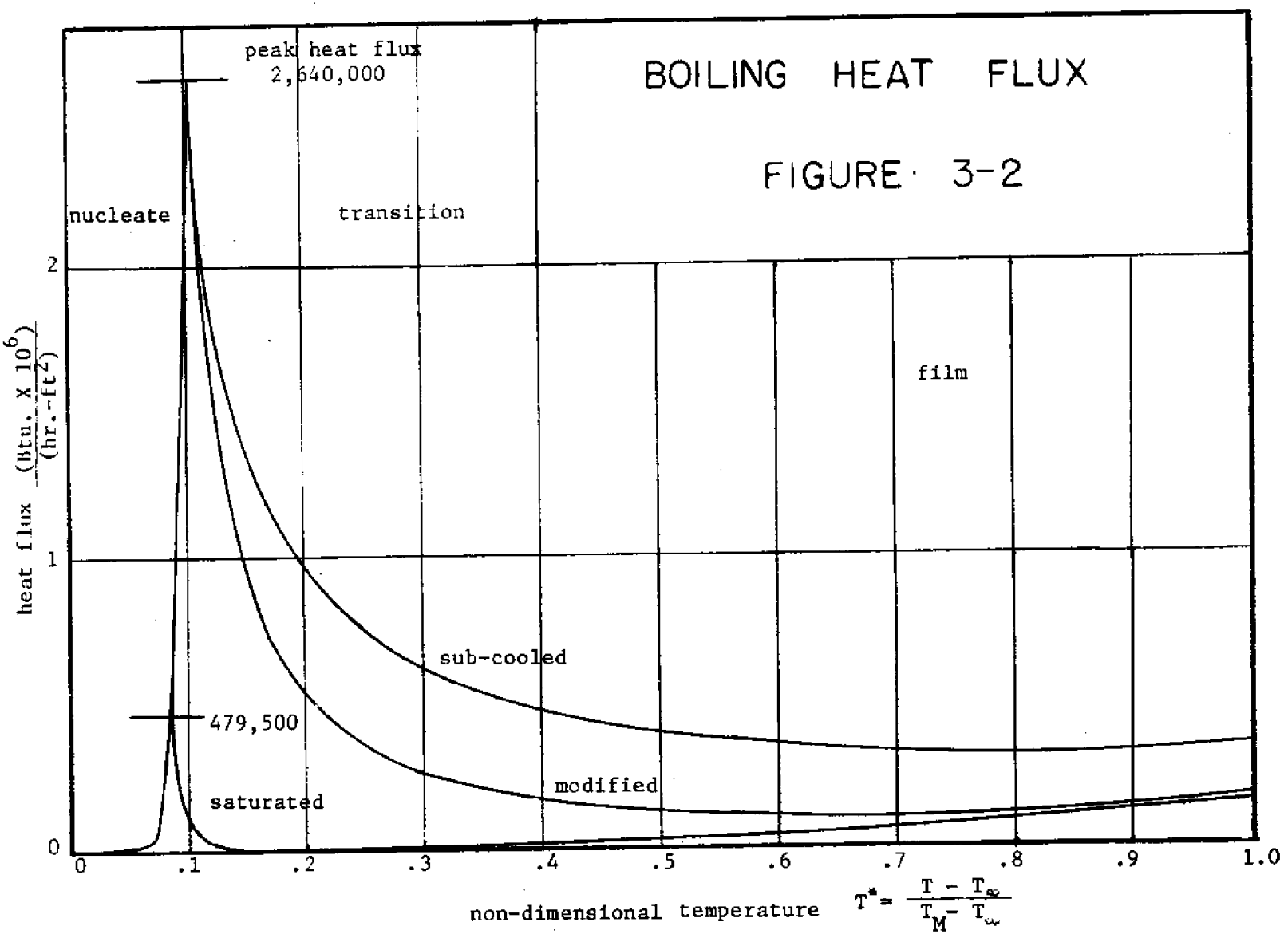
BOILING HEAT FLUX
FIGURE 3-2
peak heat flux
2,640,000
nucleate
transition
film
sub-cooled
479,500
modified
saturated
heat flux (Btu. X 10^6)/(hr.-ft^2)
0
1
2
0
.1
.2
.3
.4
.5
.6
.7
.8
.9
1.0
non-dimensional temperature T* = (T - T∞)/(TM - T∞)

to account for this. However, the precise method of bubble growth and heat transfer is not fully understood.

Forster and Grief proposed the following. (ref. 17) As a bubble grows and subsequently collapses, a volume of hot liquid is forced away from the heated surface and new liquid flows in to take its place. The attractive aspect of this mechanism lies in its insensitivity to the degree of sub-cooling due to combined effects cancelling each other. It can be assumed that:

$$\dot{q} \propto R_{MAX}^{3} \left(\Delta T_{SAT} + \Delta T_{SUB} \right) \frac{1}{\tau}$$

As sub-cooling increases (ΔT_{sub} increases), and the bubble period (τ) decreases, these effects are compensated for by a decrease in R_{max}. This insensitivity of nucleation to sub-cooling has been substantiated by a number of investigators. The only weakness is that Forster and Grief's final correlation does not show sufficient influence of fluid and surface properties. The Rohsenow correlation is the most widely accepted correlation of nucleate boiling. Considering this apparent insensitivity to sub-cooling and using the Rohsenow correlation leads to the following equation: (ref. 18)

$$\frac{C_{PL}(T-T_{SAT})}{h_{fg}} = C_{sf}\left\{\frac{\dot{q}_{NUC}}{\mu_L h_{fg}}\left[\frac{g_o\sigma}{g(\rho_L-\rho_V)}\right]^{1/2}\right\}^{1/3} Pr^{1.7}$$

or normalized

$$\dot{q}_{NUC} = 1.663\left[T^*(T_M-T_\infty)+T_\infty-T_{SAT}\right]^3 \frac{Btu}{hr.-ft.^2}$$

Assumed values for physical constants are listed in Table 3-1.

3.22 Peak Heat Flux

The bubble population greatly increases with plate superheat, and a point of peak heat flux is reached where the outgoing bubbles essentially jam up the flow and the liquid-vapor columns become unstable.

When two fluids flow relative to each other with an interface between them, there is a maximum relative velocity above which a small disturbance of this interface will blow up, and thereby distort the flow. This Helmholtz instability is the most widely accepted

explanation for peak heat flux. A two-dimensional schematic of this process is shown in figure 3-3.

Using Helmholtz instability analysis, Zuber derived the following equation for peak heat flux: (ref. 19)

$$\dot{q}_{peak} = .18\left[\frac{\sigma(\rho_L-\rho_v)g g_c}{\rho_v^2}\right]^{1/4}\left[\frac{\rho_L}{\rho_L+\rho_v}\right]^{1/2}\rho_v h_{fg}$$

Evaluating this for water at saturation temperature yields:

$$\dot{q} = 479{,}500 \ \frac{Btu.}{ft^2\text{-}hr.}$$

The limitation of this equation is again that it applies only to a liquid at its saturation temperature. Fortunately a number of investigators have considered peak heat flux in sub-cooled liquids. Their analysis involved the effect of intermittent or transient conduction to a sub-cooled rather than a saturated liquid. The Ellion and Ivy-Morris correlations for water are presented below. (refs. 20 and 21)

LIQUID-VAPOR FLOW & HELMHOLTZ INSTABILITY IN NUCLEATE BOILING

FIGURE 3-3

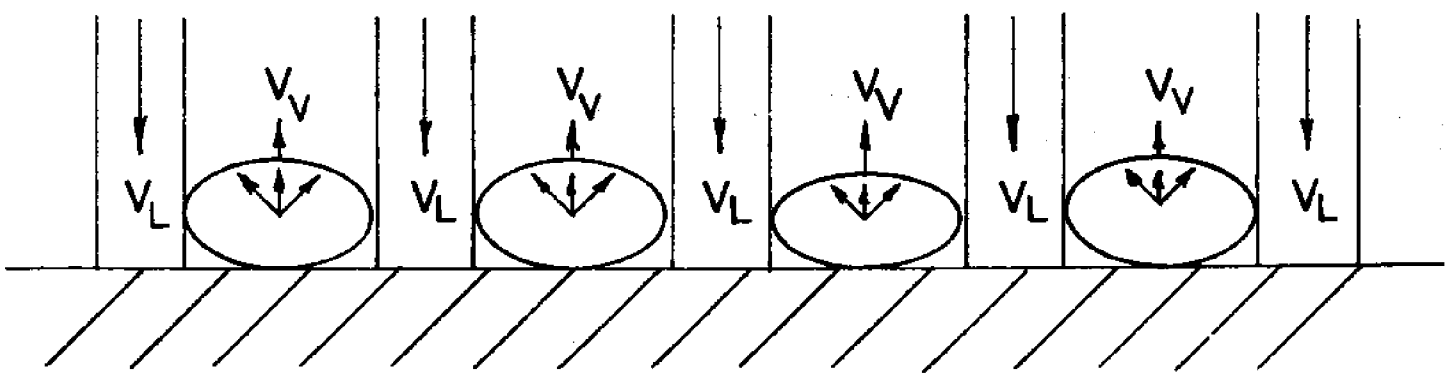

$$(\dot{q}_{MAX})_{Ellion} = \dot{q}_{\substack{MAX \\ SAT}} \left\{ 1 + \left(\frac{2K_L(T_{SAT}-T_\infty)}{(\pi\alpha_L t)^{1/2}} \right) \left(\frac{24}{\pi h_{fg} \rho_v} \right) \left(\frac{c_p \rho_L (T_{SAT}-T_\infty)}{h_{fg} \rho_v} \right)^{1/4} \right\}$$

$$(\dot{q}_{MAX})_{Ivy\text{-}Morris} = \dot{q}_{\substack{SAT \\ MAX}} \left\{ 1 + .1 (\rho_v/\rho_L)^{1/4} \left[\frac{c_p \rho_L (T_{SAT}-T_\infty)}{h_{fg} \rho_v} \right] \right\}$$

$$(\dot{q}_{MAX})_{Ellion} = 5.7 \, \dot{q}_{\substack{MAX \\ SAT}}$$

$$(\dot{q}_{MAX})_{Ivy\text{-}Morris} = 5.16 \, \dot{q}_{\substack{MAX \\ SAT}}$$

Choosing between these correlations and that for saturation boiling or choosing something in betwen posed a difficult problem. As a decision had to be made, a value of 5.5 was chosen to modify the saturation peak and both the saturated and the modified models were tested as possible solutions. This choice will be discussed more

fully in the conclusion.

Using 5.5 as the adjusting factor yields:

$$\left(\dot{q}_{MAX}\right)_{MCD} = 2{,}640{,}000 \frac{Btu.}{ft.^2\text{-}hr.}$$

Given these two values for peak heat flux and using the correlation for nucleate boiling, the corresponding peak temperatures were determined.

$$\left(T-T_{SAT}\right)_{\substack{MAX \\ SAT}} = 66^\circ F.$$

and

$$\left(T-T_{SAT}\right)_{\substack{MAX \\ MCD}} = 116^\circ F.$$

3.23 Film Boiling

As the temperature continues above the peak, the bubble stream becomes more and more jammed until a continuous film begins to form. Film boiling on horizontal plates facing up, and submerged in a liquid at its saturation temperature, has been considered by a number of investigators. The most widely accepted theories at present are based on stability phenomena of the liquid-vapor interface. The applicability of these theories for describing phenomena in underwater welding is again limited by the effect of a sub-cooled rather than a saturated liquid environment.

The existence of a continuous vapor film over the plate demands an interface with vapor contained beneath liquid. The hydrodynamic instability of this situation necessitates a continuous vapor flow due to evaporation. Such an instability is called Taylor instability.

Taylor developed a mathematical model for this liquid-vapor interface which after certain simplifying assumptions for infinite fluid depth and thin film thickness yields: (ref. 22)

$$\eta = \eta_0 e^{bt} \cos mx \qquad m = \frac{2\pi}{\lambda}$$

$$b = \left[\frac{\rho_L \rho_v V_v m^2}{(\rho_L + \rho_v/ma)^2 ma} + \frac{g(\rho_L - \rho_v)m}{\rho_L + \rho_v/ma} + \frac{g_c \sigma m^2}{\rho_L + \rho_v/ma} \right]$$

Disregarding fluid properties, the vapor velocity and vapor film thickness are the only unknowns in the above equation for film growth. The growth rate, b, is normally greater than zero indicating the instability of this interface. See figure 3-4.

Berensen (ref. 23) derived an equation for film boiling heat transfer using Taylor instability analysis. His work was of course for a saturated liquid and was based on a number of empirical observations. Such a solution for a sub-cooled liquid is much more complicated as heat is dissipated in two basic ways rather than one:

1. The heat produces steam which results in a vapor flow to the bubble.
2. In the sub-cooled case heat is also conducted to the liquid in a transient manner beginning with each cycle of bubble growth.

Again it was necessary to make a decision. Could the saturation model be applied to the sub-cooled case, or was some correction necessary. It was decided to test three separate models in this case:

1. A purely saturated boiling model
2. A model with both peak and minimum heat flux modified using the 5.5 factor
3. A model using the modified peak heat flux and a minimum heat flux derived using Berensen's methods, but considering transient conduction. This derivation is done in Appendix D.

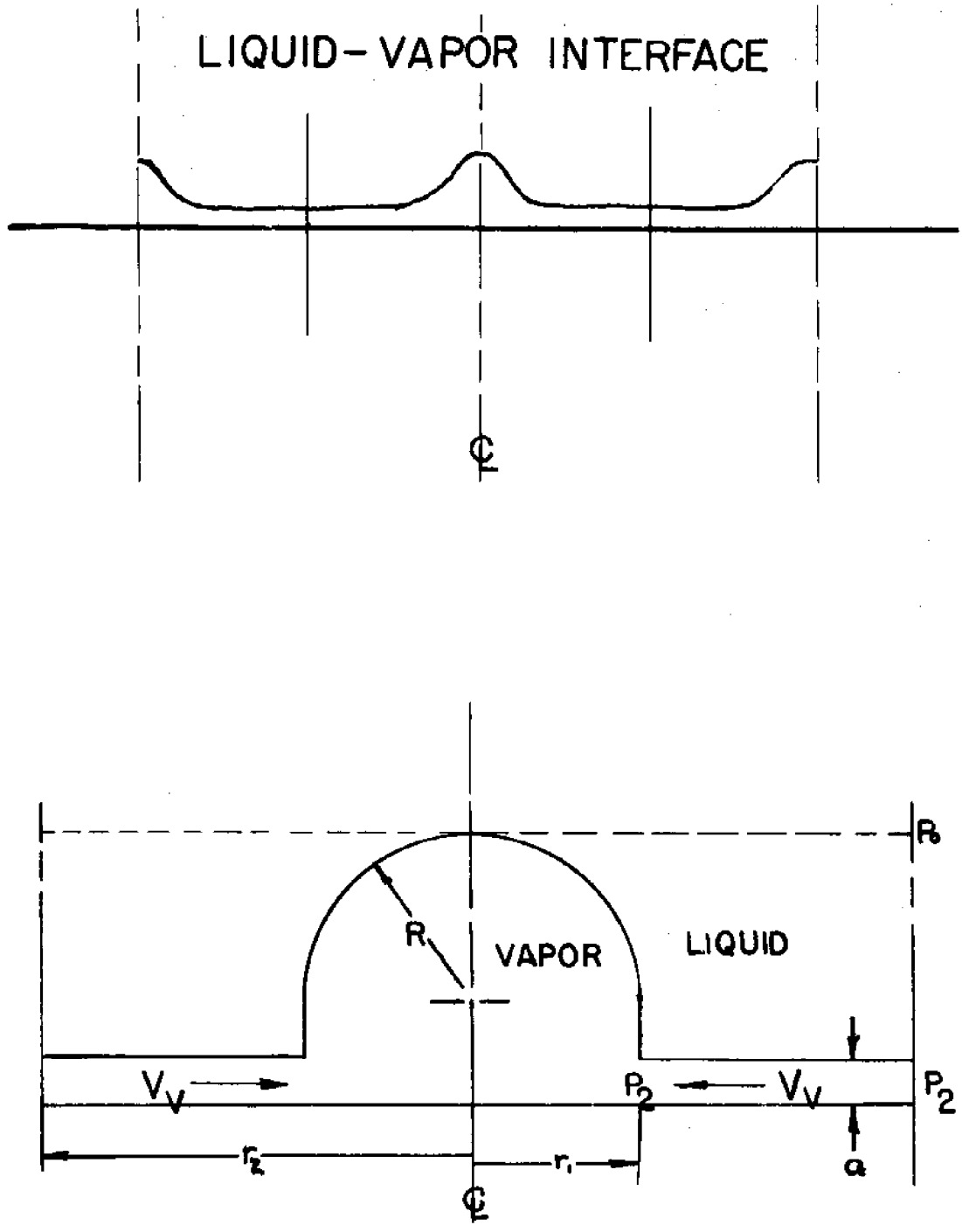

IDEALIZED FILM BOILING MODEL

FIGURE 3-4

The saturated film boiling heat transfer is determined using Berensen's equation for saturated liquids:

$$\left(\dot{q}_{film}\right)_{SAT} = .531\left[\frac{K_v^2 g \rho_v(\rho_L-\rho_v) h_{fg}}{\mu_L[\sigma g_o/g(\rho_L-\rho_v)]^{1/2}}\right]^{1/4}(T-T_{SAT})^{.75}$$

or nondimensionalized:

$$\left(\dot{q}_{Film}\right)_{SAT} = 84\left[T^*(T_M-T_\infty)+T_\infty-T_{SAT}\right]^{.75}$$

Also from Berensen's analysis comes an expression for the minimum heat flux:

$$\dot{q}_{\substack{MIN\\SAT}} = .09\rho_v h_{fg}\left[\frac{g(\rho_L-\rho_v)}{\rho_L+\rho_v}\right]^{1/2}\left[\frac{g_o\sigma}{g(\rho_L-\rho_v)}\right]$$

$$\dot{q}_{\substack{MIN\\SAT}} = 5980\ \frac{Btu}{ft^2\text{-}hr.}$$

Substituting this value for minimum heat flux into the film boiling equation yields the temperature at minimum heat flux.

$$(T-T_{SAT})_{\substack{MIN \\ SAT}} = 296°F$$

The modified version of this model can be derived by multiplying the minimum heat flux by 5.5 resulting in:

$$\dot{q}_{\substack{MIN \\ MOD}} = 33{,}000 \ \frac{Btu.}{ft.^2\text{-}hr.}$$

Substituting this into the film boiling heat flux equation yields the modified temperature at minimum heat flux:

$$(T-T_{SAT})_{\substack{MIN \\ MOD}} = 2877°F$$

This value indicates that film boiling will not occur within the range of the welding model. This leaves only nucleate boiling and transition boiling to consider.

The final sub-cooled or transient conduction model is derived in Appendix D. The results of this derivation state that

$$\dot{q}_{\substack{MIN \\ SUB}} = 5980 + 692.6\,(T_{SAT} - T_\infty)\ \frac{Btu}{ft^2\text{-}hr.}$$

and

$$(T-T_{SAT})_{\substack{MIN \\ SUB}} = .0494\ \dot{q}_{\substack{MIN \\ SUB}}$$

For normal ranges of sub-cooling this welding model will not reach film boiling.

3.24 Transition Boiling

Lying between peak and minimum heat flux is a regime of boiling which no one knows very much about. It is the regime in which the smooth bubble flow at peak heat flux jams up, transforming eventually into a continuous vapor film at minimum heat flux. Characteristic of all other regimes has been the form of their heat flux equations:

$$\dot{q} = M (T - T_{SAT})^{b}$$

Assuming this to hold for the transition regime and noting the conditions at its end points, the characteristic equation can be determined for each model:

Saturation:
1. $\Delta T = 66^{\circ}$, $\dot{q} = 479{,}500$ Btu./ft.^{2}-hr.
2. $\Delta T = 296^{\circ}$, $\dot{q} = 5{,}980$

Modified:
1. $\Delta T = 116^{\circ}$, $\dot{q} = 2{,}640{,}000$ Btu./ft.^{2}-hr.
2. $\Delta T = 2877^{\circ}$, $\dot{q} = 33{,}000$

Subcooled:
1. $\Delta T = 116^{\circ}$, $\dot{q} = 2{,}640{,}000$ Btu./ft.^{2}hr.
2. $\Delta T = .0494\dot{q}$, $\dot{q} = 5980 + 692.6\Delta T_{sub}$

Solving for M and b using the two equations generated at the end points yields:

$$\left(\dot{q}_{TRANS}\right)_{SAT} = 1.029 \times 10^{11} \left(T - T_{SAT}\right)^{2.93}$$

$$\left(\dot{q}_{TRANS}\right)_{MOD} = 1.76 \times 10^{9} \left(T - T_{SAT}\right)^{1.367}$$

$$\left(\dot{q}_{TRANS}\right)_{SUB} = M \left(T - T_{SAT}\right)^{b}$$

where M and b in the sub-cooled case are functions of the degree of sub-cooling.

This concludes the boiling portion of the heat transfer model. It applies to the top surface of a horizontal flat plate. It can be assumed that boiling heat flux from the bottom side of the plate will be negligible as a completely stable vapor film will be formed there.

3.25 Radiation

The radiation model is quite a bit more straight forward than the boiling model. The plate (emissivity = .8) radiates into the surrounding water (e_w = .95) whose

temperature is approximately at saturation. Saturature temperature is chosen as most radiation is into the vapor film or bubble. The electrical analogy for this process is shown in figure 3-5. The mathematical solution for this circuit is simply:

$$\dot{q}_{RAD} = \frac{\sigma (T^4 - T_{SAT}^4)}{1/e_p + 1/e_w - 1} \quad \frac{Btu}{ft.^2\text{-}hr.}$$

Nondimensionalized this yields:

$$\dot{q}_{RAD} = 1.317 \times 10^{-9} \left\{ \left[T^* (T_M - T_\infty) + T_\infty \right]^4 - T_{SAT}^4 \right\}$$

The total heat transfer for each of the three models discussed is shown in figure 3-2.

3.26 Spread Heat

Using the molten pool as the inner boundary to plate conduction makes it possible to overlook the very complicated process involved in energy transfer from the arc to the molten pool.

Staub's work was based on the conclusion that the surrounding water would prevent any direct energy

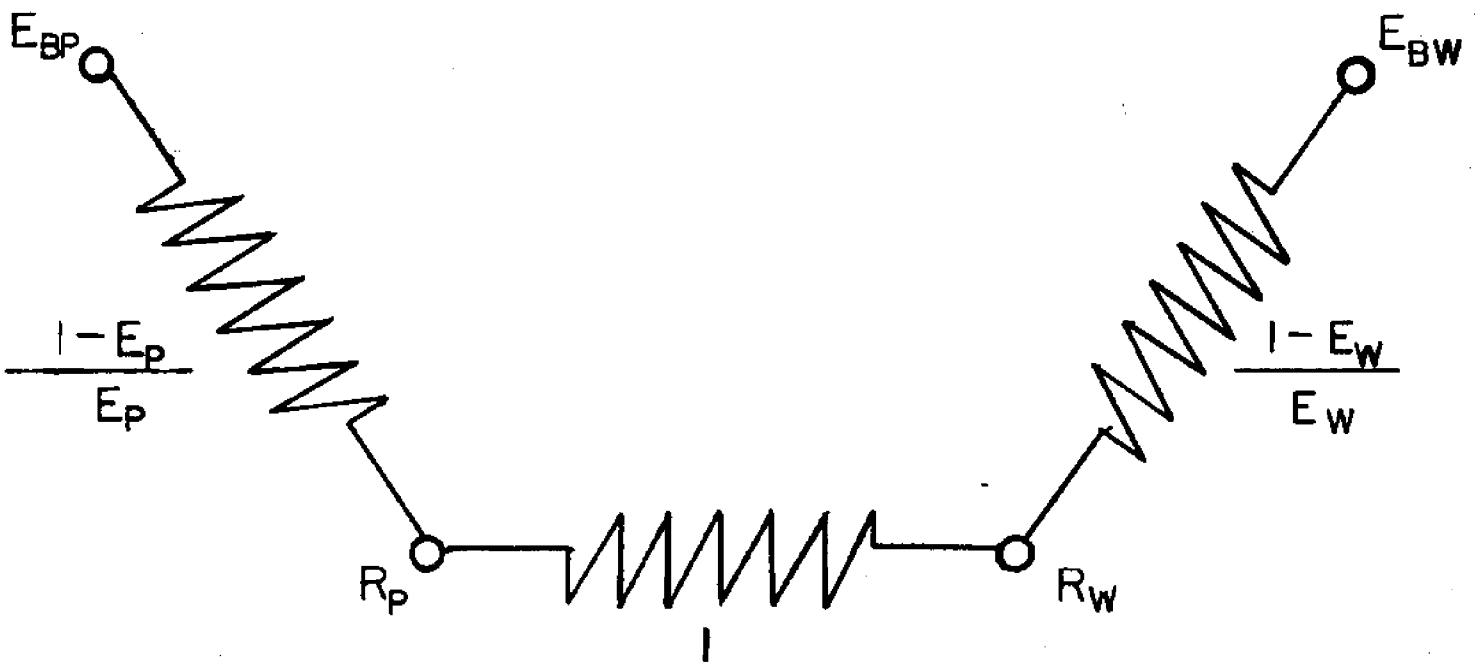

RADATION CIRCUIT ANALOGY

FIGURE 3-5

exchange between the arc and the solid portion of the plate. Predicting the pool shape and thus establishing the inner boundary on plate conduction accounted for the only energy input to his model. Although this is a valid argument when considering a submerged arc process, Staub's over-rapid cooling predictions coupled with the observation of a gaseous void around the tip of the welding electrode indicate that this arc to plate energy exchange may be significant and must be accounted for.

This energy addition is called spread heat. It will be computed in terms of a distribution extending from the tip of the electrode and diminishing out to infinity. When actually added as an energy input to the model, however, two things must be recognized:

1. By establishing the shape of the molten pool, spread heat within this region has already been accounted for.
2. The effect of the spread heat must terminate at the edge of the void surrounding the arc.

Therefore, spread heat is added only between these bounds.

Pavelec (ref. 14) and Nestor (ref. 24) state that experimental data indicates that the spread heat distribution appears as a normal distribution function somewhat steeper than Gaussian. They experimented with various decaying exponentials, and Pavelec eventually sided with

Rykalin (ref. 25) and settled on the following distribution which will also be used here: (see fig. 3-6)

$$\dot{q}_D(r) = q(0)\, e^{-Cr^2}$$

Integrating this from the arc out to infinity yields

$$q_{TOT} = \int_0^\infty q(r)\, 2\pi r\, dr = \int_0^\infty q(0) e^{-Cr^2} 2\pi r\, dr = \frac{q(0)\pi}{C}$$

or

$$q(0) = \frac{C\, q_{TOT}}{\pi}$$

There is generally a region immediately under the arc where a large portion of the arc heat is concentrated. This is called the hot spot and has a radius r_h. If r_h is defined as that radius where $\dot{q}_D(r)$ drops to $.05\dot{q}(0)$ we find the following

$$q(r_H) = q(0)\, e^{-Cr_H^2} = .05\, q(0)$$

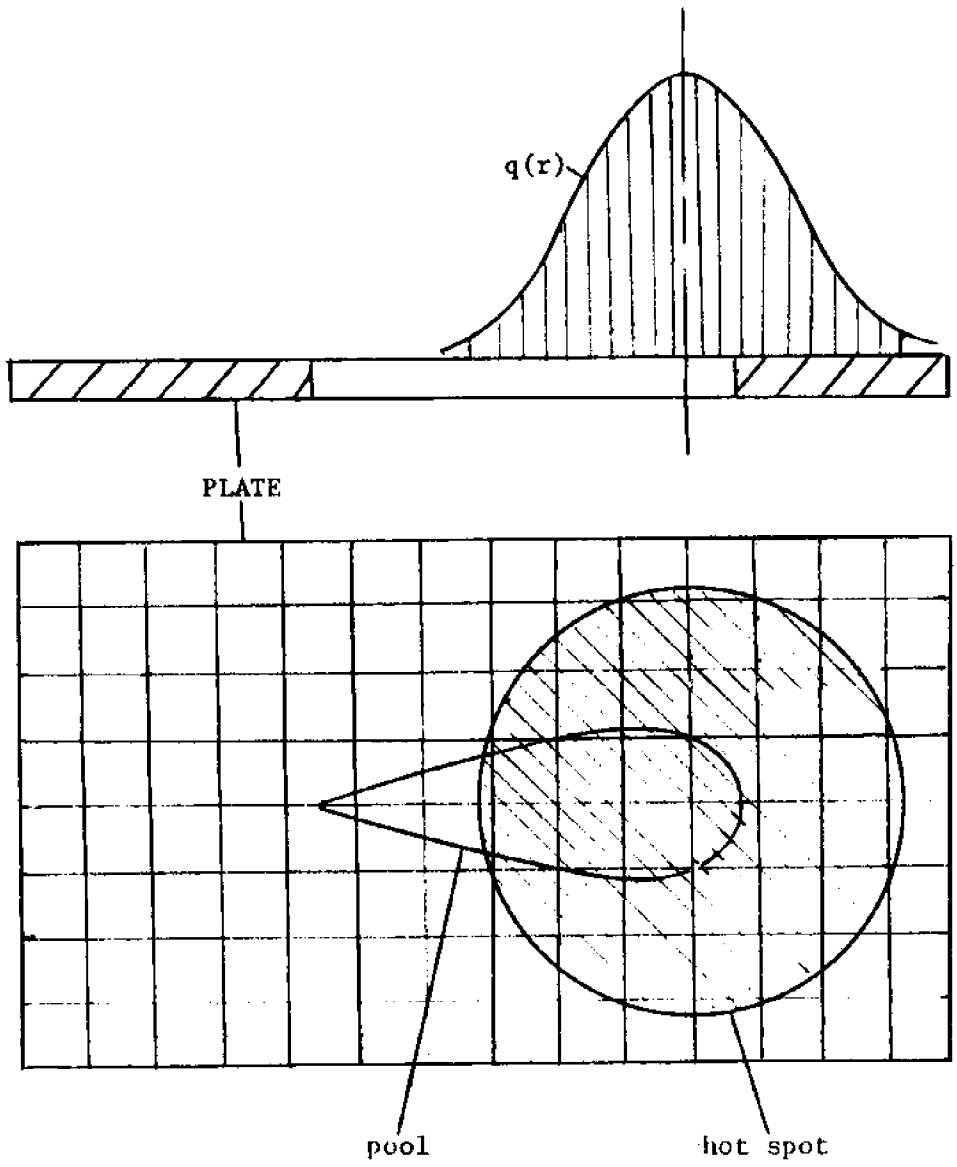

SPREAD HEAT DISTRIBUTION

FIGURE 3-6

or

$$C r_H^2 = \ln 20 = 3.0$$

which yields:

$$C = \frac{3.0}{r_H^2}$$

and

$$q(0) = \frac{3.0\, q_{TOT}}{\pi r_H^2}$$

It now remains only to measure the hot spot for a particular process and to determine the efficiency of the process since:

$$q_{TOT} = 3.415\, \eta EI$$

or

$$q_D(r) = \frac{10.245\, \eta EI}{\pi r_H^2}\, e^{-\frac{3r^2}{r_H^2}}$$

3.3 Boundary Conditions

Conduction taking place in the plane of the plate is bounded on two sides. The outer boundary represents conditions far from the pool origin. This boundary can be assumed to be at ambient temperature and may be represented by:

$$T^*(\pm\infty, y^*) = \frac{T_\infty - T_\infty}{T_M - T_\infty} = 0$$

$$T^*(w^*, \pm\infty) = \frac{T_\infty - T_\infty}{T_M - T_\infty} = 0$$

The inner boundary is the melting isotherm which separates the molten pool from the solid portion of the plate. It can be assumed to be at the metal's melting temperature and may be represented by:

$$T^*\left[f(w^*, y^*)\right] = \frac{T_M - T_\infty}{T_M - T_\infty} = 1$$

To completely define these it remains only to define the shape of the molten pool, f(w*, y*).

Predicting the location of the pool contour analytically requires the use of a temperature model, but such a model is precisely what we do not have. Point source theory predicts egg-shaped contours, quite unlike the observed tear-drop shape. For these reasons reliance on entirely analytical methods is ruled out. Second best to an entirely analytical approach is analytical correlation of empirical data. This was done using Rosenthal's point source temperature equation:

$$T - T_o = \frac{\dot{Q}}{L} \frac{1}{2\pi\bar{K}} e^{-\bar{\lambda} V w} K_o(\bar{\lambda} V r)$$

By employing this equation along with certain geometric aspects of the weld pool a lumped welding parameter was derived:

$$N^* = \frac{3.415\ EI}{2\pi\bar{\alpha} L H_m}$$

It is shown in Appendix B that this welding parameter may be used to correlate values for maximum pool length and width. (see figure 3-7) The correlation results in expressions of the form:

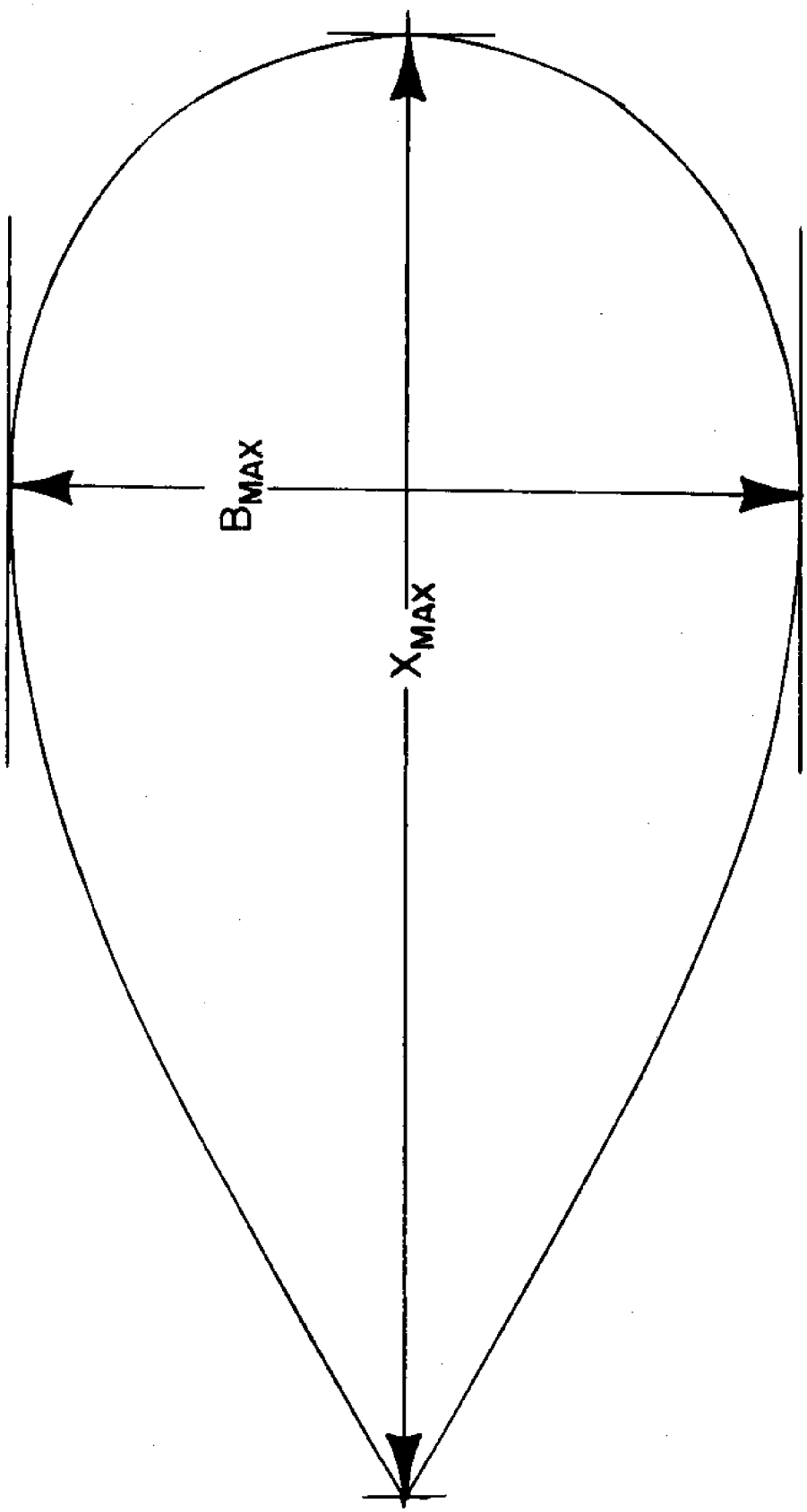

FIGURE 3-7

$$X_{max} = A N^{*B}$$

$$B_{max} = C N^{*D}$$

The constants A, B, C, D depend on the particular process used.

The two dimensions for maximum width and length establish three points on the weld contour. From these it is necessary to determine a shape function which describes the entire contour. A curve was fit by Pavelec based on the following boundary conditions.

1. $y=0;\ x=0$
2. $y=0;\ x=-X_m$
3. $y'=0;\ y=B_{max}/2$
4. $y'=\infty;\ y=0;\ x=0$

Given the shape of the weld pool and all source and loss terms the quasi-static equation for heat conduction is ready to be solved. (see figures 3-8 thru 3-17)

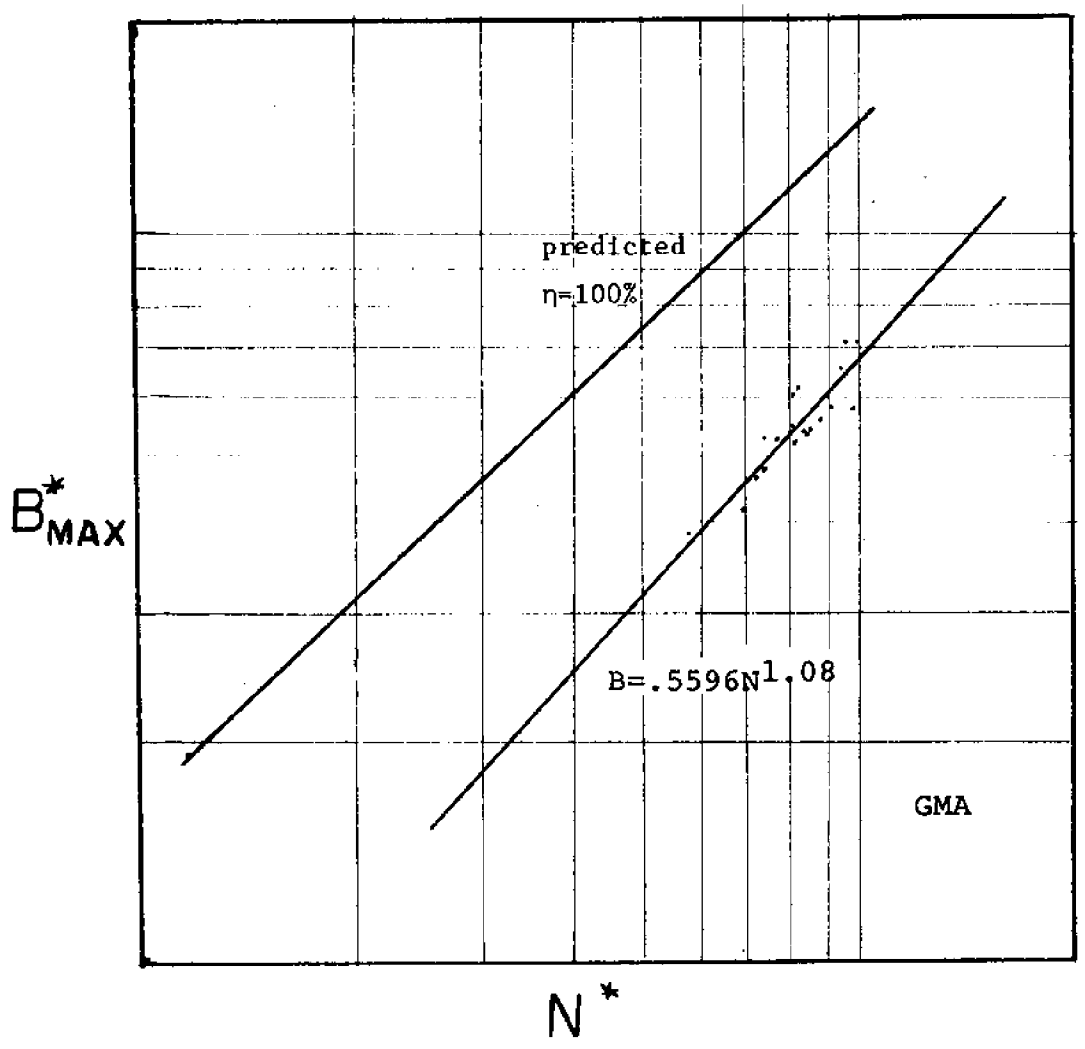

FIGURE 3-8
POOL CORRELATION

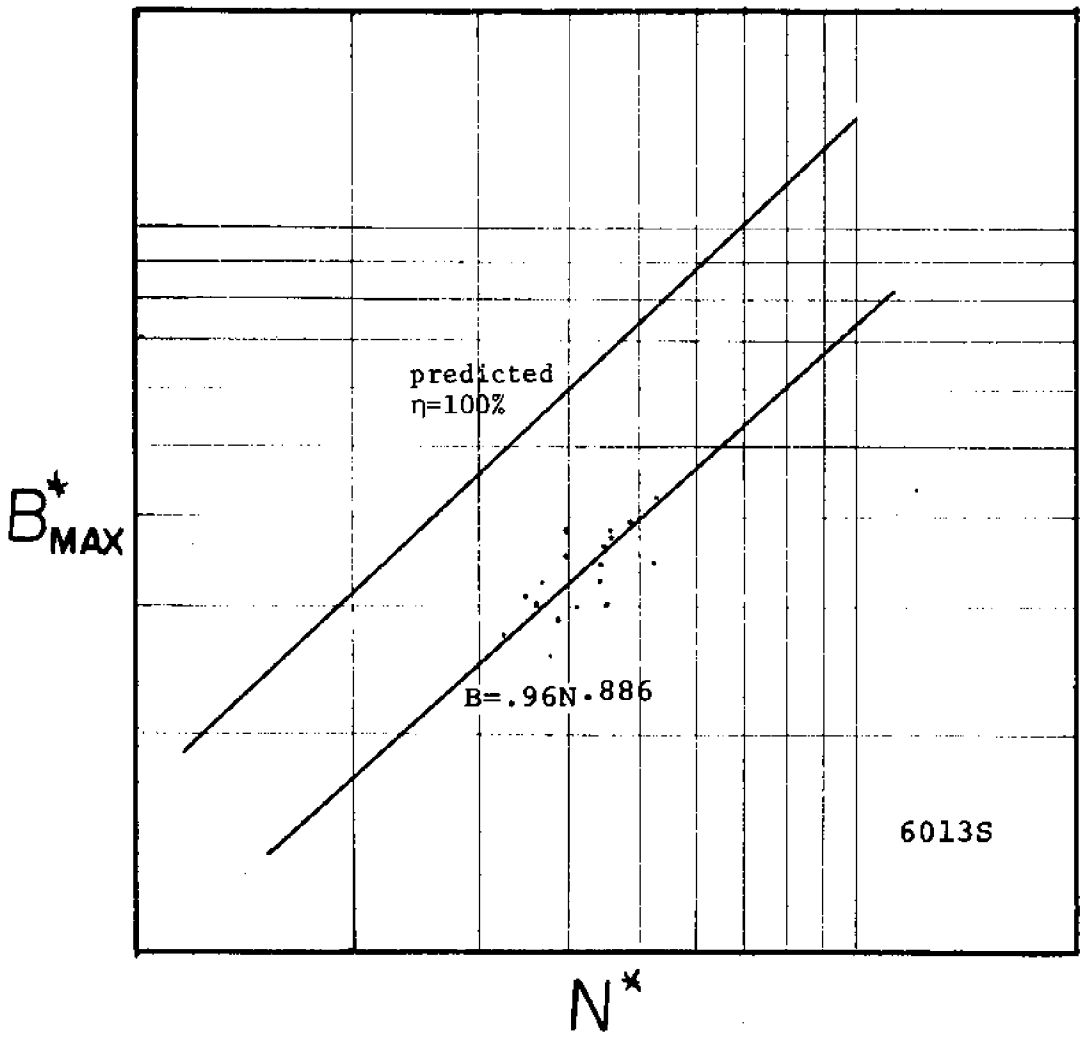

FIGURE 3-9

POOL CORRELATION

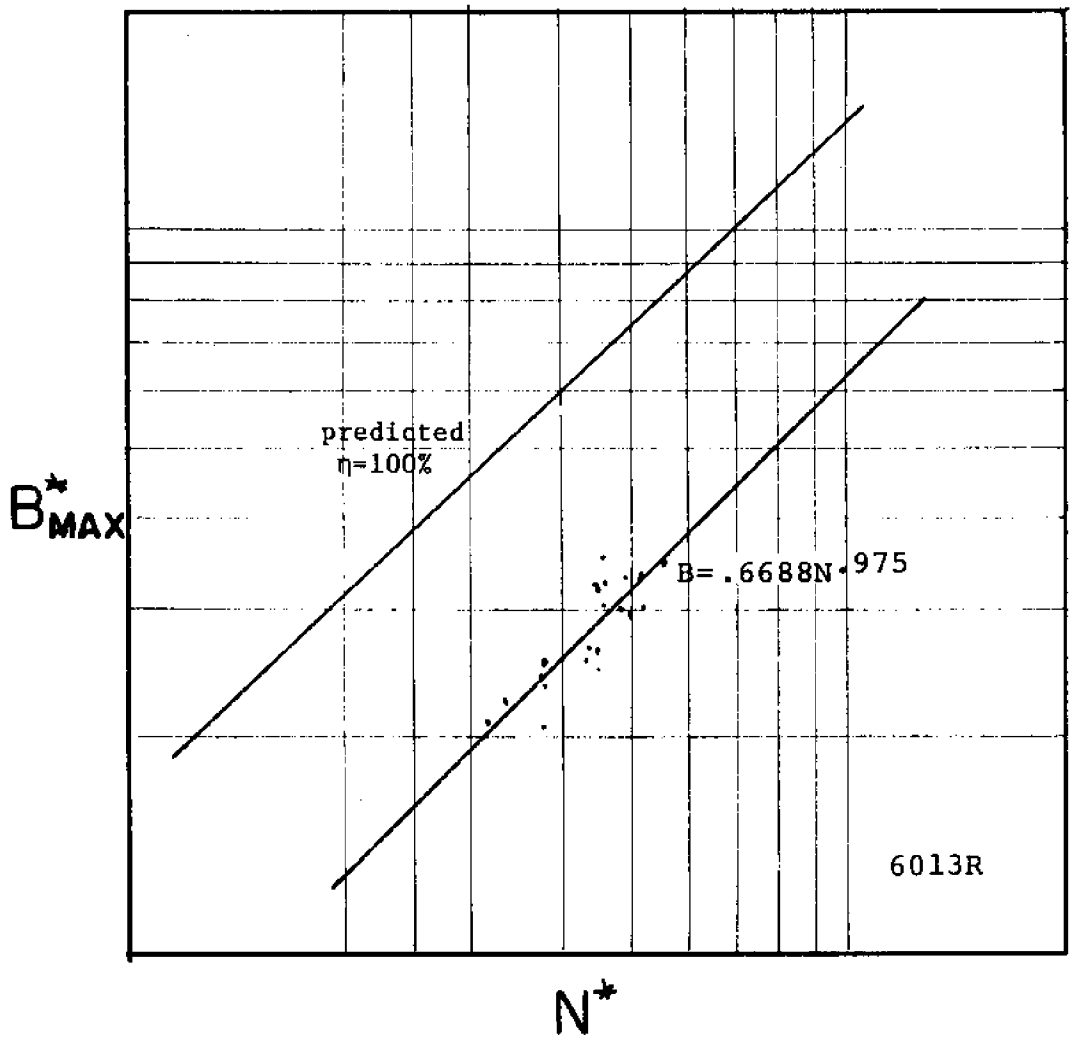

FIGURE 3-10
POOL CORRELATION

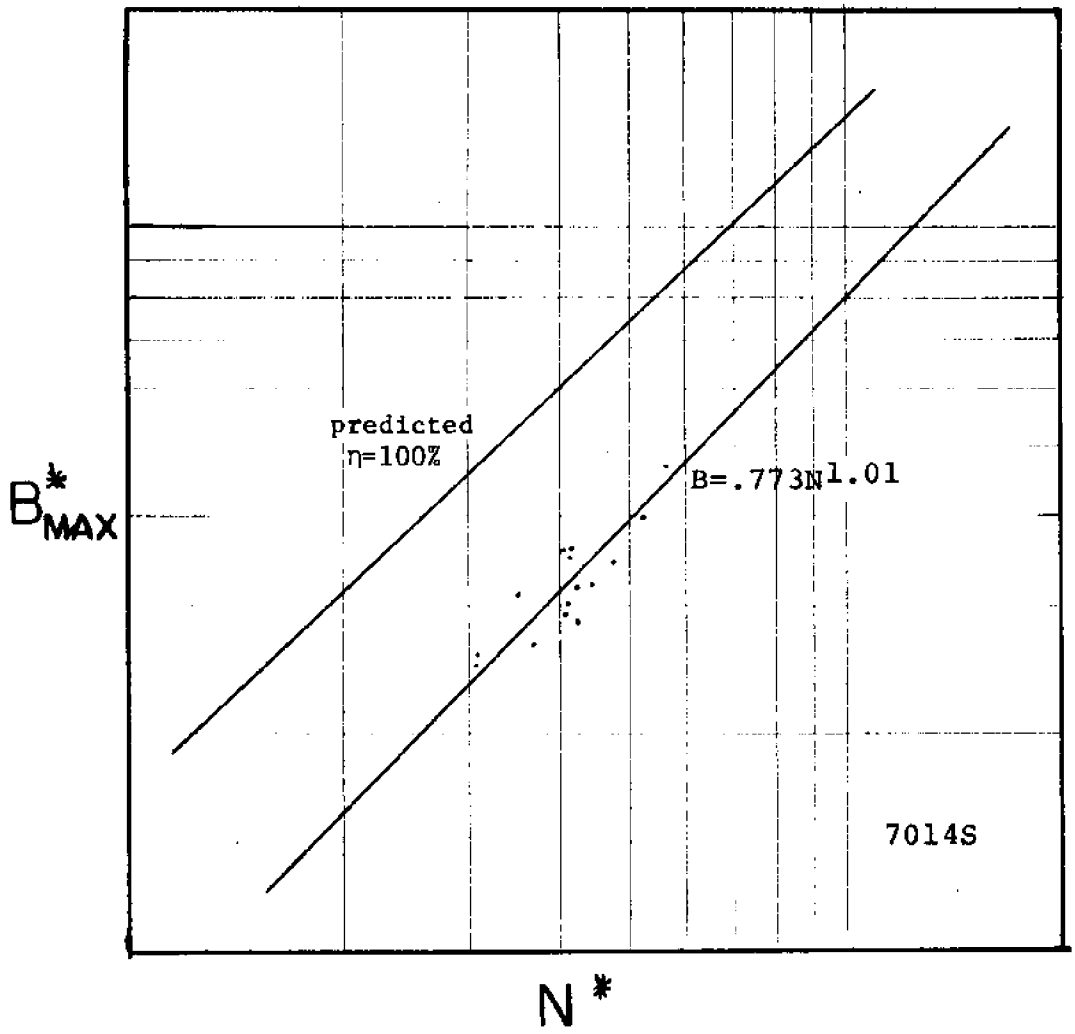

FIGURE 3-11
POOL CORRELATION

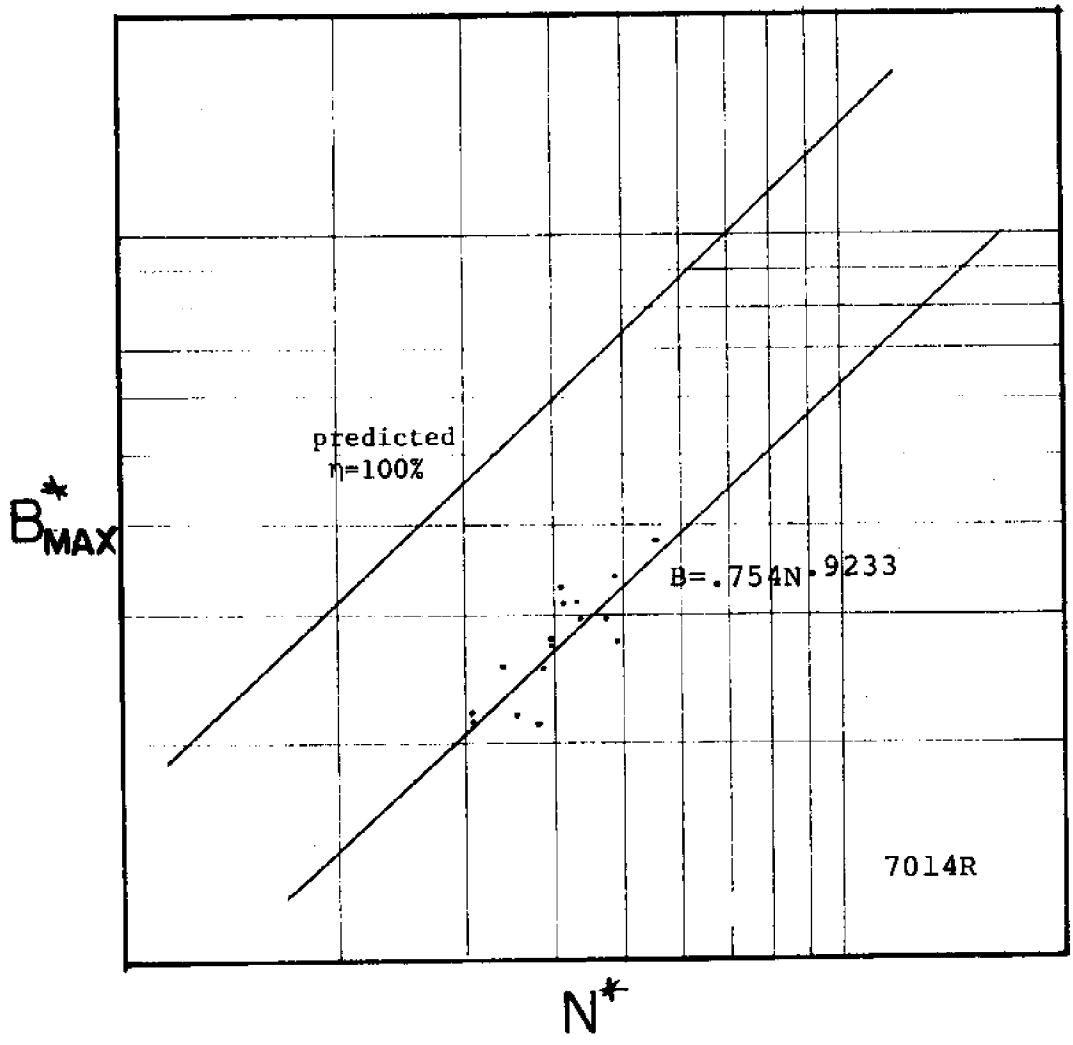

FIGURE 3-12

POOL CORRELATION

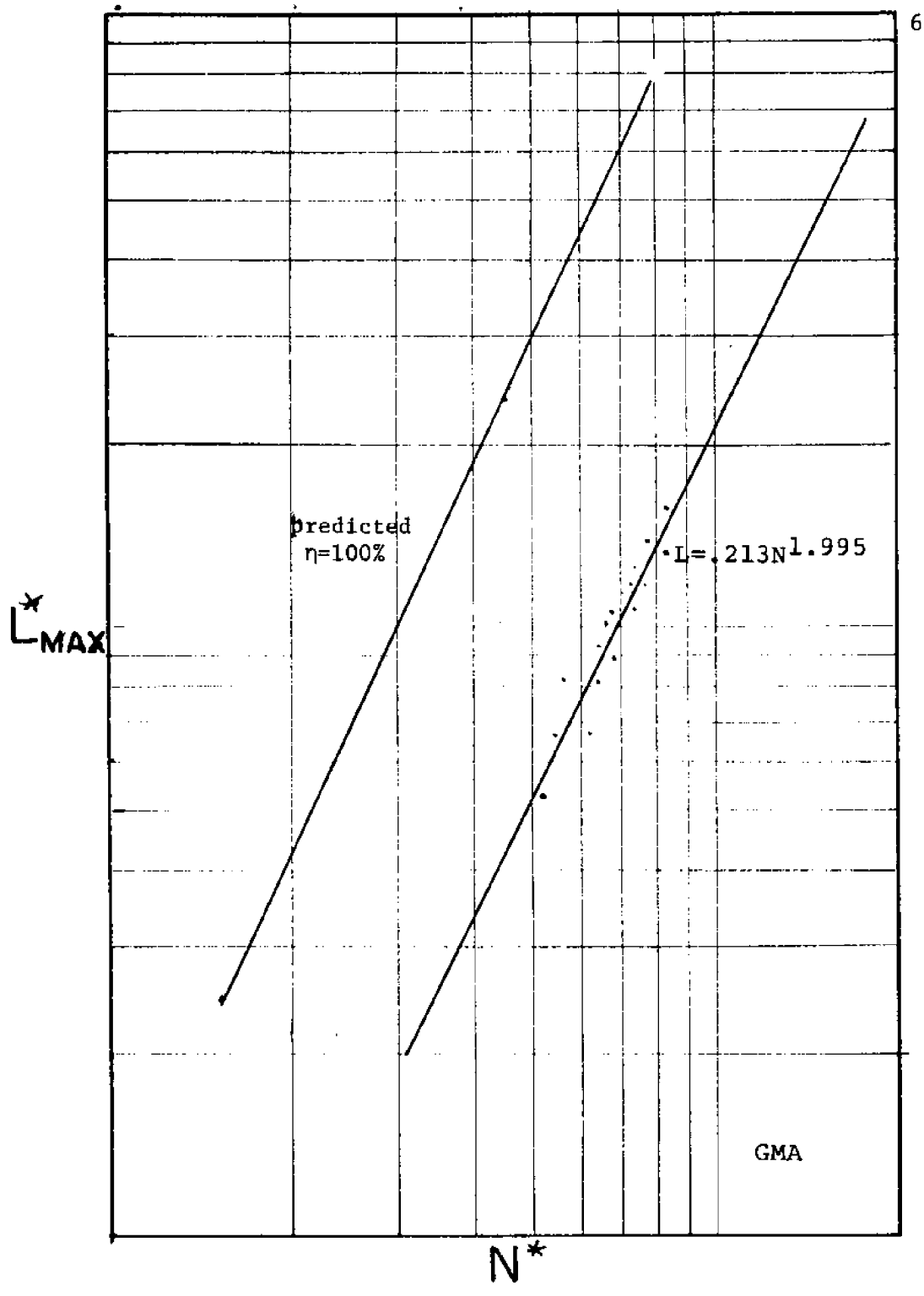

FIGURE 3-13
POOL CORRELATION

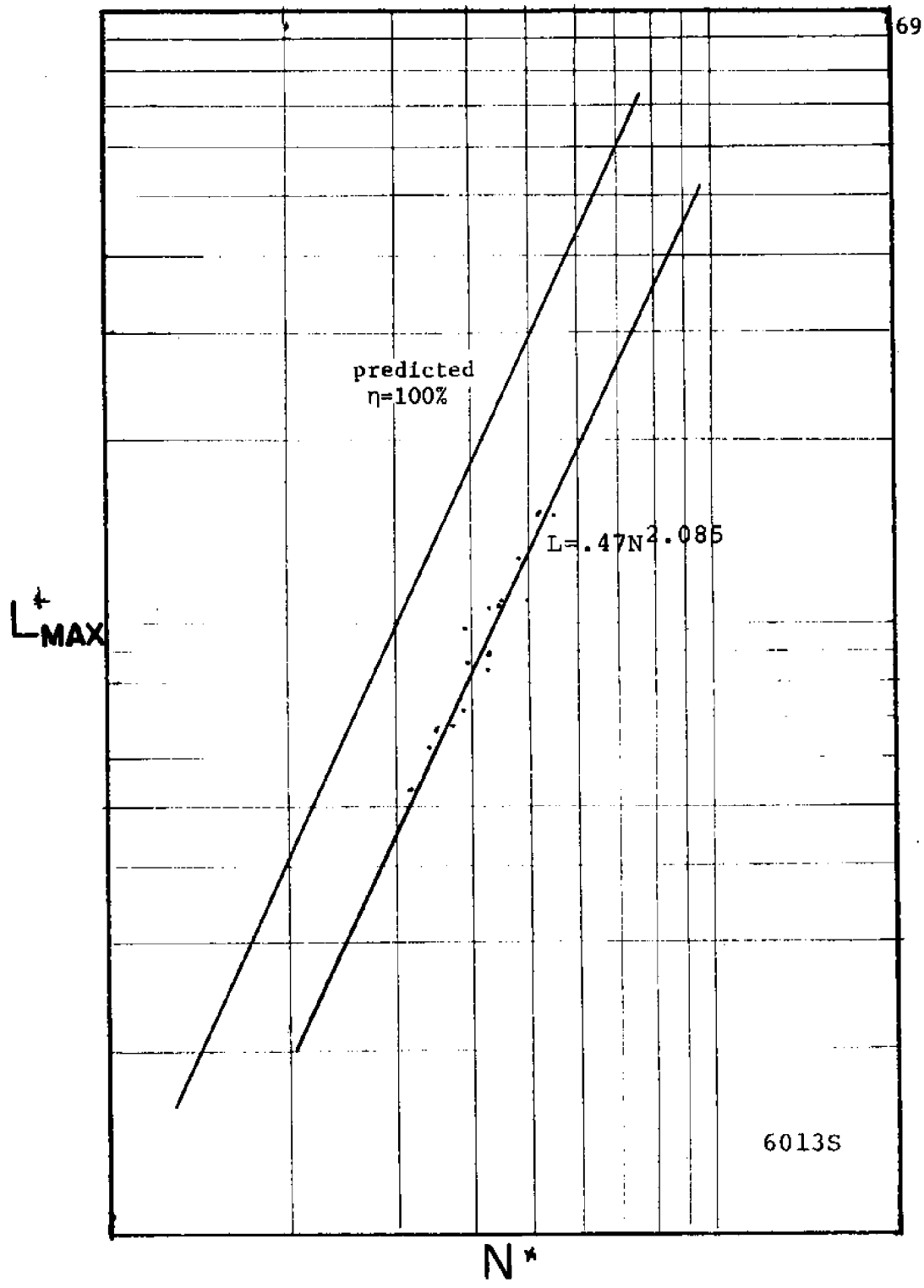

FIGURE 3-14
POOL CORRELATION

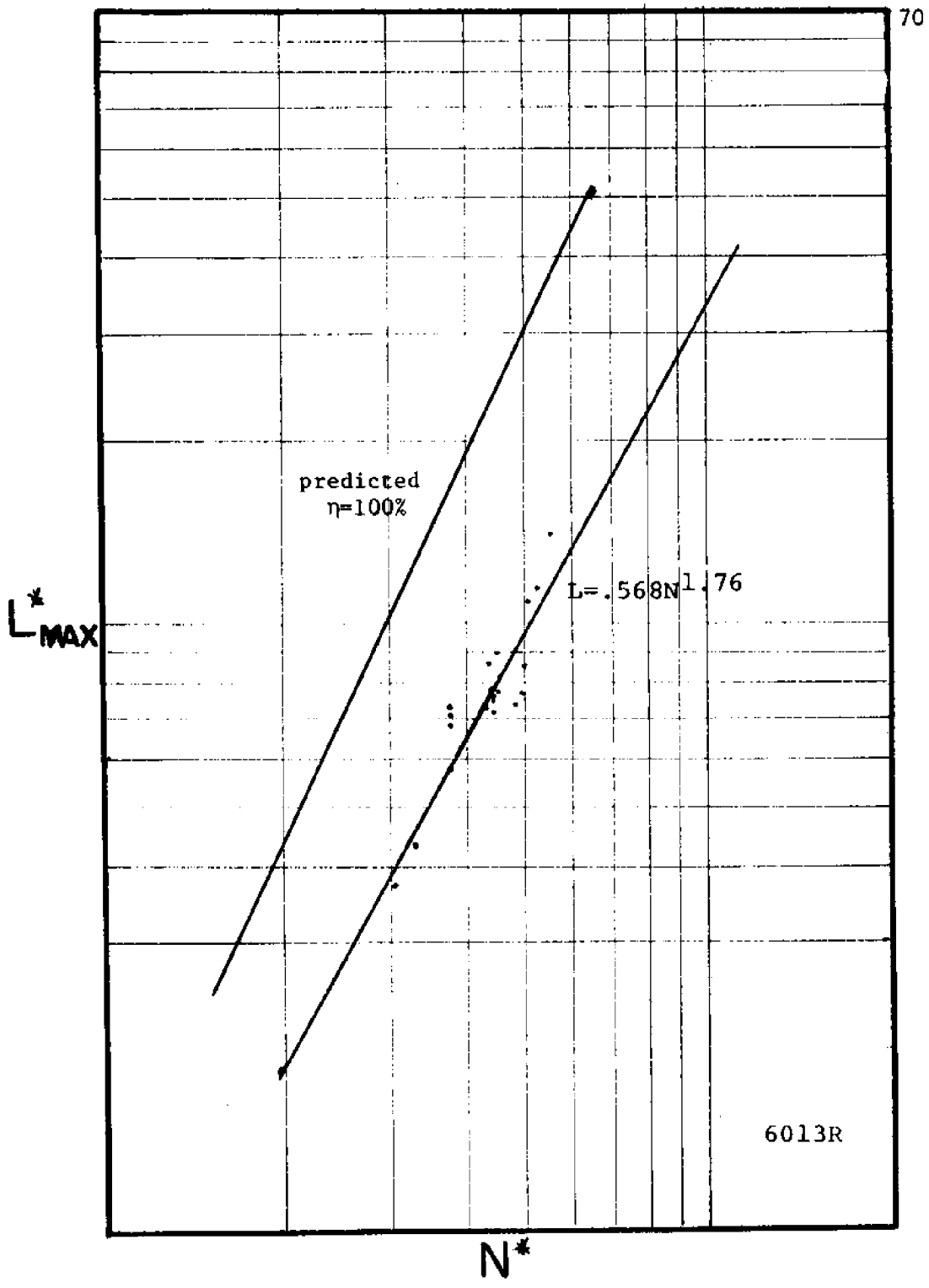

FIGURE 3—15
POOL CORRELATION

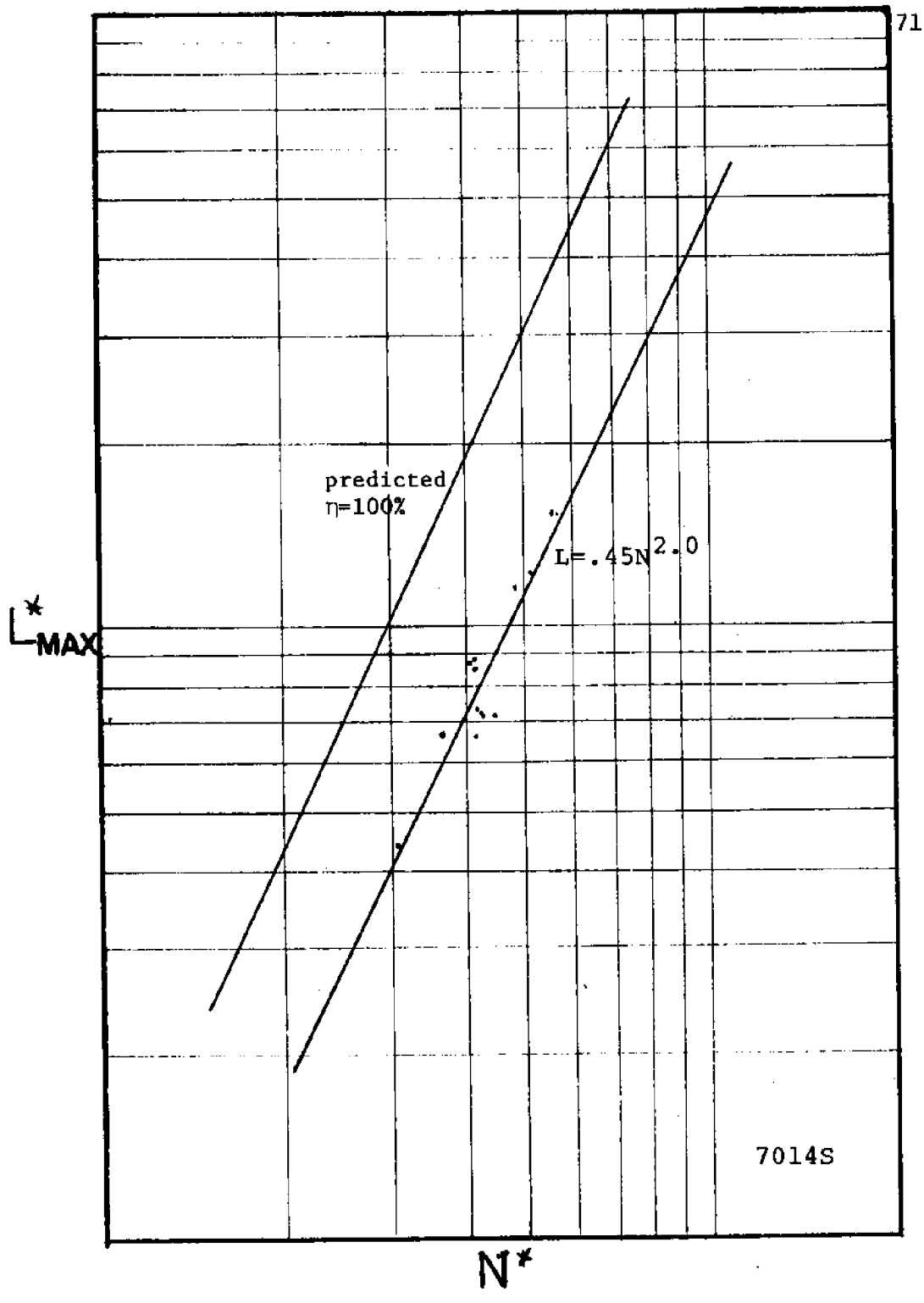

FIGURE 3-16
POOL CORRELATION

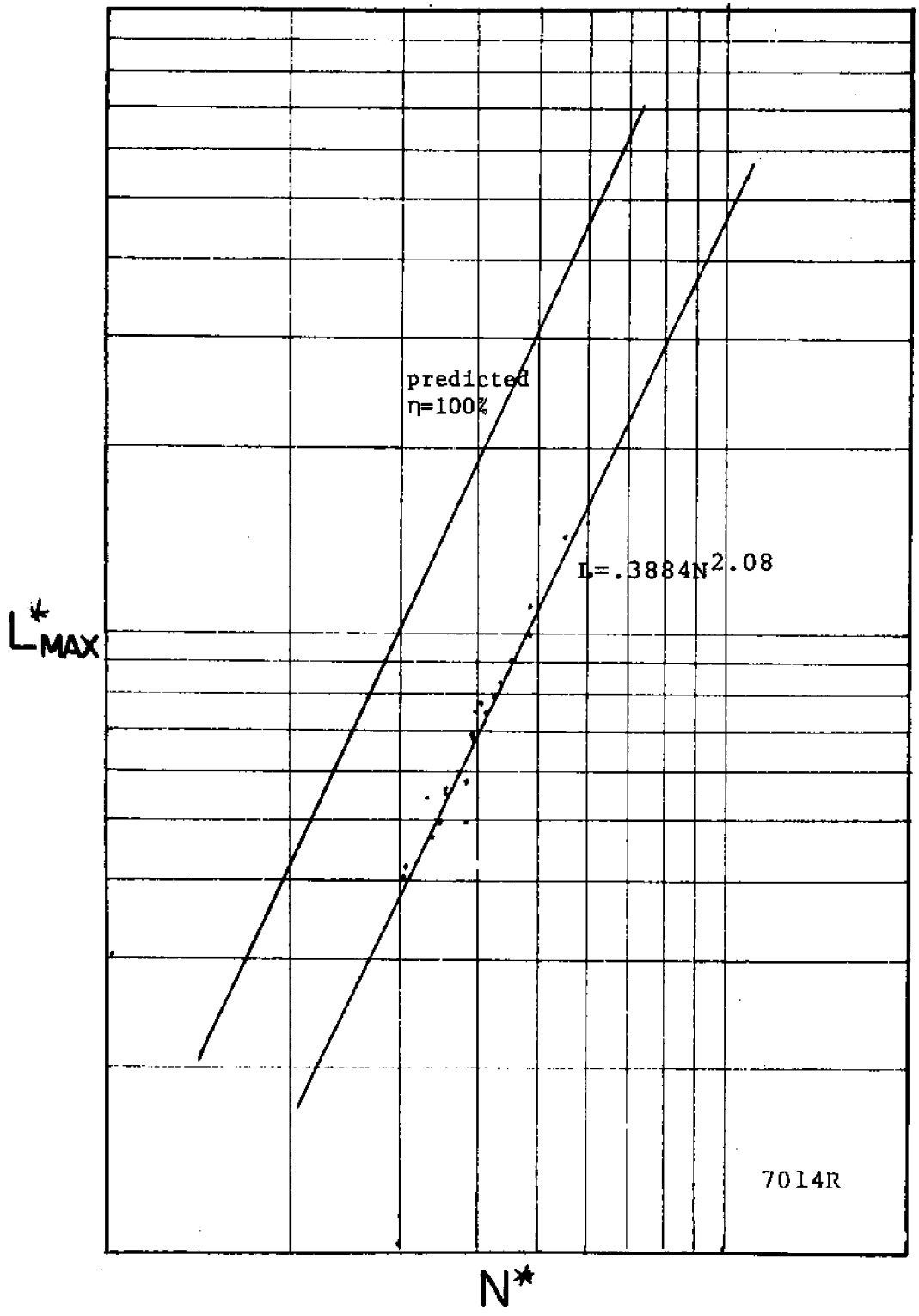

FIGURE 3-17
POOL CORRELATION

CHAPTER IV

EXPERIMENTAL PROCEDURE

Three basic types of experiments were conducted:

1. Temperature measurements
2. Molten Pool blow-outs
3. High speed cinematography

Each of these experiments were conducted for each of the three basic processes; but before anything could be done, welding techniques and procedures had to be mastered (for each process). This in itself required a great deal of time and effort. Once good welds could be made consistently with each of the processes experimentation could begin. The methods used for temperature measurement and blow-out again follow along the lines of Staub and Pavelec. Precise descriptions of all materials and equipment used can be found in Appendix C.

4.1 Welding Underwater

Underwater welding is usually performed by a hard-hat diver with an experienced surface crew and some elaborate equipment. Such an arrangement was impractical for the laboratory, so an indoor tank and machine was

used. (figure 4-1) Using this method it was possible to keep the electrode holder (or GMA gun) above the free surface of the tank with the electrode (or extension tube) penetrating the surface to the plate. Placing the plate about eight inches below the free surface allowed underwater conditions to be simulated.

Optical experiments were conducted in a 2 Ft. x 2 Ft. x 4 Ft. plexiglass tank. (ref. 26 and figure 4-1). All other experiments were conducted in a similar steel tank. Problems encountered in the actual welding can be summarized as follows:

1. Equipment setup, insulation, grounding
2. Visibility and electrode manipulation
3. Establishing feasible ranges for welding conditions

Each of these will be considered in detail.

4.11 Welding Equipment

Common to each process is the problem of proper grounding and insulation. A direct insulated ground was connected from the welding machine to the workpiece. The workpiece was in turn insulated from the tank by setting it up on oven bricks. Welding gloves were worn and rubber mats provided to stand on.

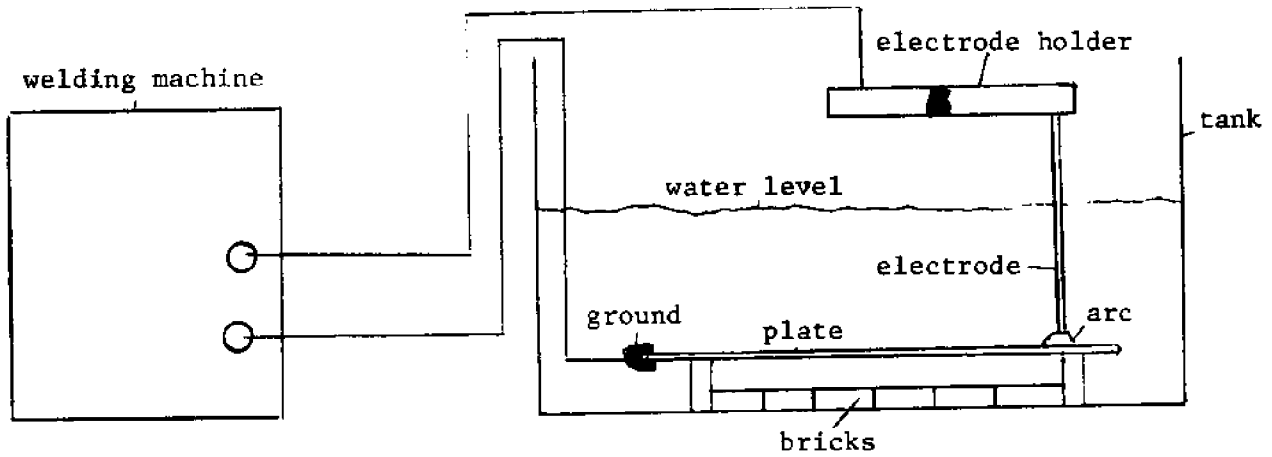

WELDING ARRANGMENT

FIGURE 4-1

The length of the welding electrode in SMA was quite adequate for reaching through the free surface to the plate. During use the electrode was replaced when the holder approached the free surface. This allowed a normal surface holder and rig to be used.

The shrouded process was set up in the same manner as SMA. In order to photograph the dynamics of this process a clear plastic shroud was used. This shroud was fashioned from a plastic dome-like cover of an old-fashioned clock. (see figure 4-2) This worked very well except that the shroud's buoyancy had to be compensated for by adding additional weight. This was done by balancing a nut and bolt between the ports.

The final process, GMA, was a bit more difficult to set up. It was necessary to modify the nozzle of the semi-automatic gun so that it would extend through the free surface to the plate without having to submerge the gun. Figure 4-3 shows the nozzle before and after changes were made. The inner contact tube was replaced with a 10 inch one machined from copper tubing. An eight inch extension was brazed onto the outer barrel. This provided more than enough length to reach the plate.

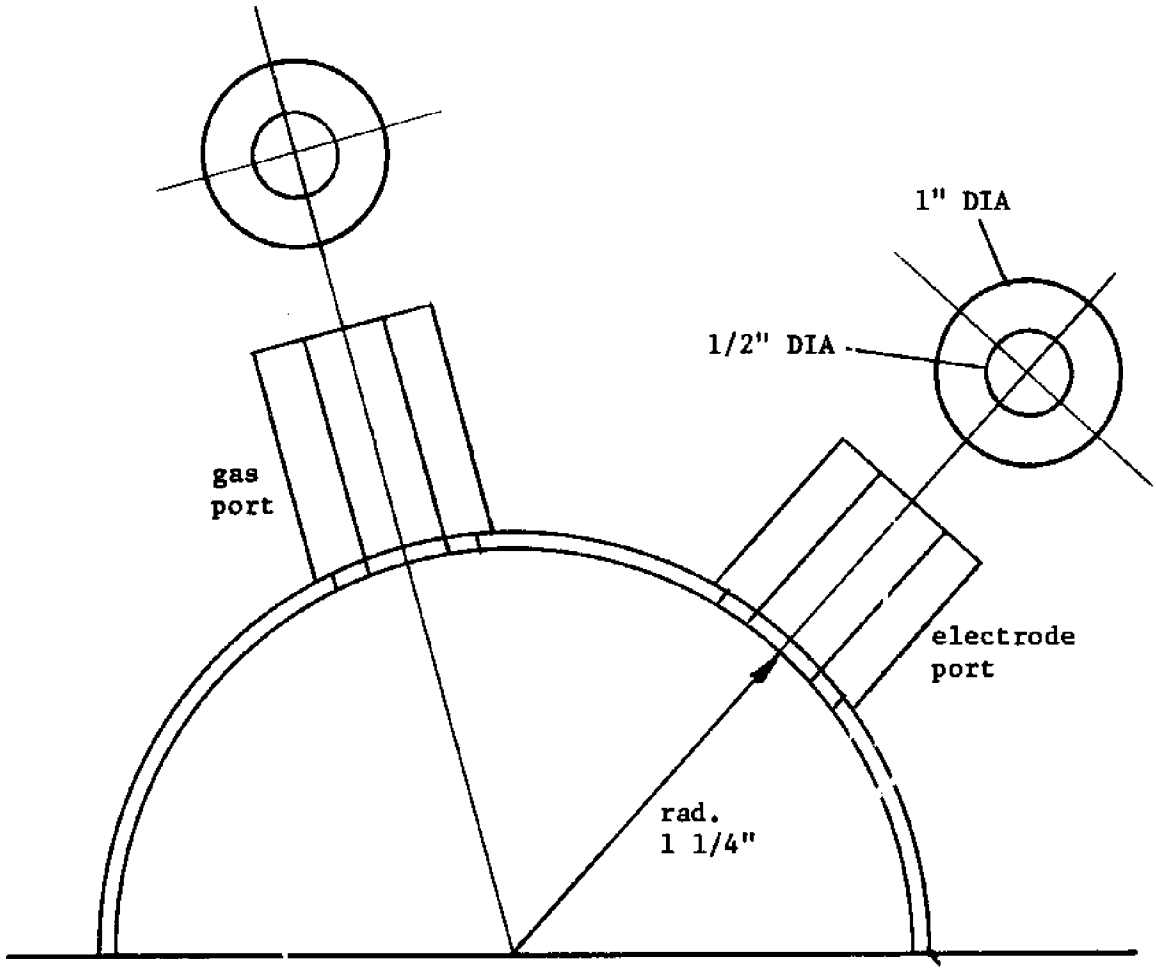

PLASTIC SHROUD

FIGURE 4-2

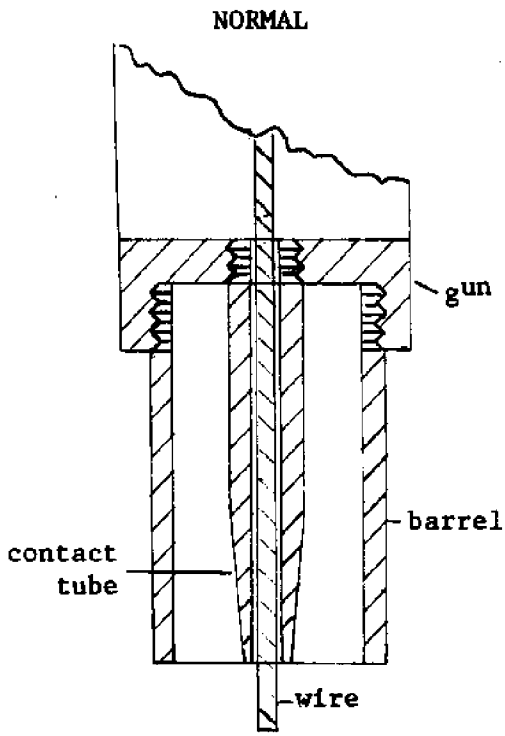

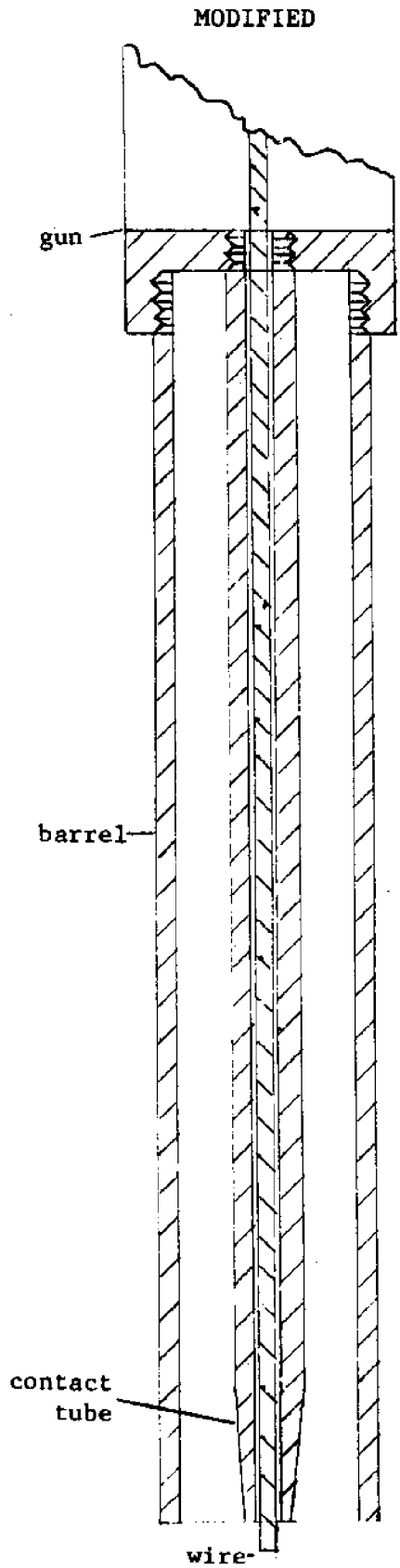

GMA

HARDWARE

FIGURE 4-3

4.12 Electrode Manipulation

The very first thing one discovers when trying to weld through a free surface is that visibility is non-existent. Fortunately, the "drag manipulation" nature of shielded electrodes eliminates difficulties with maintaining the arc. The non-consuming nature of GMA also serves to do this. The major problem then is maintaining a straight line motion and continuous speed.

Attempts were made to use a gravity feed welder to solve this problem, but weld quality was poor. Finally a manual straight-edge method was used. (see figure 4-4) A wooden straight edge was extended out over the workpiece in a direction parallel to the desired motion. The electrode or gun barrel could then be drawn along this straight edge. The edge was measured off and marked so that a metronome could be used to synchronize the welding speed with the passing of marks. This allowed a consistent and relatively prescribed speed to be kept. After many trials it was found that if a steady touch was kept, the angle between the electrode and horizontal (lead angle) would set and keep a consistent weld speed.

Starting the electrodes was often a problem because they would stick. Once started, however, they could be restarted without difficulty. This was due to

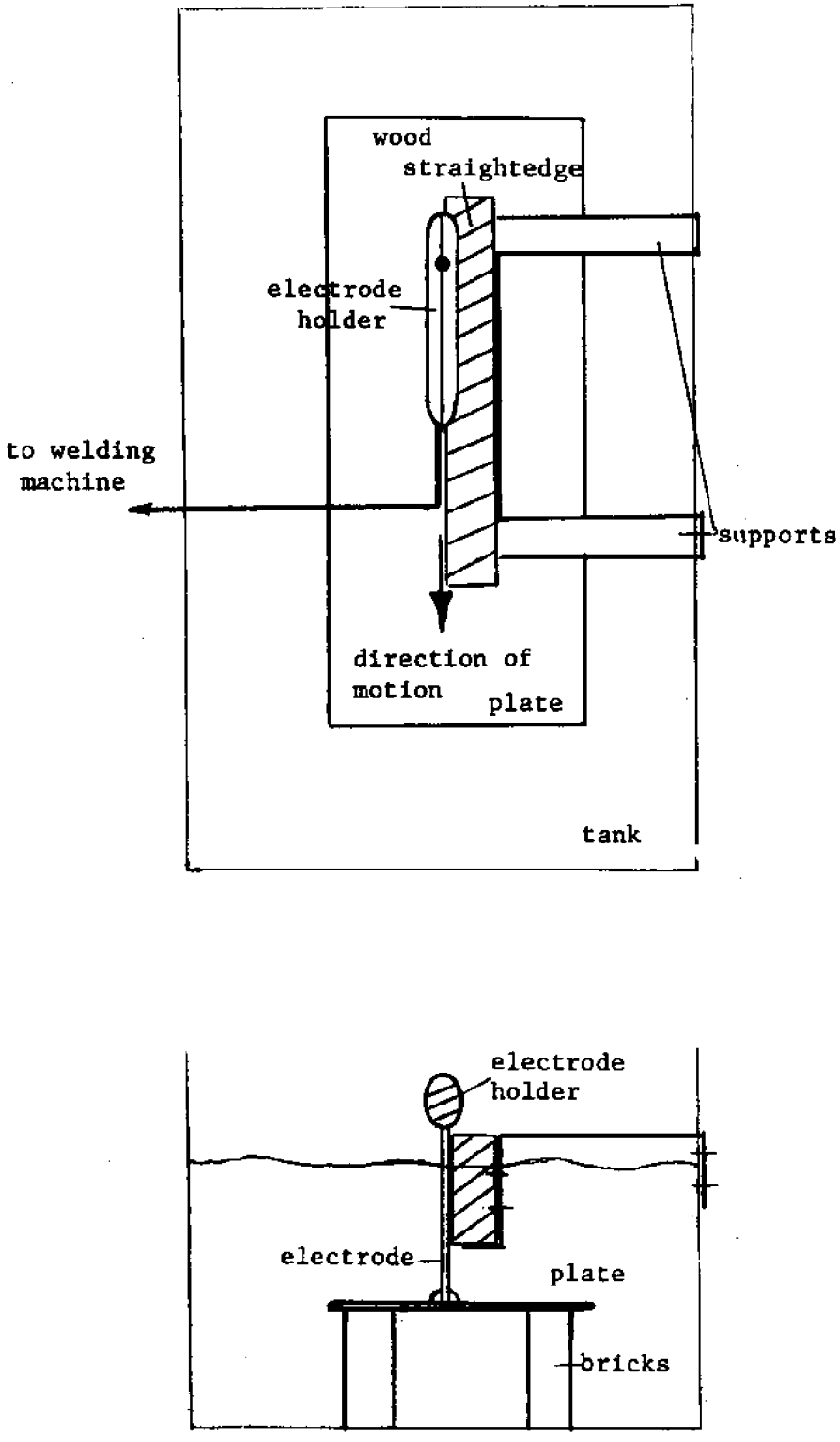

STRAIGHT EDGE TECHNIQUE

FIGURE 4-4

the flux barrel formed around the tip which maintained a proper arc length. Care should be tken when starting the electrode to insure that the flux is at least even with the end of the metal.

The steps for successful operation of the GMA process are:

1. Start with about 1/2 inch of wire extending
2. Put the wire against the plate with the barrel vertical
3. Press the button
4. Maintain a constant waterline on the barrel

If the machine and feed are set properly, this should work the first time.

4.13 Welding Conditions

It was next necessary to establish a set of welding conditions which were consistent with the desired experiments. This meant determining plate thickness, machine settings, wire feed, welding speed, etc.

Most important in these calculations was the requirement for two-dimensionality. From the heat transfer standpoint this required as thin a plate as possible. (maximum of 1/4 inch) In order to maintain a two-dimensional weld pool (figure 4-5) combinations of welding speed and current were also limited. When the

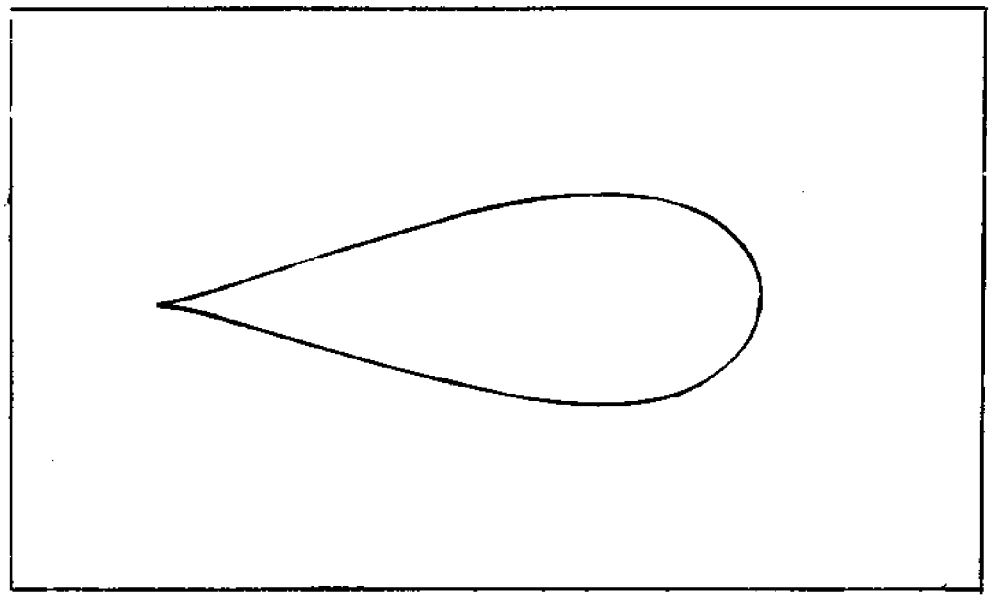

TWO-DIMENSIONAL
WELD POOL

FIGURE 4-5

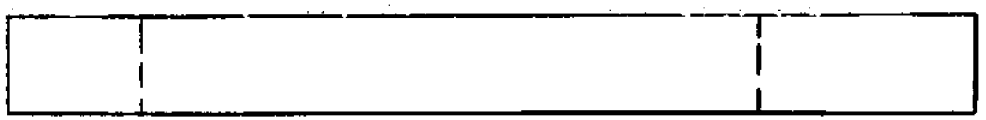

plate got too thin, burnthrough was very excessive. Considering the above 1/8 inch mild steelplate was chosen for the experiments. Welding speeds and currents were then determined by trial and error. Results for these are tabulated in tables 4-1 and 4-2. Approximate welding speeds for various currents are shown in figures 4-6 and 4-7. The two electrodes (E6013 and E7014) behaved very similarly in terms of required welding speed. Straight polarity required a slightly faster speed than reverse for both electrodes. During the blow-out experiments the 1/8 inch stock obtained ran slightly thick (.130 inch). The required welding speed was extremely sensitive to this change and had to be reduced. So it should be noted that figure 4-6 and 4-7 apply only for .125 inch stock on a specific machine.

Table 4-1

Current Characteristics for Underwater SMA Welding

(E6013 and E7014 electrodes)

I (amperes)	Description
150 amps	The bead was eratic and the arc was very difficult to start
180 amps	Although starting was still difficult, the bead was smooth and the penetration sufficient. Minimum current in experimental range.
220 amps	Starting was easier and the weld bead smooth. Probably the optimum current found.
250 amps	Burnthrough became a problem and welding speed was very fast. Maximum current in experimental range.

Table 4-2

Current and Machine Settings for Underwater GMA Welding

Machine Settings		Resulting	
Arc Length	Wire Feed	Current	Comment
5	4.8	250 amps	Minimum of possible range Bead piles up in globs due to short circuit transfer.
6	5.2	300 amps	Good welding range Moderate penetration Smooth bead
7	5.7	340 amps	
8	6.0	370 amps	Beyond this point burnthrough is uncontrollable even at fast welding speeds.

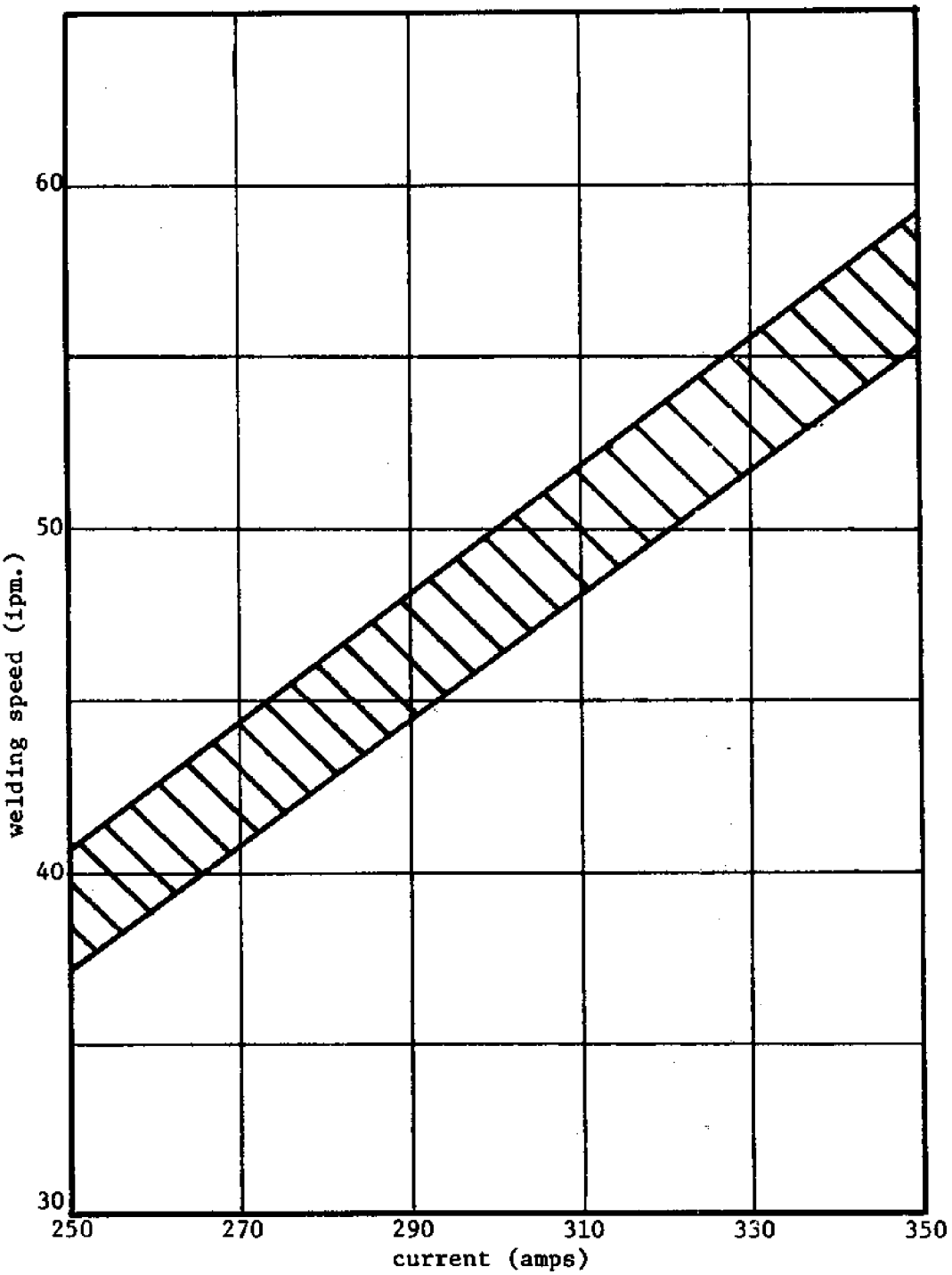

RANGE OF WELDING SPEEDS — GMA

FIGURE 4-6

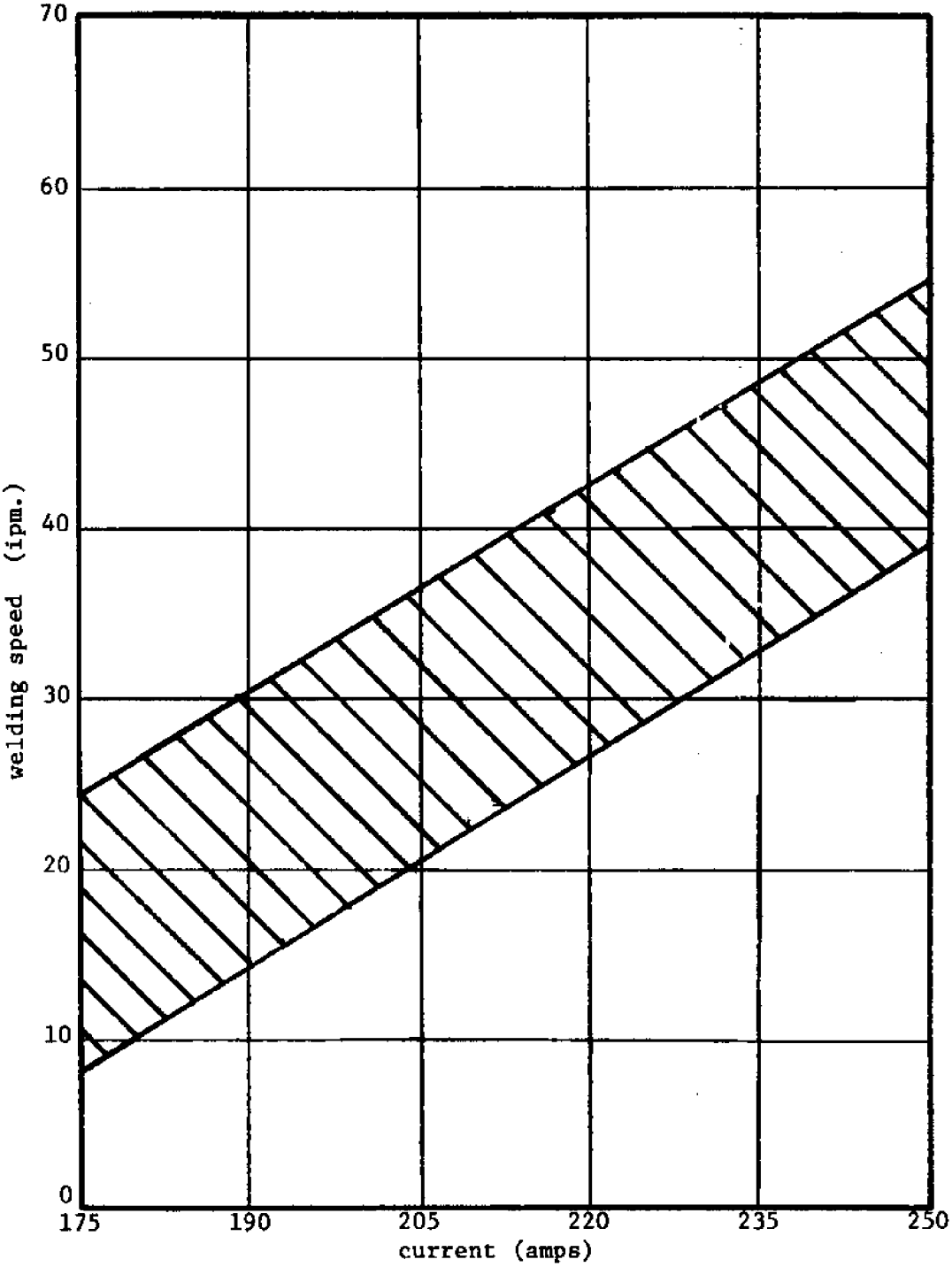

RANGE OF WELDING SPEEDS — SMA

FIGURE 4-7

4.2 Temperature Measurements

In order to determine the accuracy of the mathematical model it was necessary to generate a set of temperature distributions for actual welding runs. The basic steps involved in this experimentation are:

1. Mount the thermocouples
2. Mount the plate in the tank
3. Attach thermocouple leads to the recorders
4. Set up the welding system
5. Attach voltage and current recorders
6. Flood the tank
7. Turn on the power
8. Lay the weld bead and record temperature, voltage, current, and time
9. Measure bead length and distance from centerline to each thermocouple
10. Process and plot the data

Mounting the thermocouples was the most tedious operation and required a certain amount of trial and error. This will be discussed in detail.

Four thermocouples were mounted in each plate. Asbestos wrapped chromel-alumel thermocouple wire served as both the thermocouples and the leads. Staub's method of jamming these leads into a tight hole in the plate and then peening the hole shut was tried without success. This was probably due to a poor thermocouple junction as well as poor contact with the plate. Steps involved in the method finally chosen are as follows:

1. Drill and counter drill 4 holes in each plate as shown in figure 4-8.
2. Bare about 1/2 inch on each wire, twist the ends together and insert them through the plate (figure 4-8).
3. Using a gas torch melt this twisted end down until a small bead is formed.
4. Pull the bead to the plate and peen flush.
5. Seal the underside with porcelain cement. Let dry and waterproof with mild acetic acid.

This setup insured a good junction and metal contact. Its results were quite satisfactory.

The thermocouple leads were connected, two to each of two recorders. The sensitivity settings for the recorders were 1 mv/div for three channels and 2 mv/div for the fourth. The fourth channel was connected to the thermocouple closest to the centerline of the weld. Current and voltage recorders were connected between the welder and the machine. They also recorded the duration of the run. (see figure 4-9)

Once the welding run had been made, the length of the weld bead as well as thermocouple distance from center were measured with a micrometer device. Using the length of the bead along with run time allowed the welding speed for the run to be calculated.

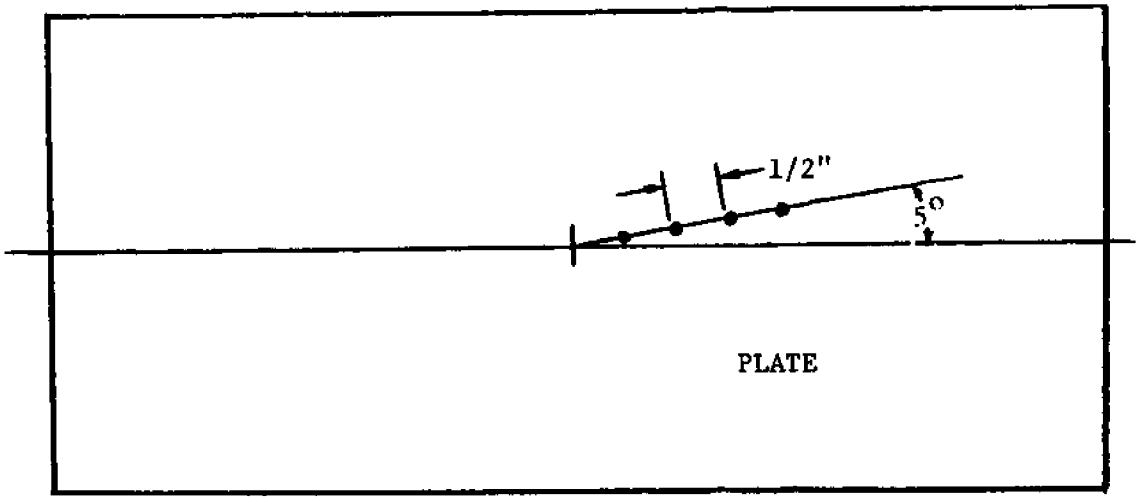

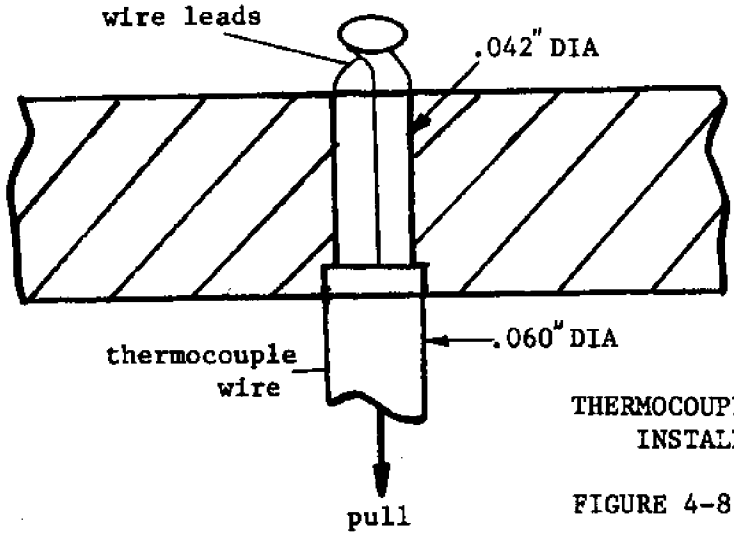

THERMOCOUPLE INSTALLATION

FIGURE 4-8

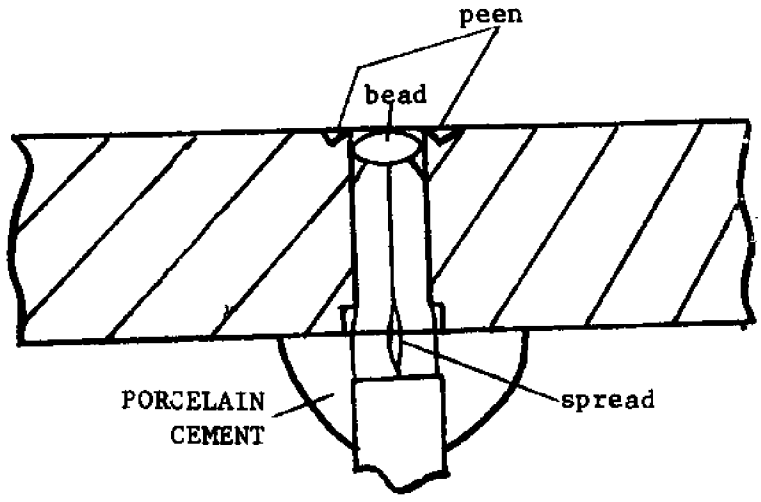

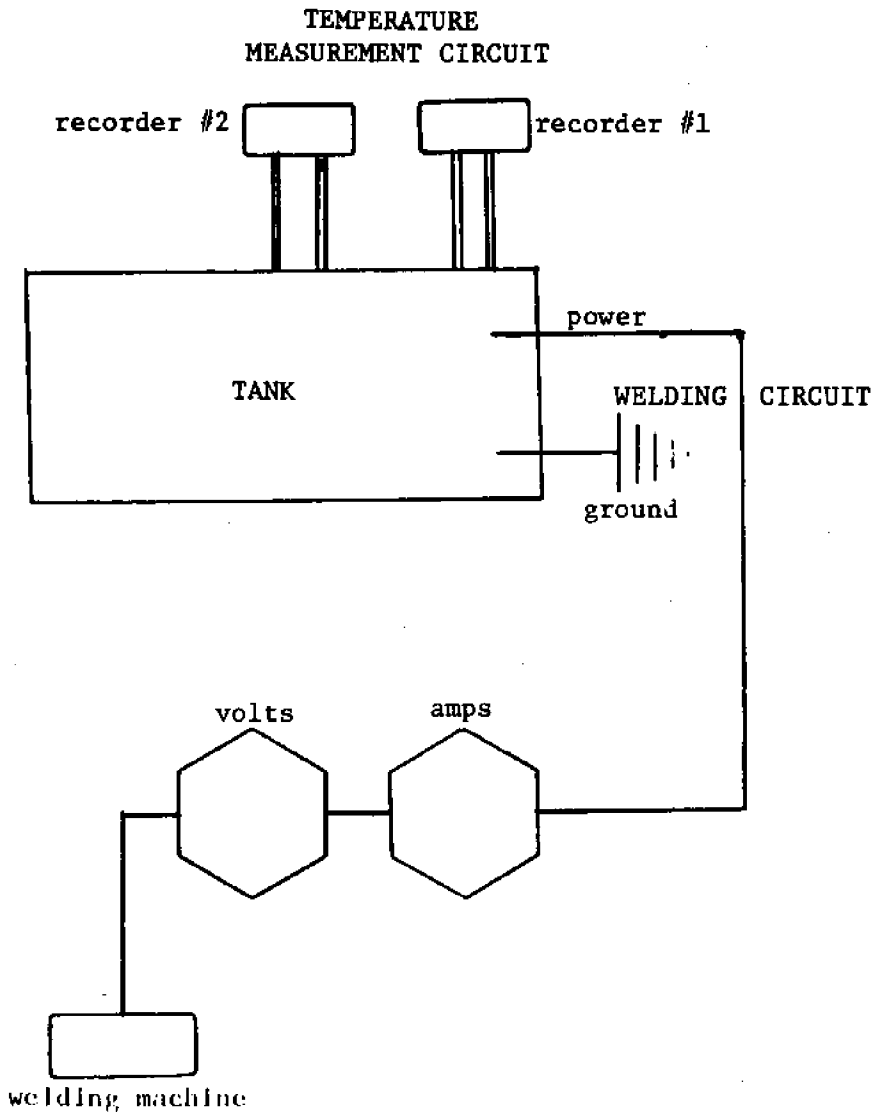

THERMOCOUPLE SETUP

FIGURE 4-9

The voltage readings from the thermocouples were converted to temperatures and everything normalized for comparison to the model. The results are displayed and discussed in Chapter 7.

4.3 Molten Pool Blow-out

In order to establish the inner boundary on plate heat transfer it was necessary to determine, for each process, the relationship between maximum pool dimensions and the lumped welding parameter. (section 3.3) This was done by laying a bead and at some point during the welding blowing a sharp blast of air towards the base of the electrode and molten pool, terminating the welding at this point. If aimed properly this blast would blow the molten metal away leaving a crater in the form of the weld puddle. These craters were measured with a micrometer and their maximum dimensions normalized and correlated as discussed in section 3.3.

Figure 4-10 illustrates the blow-out setup for the SMA process runs. After a number of trials, it was found that the blast should be aimed at an angle of 45 degrees and pointed at the front of the teardrop towards the tail. Since the apparatus was fixed to the consuming

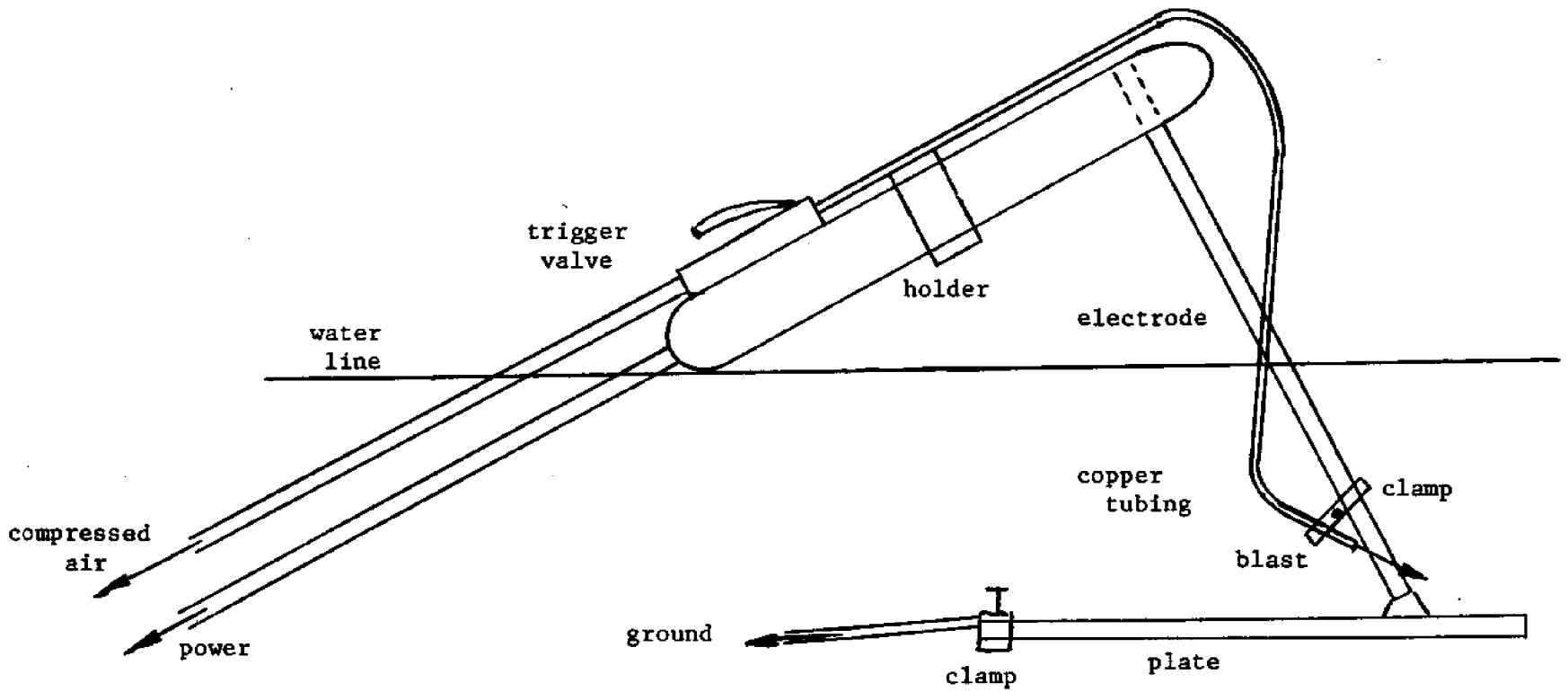

BLOWOUT SYSTEM SMA

FIGURE 4-10

electrode, it was necessary to blow out just as the tubing neared the plate. This timing was crucial for a successful run. About one out of three craters was satisfactory. This meant proper shape (teardrop) and two dimensionality. The electrode was replaced after every run and the trial repeated.

The operation was much simpler for GMA as it was possible to fix the blow-out apparatus to the gun barrel and actuate it at any time. Most of the runs for this process were succussful. (figure 4-11)

High speed photographs had shown that the shroud was not functioning properly, but merely sustaining normal bubble growth within the shroud. As time could not be devoted to improving the shroud, no blow-out experiments were made for it.

Collection of this data showed excellent agreement with the derived correlation.

4.4 High Speed Cinematography

In order to determine the arc bubble mechanism it was necessary to observe it closely and to slow its action down. This was done using high speed cinematography.

The method and setup is shown schematically in

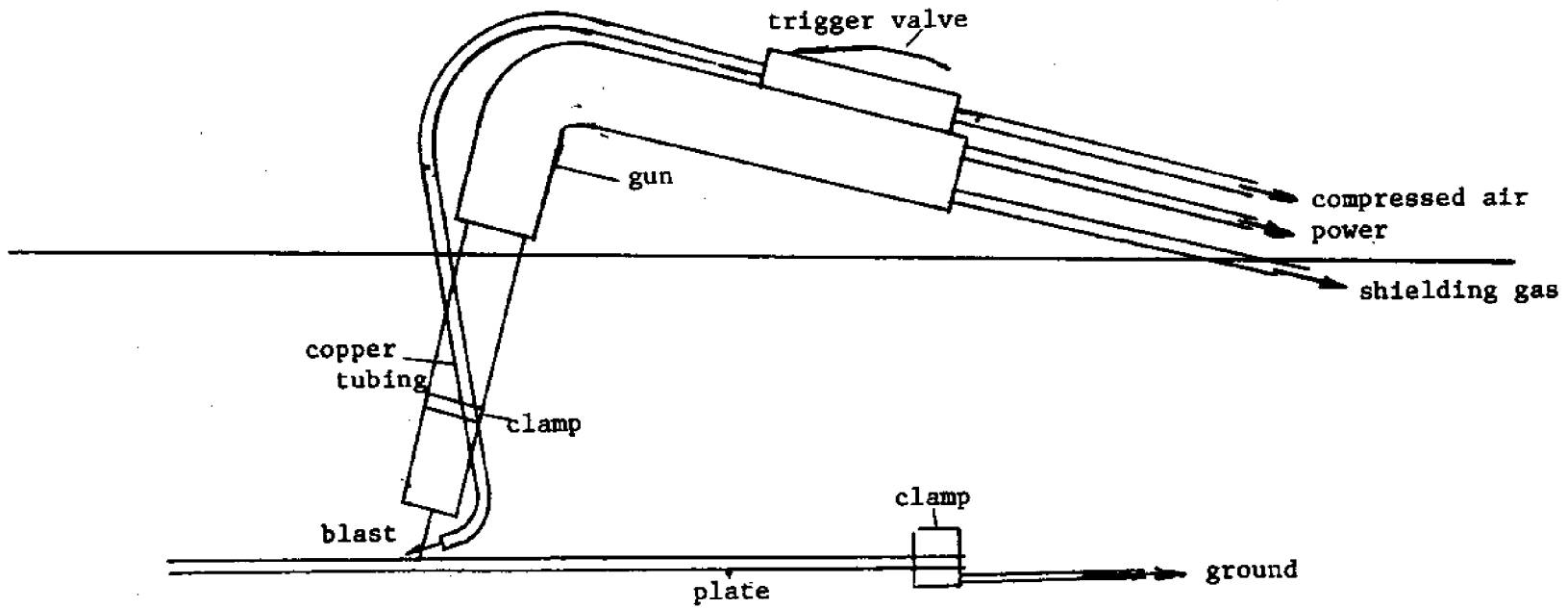

BLOWOUT SYSTEM GMA

FIGURE 4-11

figure 4-12. By welding along a line parallel to the direction of the lens it was possible to keep the camera stationary while moving the arc within its line of sight. The problems remaining to be solved were those of focus, film type, camera type, and exposure. The sequences of trials leading to the final methods for each are described in Tables 4-3 through 4-5.

The first SMA run used Kodachrome II film. These pictures showed an exceedingly bright red fireball which obscured everything. The blue-green filter used in the second run did little to lessen this problem. Ektachrome film eliminated the red glare enough to tell that the subject was out of focus and too bright. Increasing the speed in run 4 improved the exposure, but did little for the focus. Up to this time focussing was done through the lens. The depth of field was not sufficient using the 50 mm lens, so a 75 mm lens was tried. Finally the subject to camera distance was simply measured and set on the lens. This at last resulted in a satisfactory run, run six. (see figure 5-1) All remaining SMA runs were made using the same settings.

Filming the shroud required only that a new exposure be found and focus be maintained. Run 4 for the shroud proved satisfactory and required one f-stop more

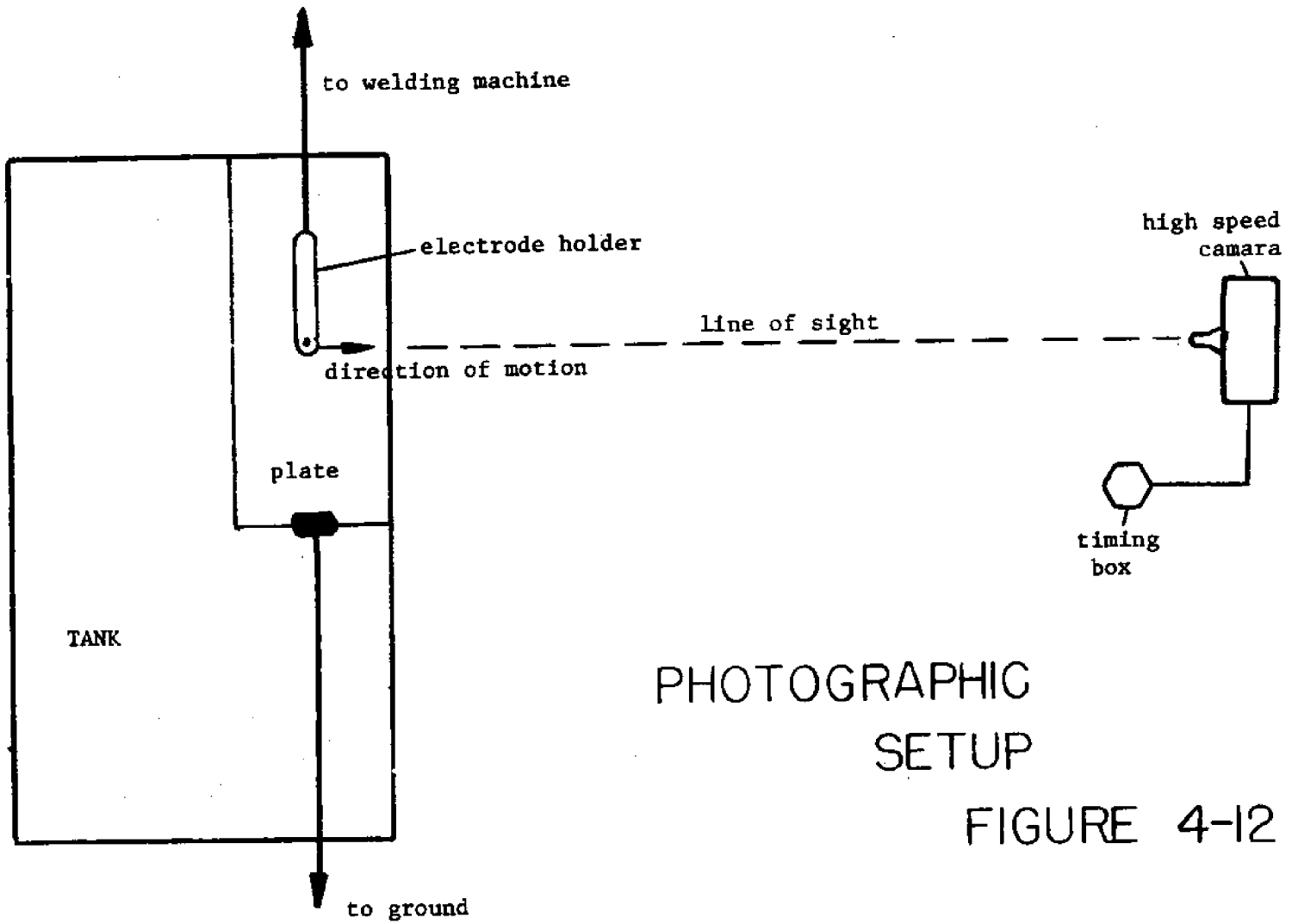

PHOTOGRAPHIC
SETUP
FIGURE 4-12

TABLE 4-3

Description of Photographic Trials

SMA

RUN	FILM	CAMERA	DISTANCE	LENS	f-STOP	SPEED	FILTER
1	Kodachrome II	Fastax	4 ft.	50mm	f2	200 fps	none
2	Kodachrome II	Fastax	4 ft.	50mm	f2	200 fps	blue-green
3	Ektachrome (Tungsten)	HiCam	6 ft.	75mm	f2.8	400 fps	none
4	Ektachrome (Tungsten)	HiCam	6 ft.	75mm	f2.8	750 fps	none
5	Ektachrome (Tungsten)	HiCam	6 ft.	75mm	f4	400 fps	polarizing
6	Ektachrome (Tungsten)	HiCam	6 ft.	75mm	f2.8	750 fps	none

TABLE 4-4

Description of Photographic Trials

Shroud

RUN	FILM	CAMERA	DISTANCE	LENS	f-STOP	SPEED	FILTER
1	Ektachrome	HiCam	10 ft.	75mm	f4	950 fps	none
2	Ektachrome	HiCam	10 ft.	75mm	f4	800 fps	none
3	Ektachrome	HiCam	10 ft.	75mm	f4	400 fps	none
4	Ektachrome	HiCam	10 ft.	75mm	f3.3	200 fps	none

TABLE 4-5

Description of Photographic Trials

GMA

RUN	FILM	CAMERA	DISTANCE	LENS	f-STOP	SPEED	FILTER
1	Ektachrome	HiCam	8 ft.	75mm	f4	400 fps	none
2	Ektachrome	HiCam	8 ft.	75mm	f4	950 fps	none
3	Ektachrome	HiCam	8 ft.	75mm	f5.6	1500 fps	none
4	Ektachrome	HiCam	8 ft.	75mm	f5.6	3000 fps	none

than SMA run number six.

The final GMA run required 5 f-stops less light than the shroud run. This value was reached after four successive reductions in exposure.

The film results for each process provided extremely valuable information, and this method is highly recommended for any future research.

CHAPTER V

DYNAMIC BUBBLE, SHROUD AND GAS MODELS

Discussion thus far has concentrated on phenomena occurring in the plane of the plate. Staub's missing link, the gaseous phenomena occurring above the plate will be described in this chapter. This phenomena either occurs naturally or is generated artificially. The three processes described here are:

1. the naturally occurring dynamic bubble
2. the underwater welding shroud
3. underwater gas metal arc

Knowledge of these taken as a whole could be the key to further advancement in underwater welding technology.

5.1 Dynamic Bubble Model

During underwater SMA welding a gaseous bubble is continuously growing and departing at the tip of the electrode. A high speed motion picture study of this bubble mechanism was conducted. (Section 4.3) Experiments using E6013 and E7014 electrodes may be summed up as follows: (figure 5-1)

1. There appears to be a gas and plasma void immediately around the arc column which is relatively stable. The arc energy is so intense here that any water in this region is immediately vaporized.

2. Within this void hydrogen gas, steam and various organic by-products are produced, causing a dynamic bubble to grow from it.

3. This bubble grows and rises continuously until its radius becomes tangent to the initial void, at which time the bubble breaks away and a new bubble begins to form.

4. It has been observed here and by Silva and Madatov (refs. 9 and 11) that varying the welding parameters (current, voltage, speed, polarity) for a given liquid environment, electrode, and depth has little effect on gas flow rate and bubble dynamics. It should be noted that the electrode coating and the salinity of the environment will affect the production of organic by-products and thereby the gas flow rate.

5. The flow rate predicted by collection (after the gases have filtered through the liquid) does not take into consideration the steam generated at the arc. Although the steam does eventually condense, leaving only hydrogen and organic by-products, it is very active during the rapid bubble growth process and augments the apparent flow rate. By considering bubble volumes and frequencies, volume flow rates in the order of 100 cc/sec. were observed rather than the 50-60 cc/sec. rate determined by collection.

6. The shape of the bubble, especially late in its growth, may be assumed spherical.

In order to predict bubble phenomena under various conditions of salinity and pressure and for various electrodes

a general model was sought which would satisfy the above observations. As nucleate boiling involves various bubble growth phenomena, this literature was searched, but an adequate model could not be derived from this literature. Davidson's work with bubble formation from an orifice (ref.27) was observed to have much in common with underwater welding bubble growth. A model using his method was derived and proved quite satisfactory.

Large flow rates made it possible to neglect surface tension, leaving only the balance of buoyant and inertial forces to control the process. It was further assumed that growth begins at a point on or just above the plate and that the gas behaves ideally. The volume at any time may then be represented in terms of mass and volume flow rates:

$$\nabla = Gt = \frac{wRT}{P} \quad cm^3$$

The apparent mass of a sphere moving perpendicular to a wall is derived in Milne-Thompson (ref. 28):

$$m = m_V + \frac{11}{16} m_L \simeq \frac{11}{16} m_L = \frac{11}{16} \rho_L \nabla$$

Equating the inertial forces to the buoyant forces yields:

$$\rho_L \nabla g = \frac{d}{dt}\left(\frac{11}{16} \rho_L \nabla \frac{dh}{dt}\right)$$

or:

$$G t_g = \frac{11}{16} \frac{d}{dt}\left(G t \frac{dh}{dt}\right)$$

The solution of this equation yields:

$$h = \frac{8}{22} g t^2 \text{ cm.}$$

The idealized bubble growth mechanism is shown in figure 5-2. Break-away occurs when the bubble is tangent to the void or when its height equals its radius plus the radius of the void. Critical height, radius, and departure time may be determined graphically by plotting height and bubble radius plus void radius on the same graph and finding their intersection:

$$R = \left(\frac{3}{4\pi} G t\right)^{1/3} \text{ cm.}$$

$$h_{max} = R_{MAX} + R_o$$

This was done for the E6013 electrode (flow rate of 100 cc/sec.) and for the E7014 electrode (flow rate of 125 cc/sec.). Plots and results are shown in figures 5-3 through 5-6, and Tables 5-1 and 5-2.

IDEALIZED BUBBLE GROWTH

FIGURE 5-2

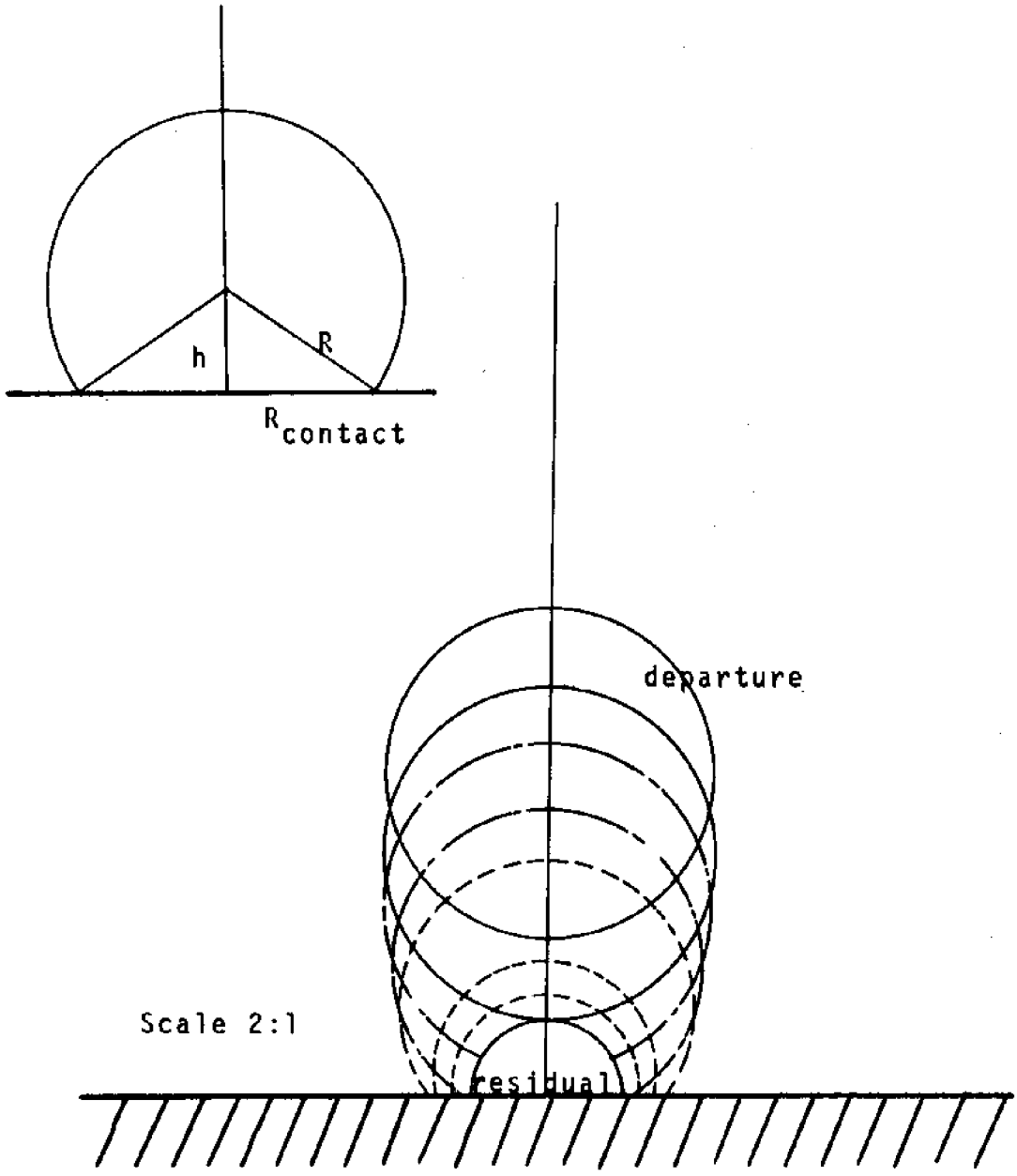

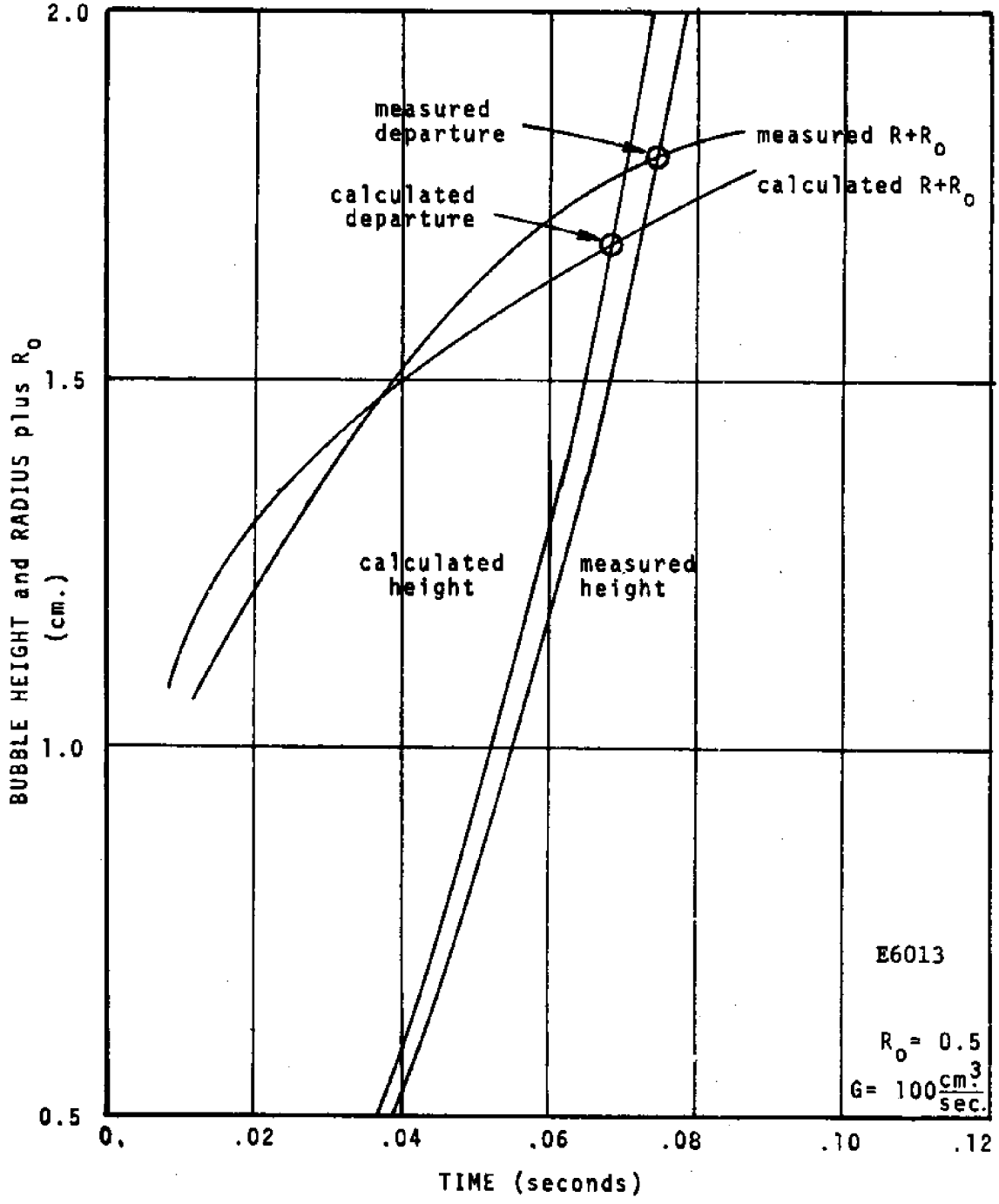

DETERMINING BUBBLE DEPARTURE

FIGURE 5-3

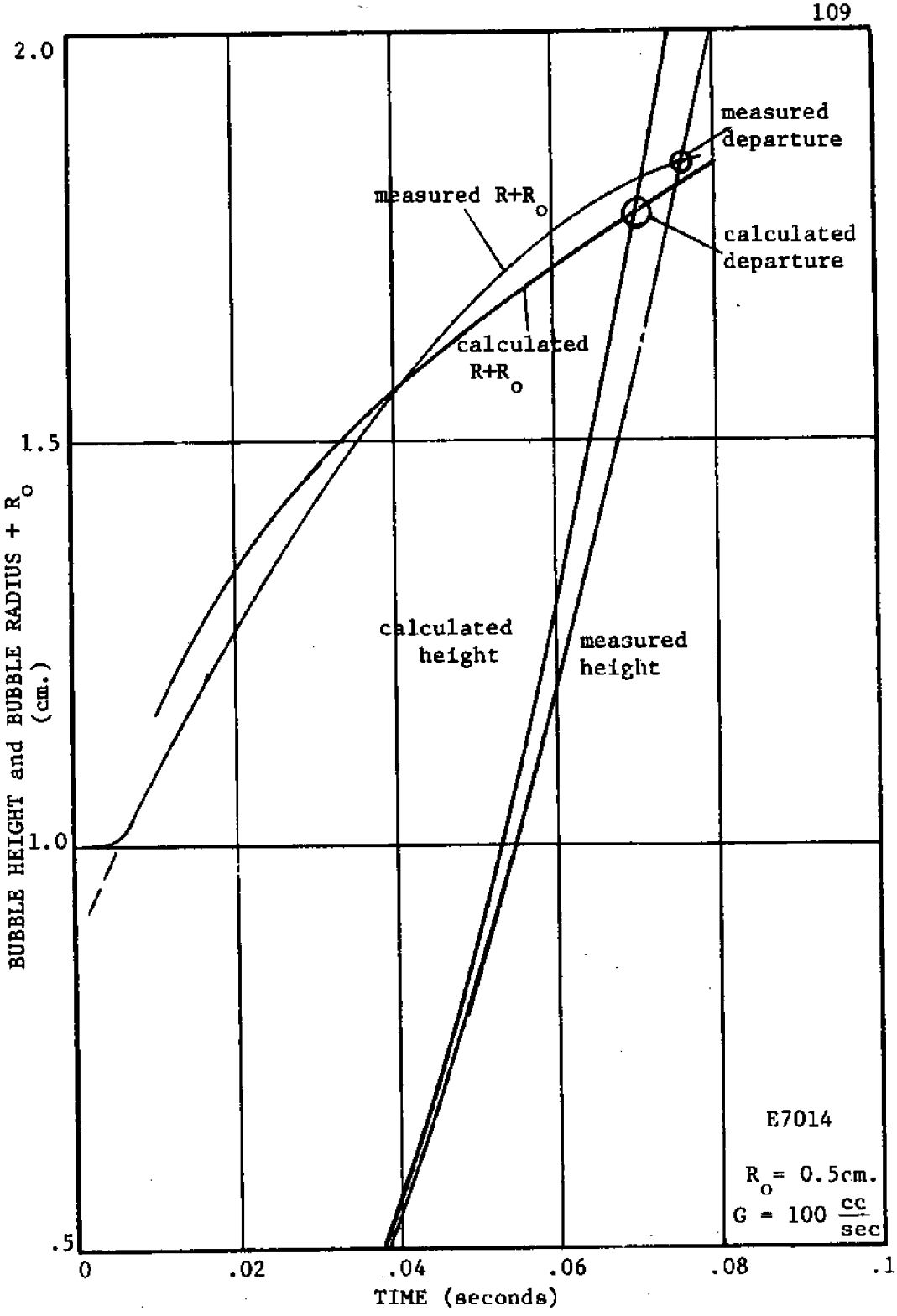

DETERMINE DEPARTURE

FIGURE 5-4

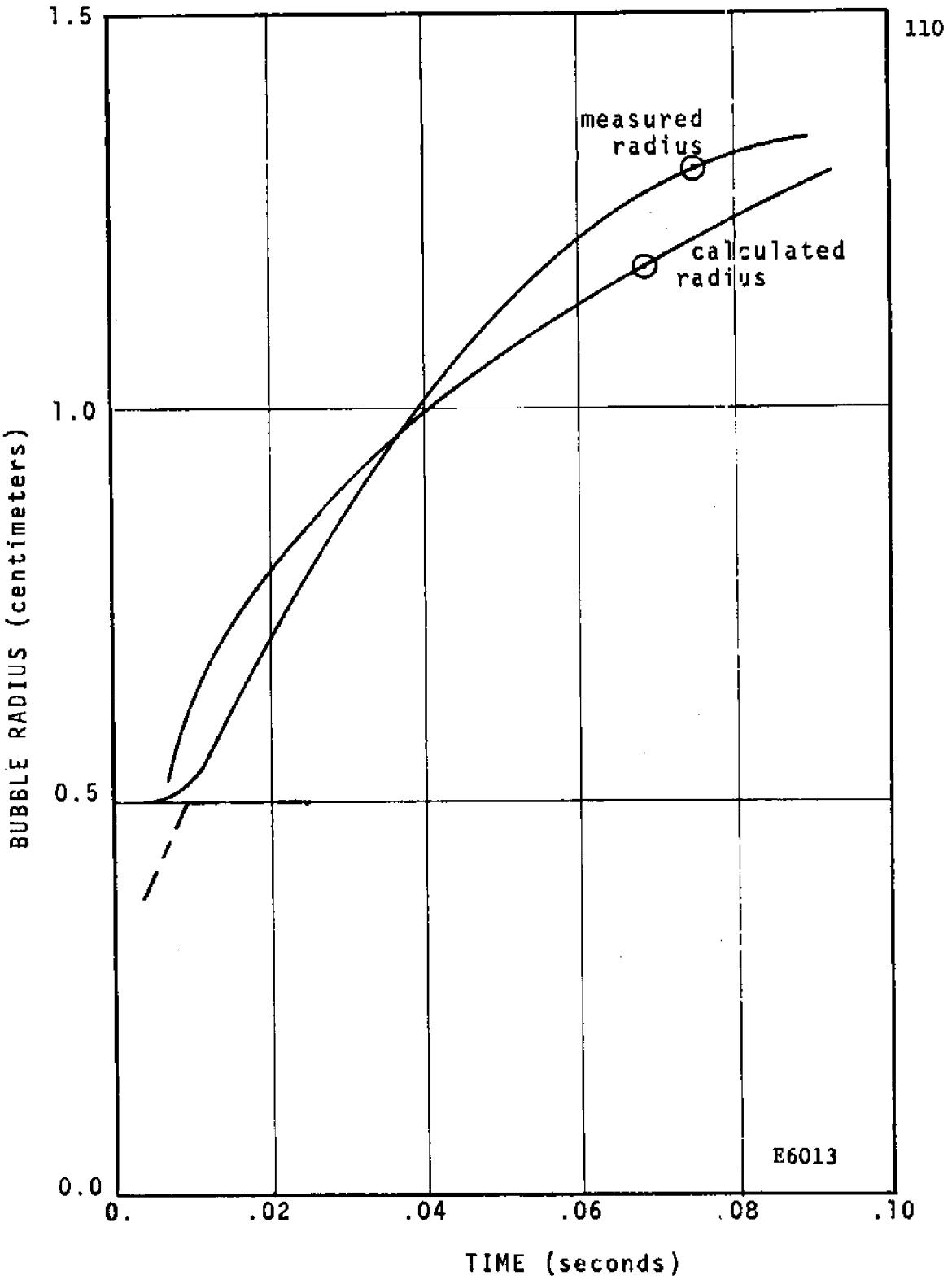
1.5
1.0
0.5
0.0
BUBBLE RADIUS (centimeters)
measured radius
calculated radius
E6013
0.
.02
.04
.06
.08
.10
TIME (seconds)

FIGURE 5-5

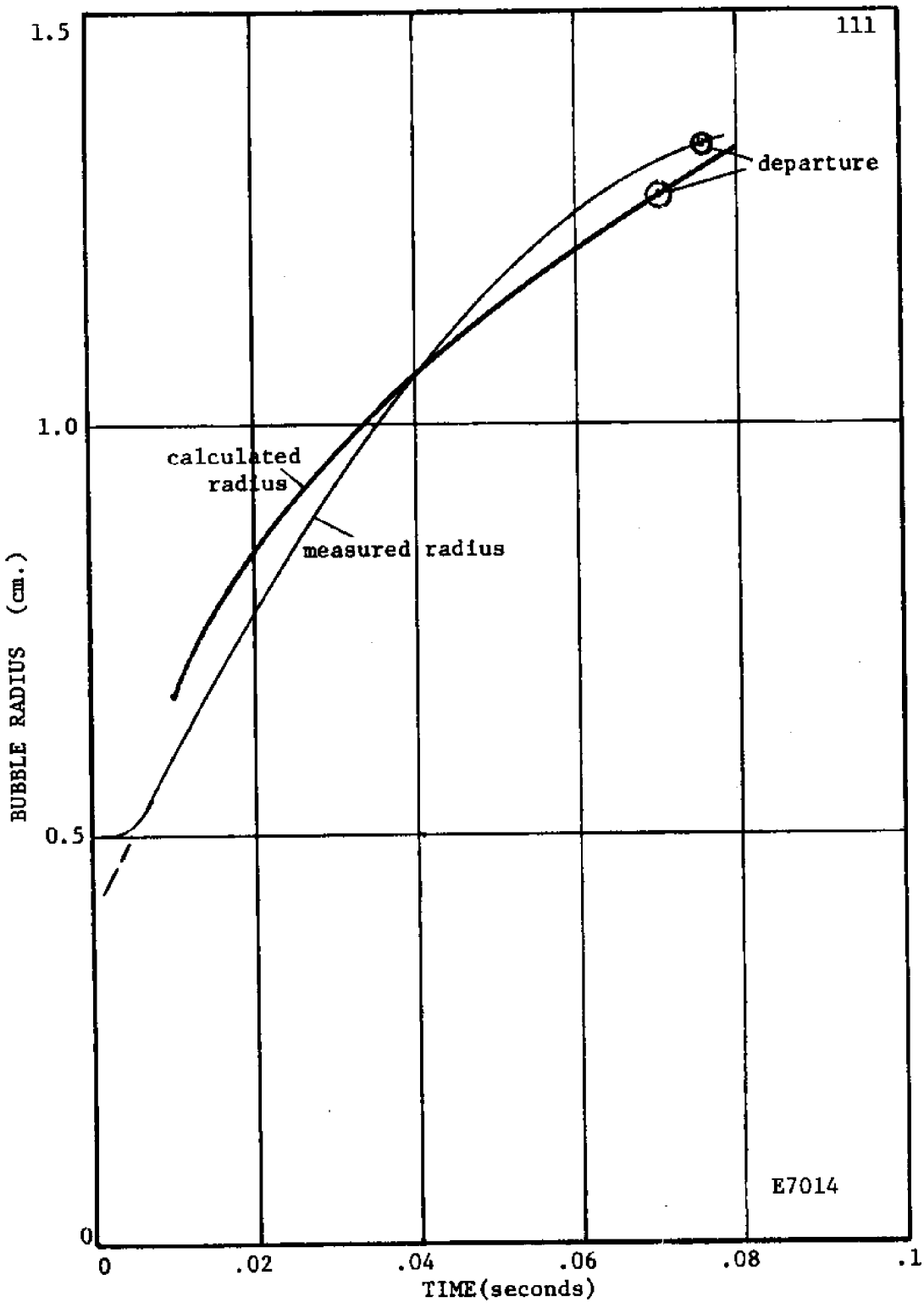
111
1.5
1.0
0.5
0
BUBBLE RADIUS (cm.)
departure
calculated radius
measured radius
E7014
0
.02
.04
.06
.08
.1
TIME(seconds)

FIGURE 5-6

BUBBLE GROWTH CHARACTERISTICS

(E6013)

Table 5-1

MEASURED		CALCULATED
.075 Sec.	Period	.068 Sec.
13 Bubbles/sec.	Freq.	15 Bubbles/sec.
.5 cm.	R_o	.5 cm.
100 cc/sec	G	100 cc/sec
1.30 cm.	R_{MAX}	1.18 cm.
1.81 cm.	H_{MAX}	1.68 cm.

BUBBLE GROWTH CHARACTERISTICS

(E7014)

Table 5-2

MEASURED		CALCULATED
.076 Sec.	Period	.071 sec.
13 Bubbles/sec.	Freq.	14 Bubbles/sec.
.5 cm.	R_o	.5 cm.
125 cc/sec	G	125 cc/sec
1.35 cm.	R_{MAX}	1.28 cm.
1.83 cm.	H_{MAX}	1.78 cm.

It can be assumed that the mass flow rate is constant for these processes and that the volume flow rate would change with pressure. Substituting new volume flow rates into the above expressions would determine bubble sizes at various depths. Unfortunately, the lack of equipment made the testing of pressure effects beyond the scope of this thesis.

Given this model for bubble growth, the actual contact radius and area must be determined, as they are critical to the plate heat transfer. (figure 5-2) It can be assumed that the maximum contact radius determines the region in which boiling is prevented as hot gases from the arc are periodically sweeping this entire area. Plots of contact radius vs. time are shown in figures 5-7 and 5-8.

$$R_{contact} = (R^2 - h^2)^{1/2} \quad cm.$$

The values chosen for the critical radii were .35 inch (E7014) and .32 inch (E6013).

5.2 The Shroud Model

Using high speed photography it was immediately

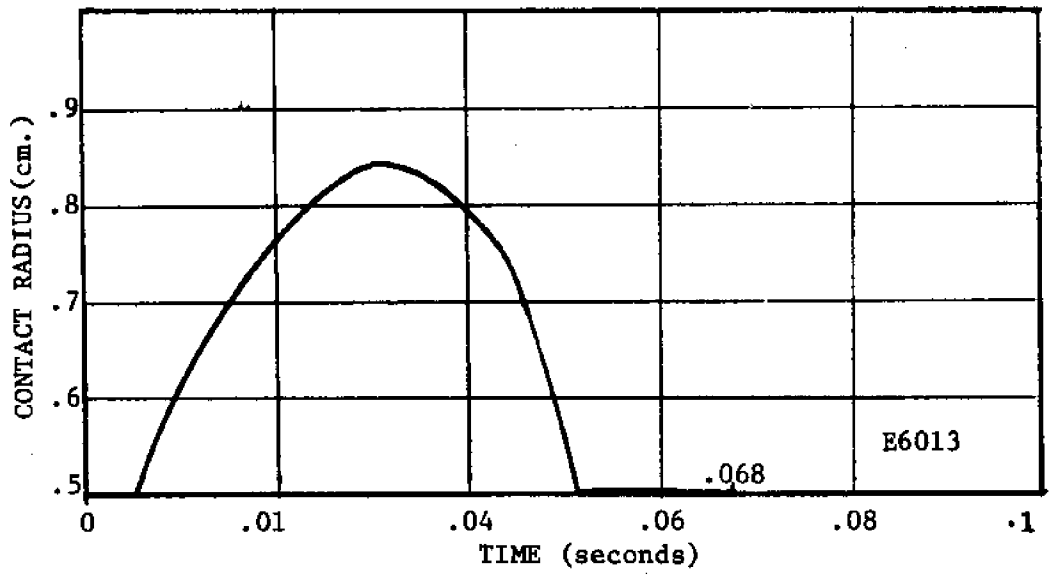

FIGURE 5-7

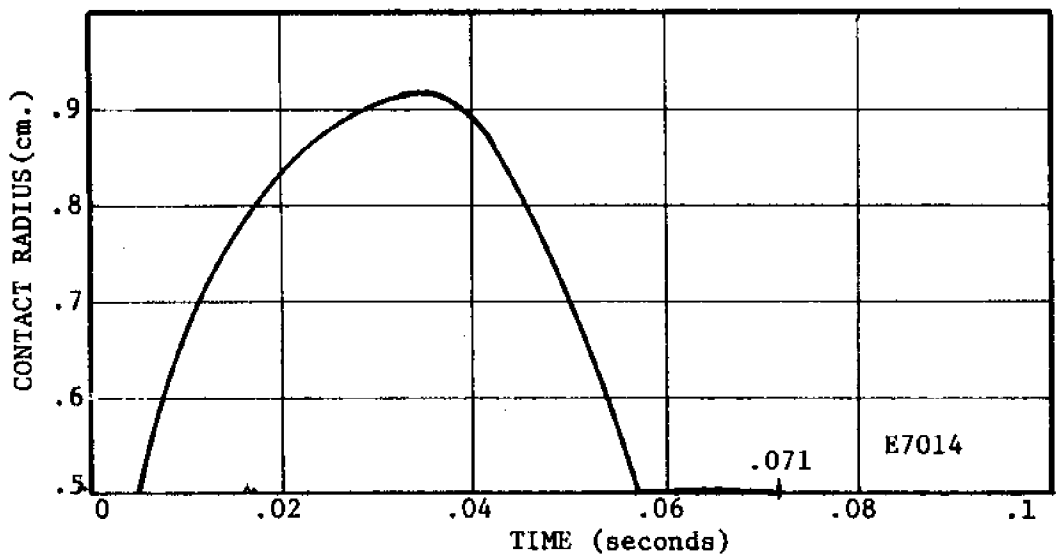

FIGURE 5-8

noticed that the acrylic shroud was not serving its purpose. The gas being produced by the arc was not sufficient to fill the shroud even with the gas escape port blocked. (figures 5-9 and 5-10) The failure of this shroud was attributed to its slightly larger size over that of Silva's. As this thesis does not encompass the development of a shroud, experiments with it were abandoned, but a vital lesson was learned. The value of this device would certainly be enhanced by an external gas source.

If the shroud were made to function properly, heat transfer within its radius would be reduced to radiation. This could be modeled by simply setting the critical radius mentioned earlier equal to the shroud radius.

5.3 Gas Metal Arc

The gas metal arc process demonstrated a combination of bubble growth phenomena. It had been expected that the gas would impinge on the plate creating some sort of gaseous shield, but instead the gas generated a second bubble phenomena. (see figures 5-11 and 5-12)

Growing from the large orifice at a volume flow rate of 70 ft^3/hr (570cc/sec) this bubble merges with the

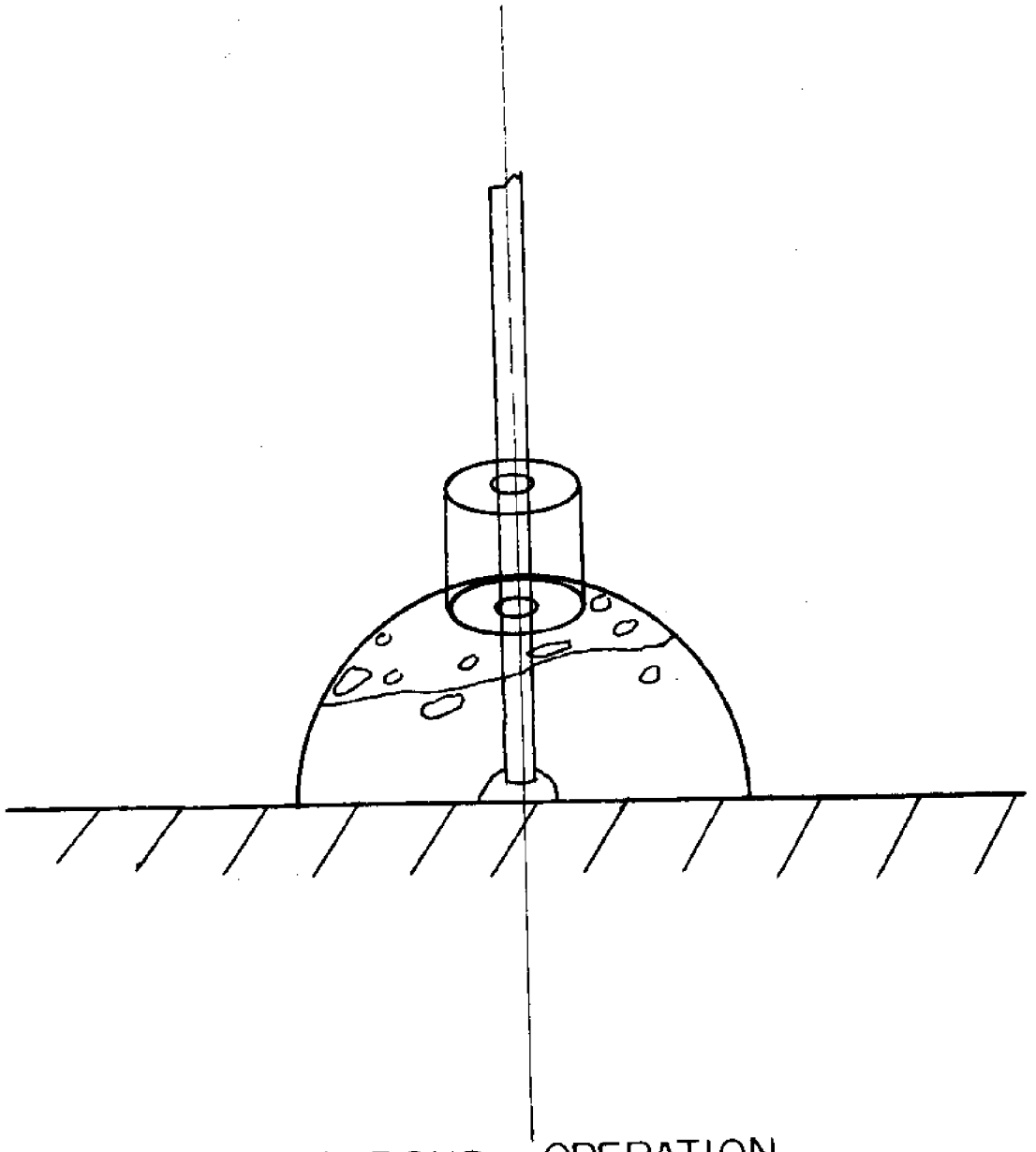

SHROUD OPERATION

FIGURE 5-10

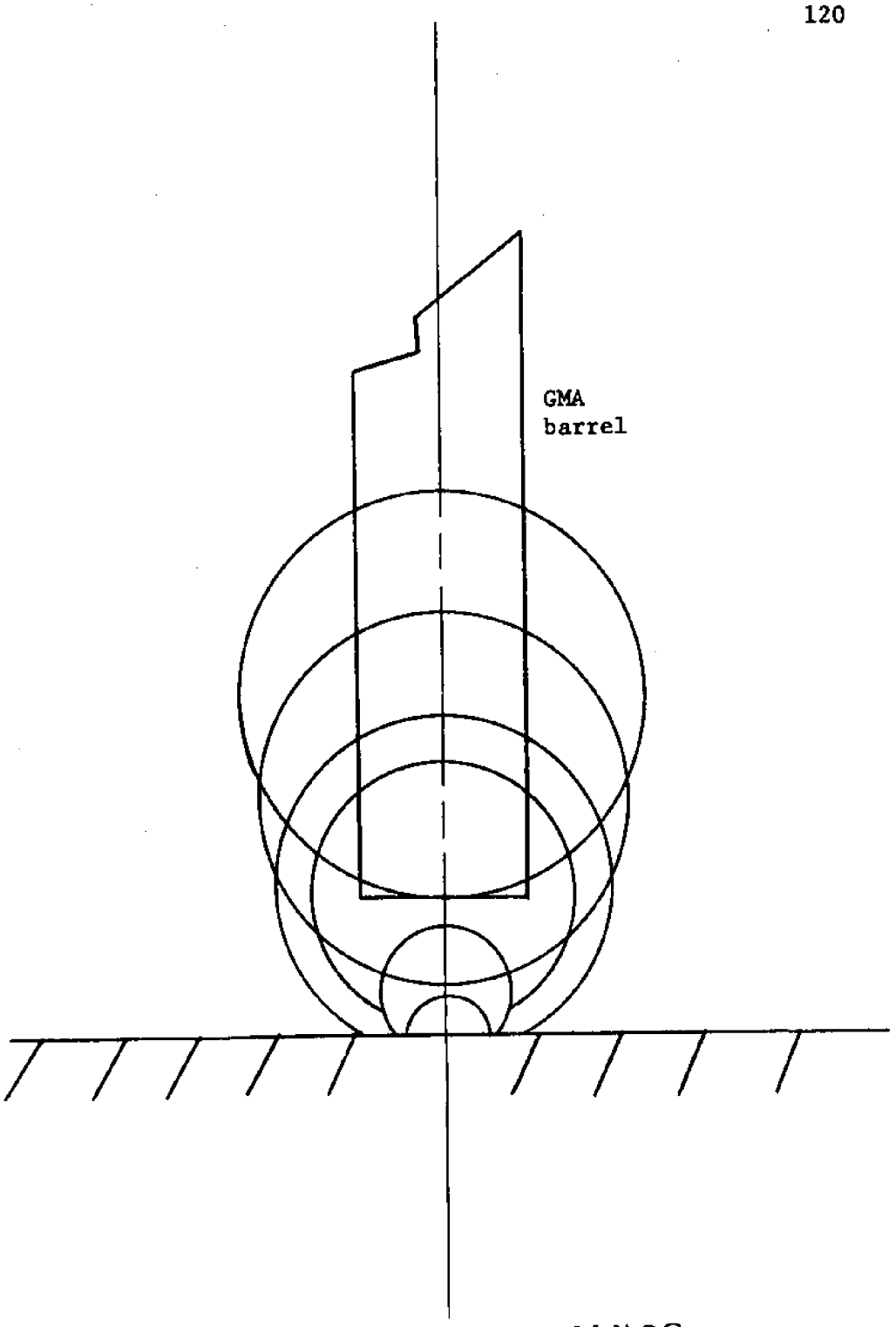

GMA BUBBLE DYNAMICS

FIGURE 5-12

normal arc bubble growing below. Due to the lack of organic materials around the GMA wire, the gas flow rate of its arc bubble was only 75 cc/sec. Assuming the Davidson model for these two flows yields the data shown in figures 5-13 through 5-16 and Tables 5-3 and 5-4. The period predicted for both bubbles was fairly accurate, but as the two volumes mixed and interacted they were difficult to measure and varied significantly from ideal. The fact that the gas orifice was maintained at 1.5 above the plate prevented the orifice bubble from intersecting the plate. Thus all shielding came from the arc bubble. The contact radius for this bubble is plotted in figure 5-17. A critical radius of .27 in (.7 cm.) was chosen.

Effective use of GMA underwater necessitates effective use of its shielding gas. This was not obtained in the above application. Future processes must use this gas in a more efficient manner.

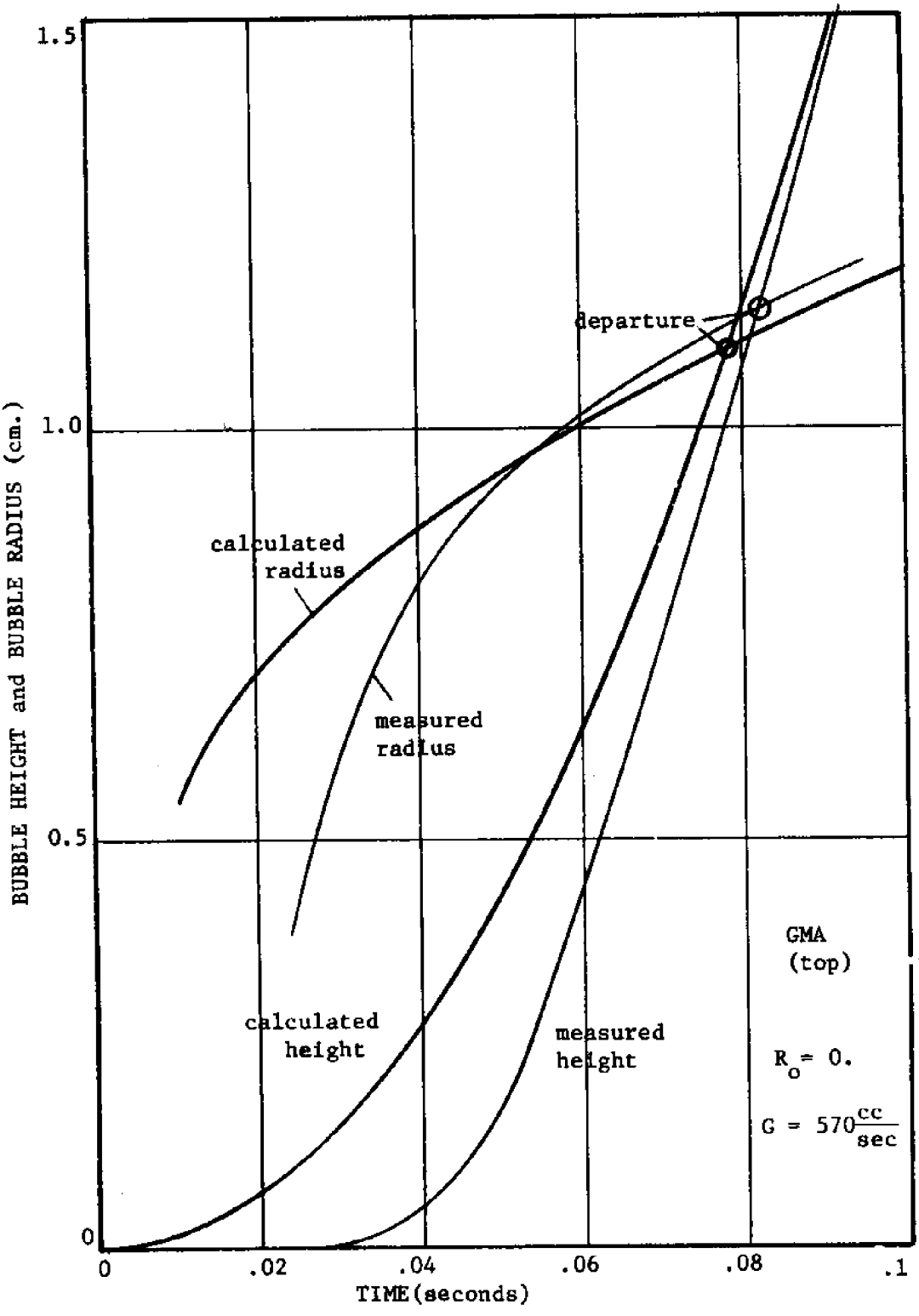

BUBBLE DEPARTURE

FIGURE 5-13

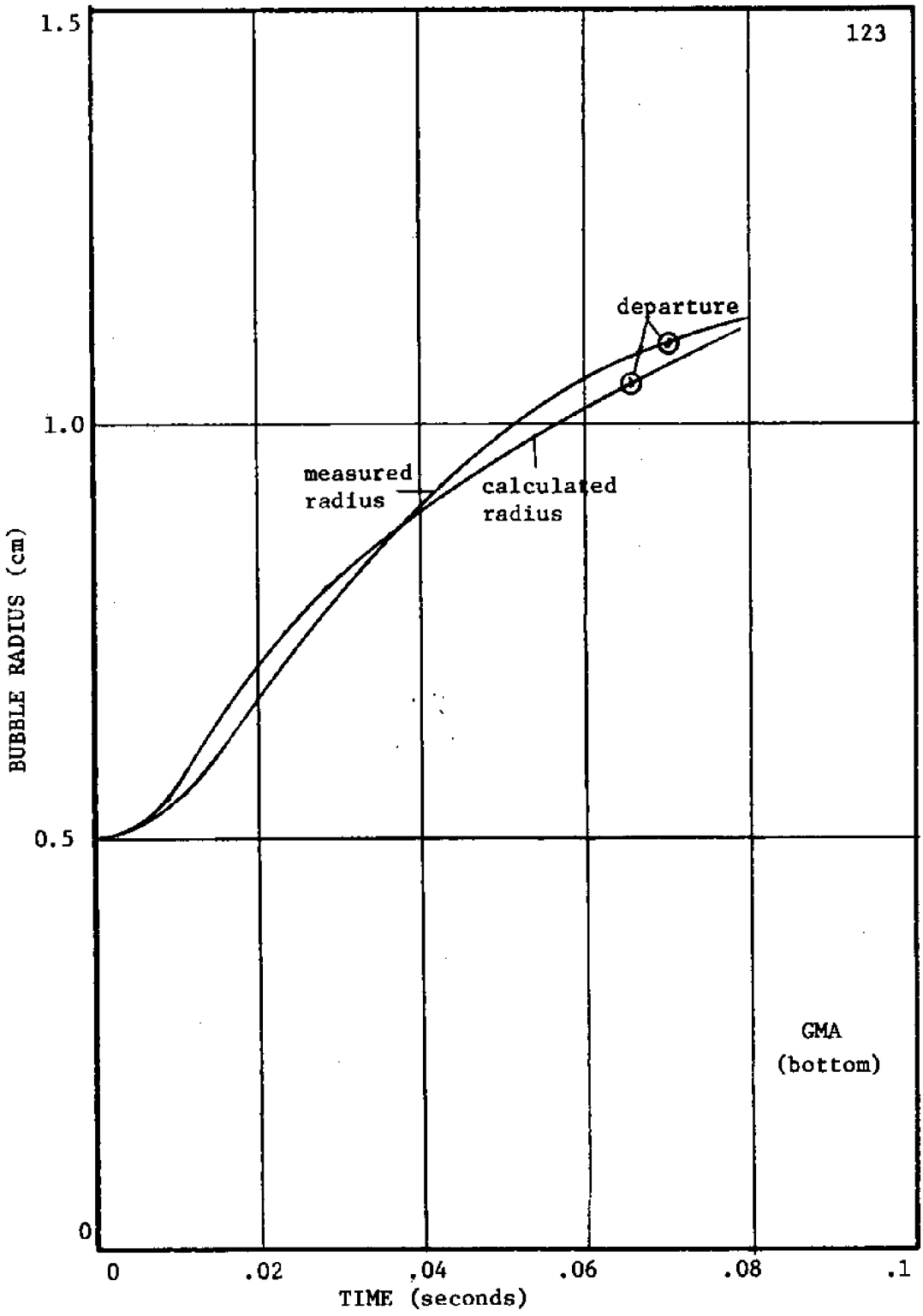
123
1.5
1.0
0.5
0
BUBBLE RADIUS (cm)
departure
measured radius
calculated radius
GMA (bottom)
0
.02
.04
.06
.08
.1
TIME (seconds)

FIGURE 5-14

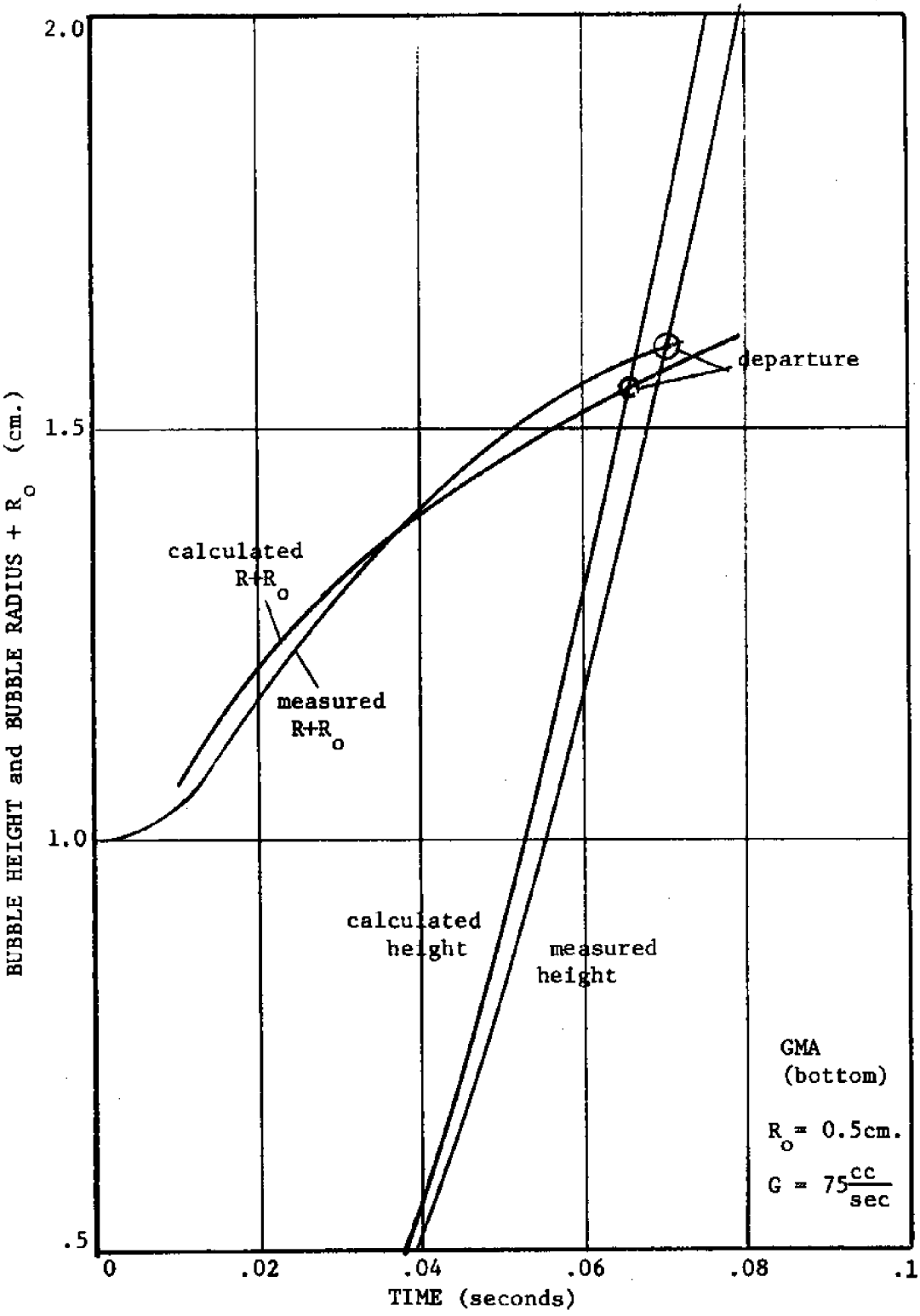

BUBBLE DEPARTURE
FIGURE 5-15

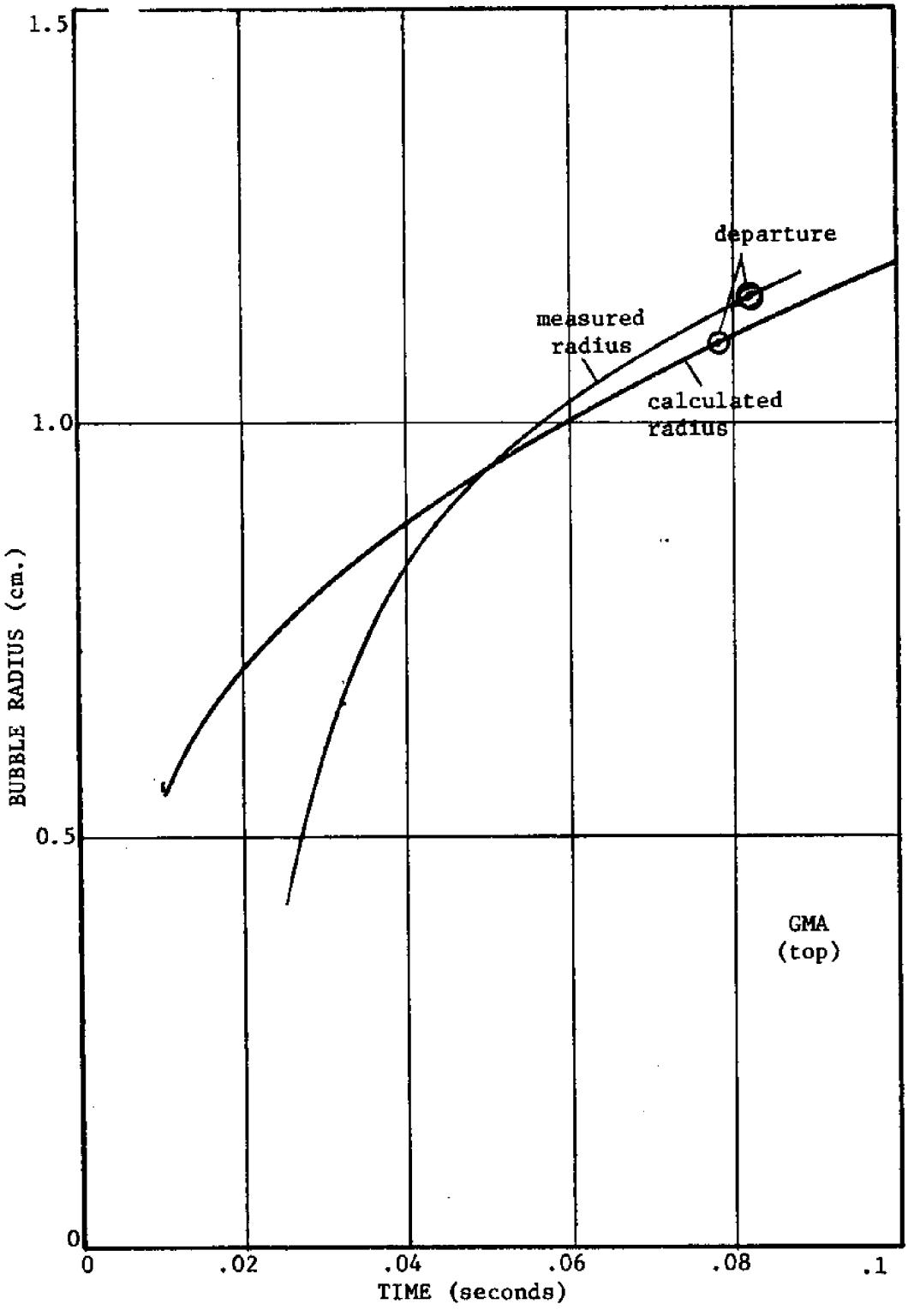
1.5
1.0
0.5
0
BUBBLE RADIUS (cm.)
departure
measured radius
calculated radius
GMA (top)
0
.02
.04
.06
.08
.1
TIME (seconds)

FIGURE 5-16

BUBBLE GROWTH CHARACTERISTICS

(GMA - bottom)

Table 5-3

MEASURED		CALCULATED
.070sec.	Period	.066sec.
14bubbles/sec	Freq.	15bubbles/sec
.5cm.	R_o	.5cm.
75ec/sec	G	75cc/sec.
1.5cm.	R_{max}	1.05cm.
1.5cm.	H_{max}	1.55cm.

BUBBLE GROWTH CHARACTERISTICS

(GMA - top)

Table 5-4

MEASURED		CALCULATED
.082sec.	Period	.079sec.
12bubbles/sec.	Freq.	13bubble/sec
0	R_o	0
570cc/sec.	G	570cc/sec.
2.7cm.	R_{max}	2.2cm.
2.7cm.	H_{max}	2.2cm.

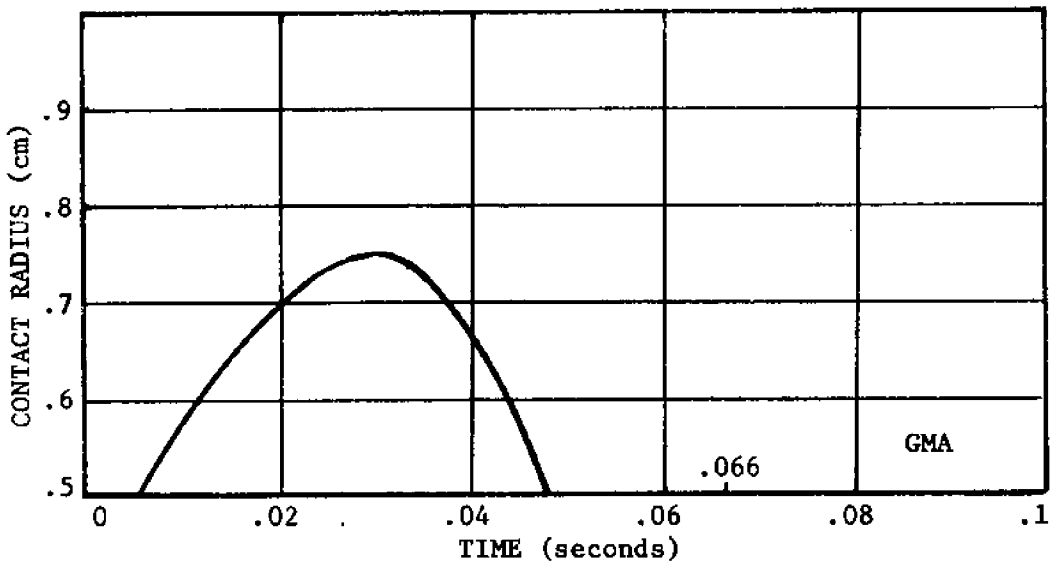

FIGURE 5-17

CHAPTER VI

THE COMPUTER MODEL

The purpose of this computer model is to verify the derived knowledge of various underwater welding phenomena. It is a purely two dimensional model, and probably has little practical application beyond testing and developing this knowledge. However, evaluation of new "above the plate" phenomena as might be involved in a shroud-GMA process could hopefully be done using this model.

The program is an adaptation of Pavelec's, so changes rather than basic program organization and methods will be stressed here. It suffices to say that the entire program is based on the heat conduction equation with source terms presented in Section 3-1. This equation is transformed into a finite difference equivalent which expresses the temperature at a point as a function of the surrounding temperatures in the grid and its value on the previous iteration. This equation along with the characteristic grid setup are shown in figures 6-1 and 6-2. Solution of this equation was done using a Gauss-Sidel iterative procedure. For specifics

FIGURE 6-1 THE FINITE DIFFERENCE EQUATION

$$T_{i,j}^{*n+1} = \left\{ T_{i+1,j}^{*n} \left(\frac{\alpha(T_{i,j}^{*n}) + a_{i-1,j}}{\alpha(T_{i,j}^{*n}) a_{i,j}(a_{i,j} - a_{i-1,j})} \right) + \left(\frac{\alpha(T_{i,j}^{*n}) + a_{i,j}}{\alpha(T_{i,j}^{*n}) a_{i-1,j}(a_{i,j} + a_{i-1,j})} \right) T_{i-1,j}^{*n+1} \right.$$

$$+ T_{i,j+1}^{*n} \left(\frac{1}{b_{i,j}(b_{i,j} + b_{i,j-1})} \right) + T_{i,j-1}^{*n+1} \left(\frac{1}{b_{i,j-1}(b_{1,j} + b_{i,j-1})} \right)$$

$$+ \frac{X_o^2 \dot{q}}{KL(T_m - T_o)} + \frac{1}{2K(T_{i,j}^{*n})} \frac{dK(T_{i,j}^{*n})}{dT^*} \left[\left\{ \left(\frac{a_{i,j} - a_{i-1,j}}{a_{i,j} a_{i-1,j}} \right) T_{i,j}^{*n} + \left(\frac{a_{i,j} T_{i+1,j}^{*n}}{a_{i,j}(a_{i,j} + a_{i-1,j})} \right) \right.\right.$$

$$\left.\left. + \left(\frac{a_{i,j} T_{i-1,j}^{*n+1}}{a_{i-1,j}(a_{i,j} + a_{i-1,j})} \right) \right\}^2 + \left\{ \left(\frac{b_{i,j} - b_{i,j-1}}{b_{i,j} b_{i,j-1}} T_{i,j}^{*n} \right) + \left(\frac{b_{i,j-1} T_{i,j+1}^{*n}}{b_{i,j}(b_{i,j} + b_{i,j-1})} \right) \right.$$

$$\left.\left. + \left(\frac{b_{i,j} T_{i,j-1}^{*n+1}}{b_{i,j-1}(b_{i,j} + b_{i,j-1})} \right) \right\}^2 \right] \Bigg\} \Bigg/ \frac{1}{a_{i,j} a_{i-1,j}} + \frac{1}{b_{i,j} b_{i,j-1}}$$

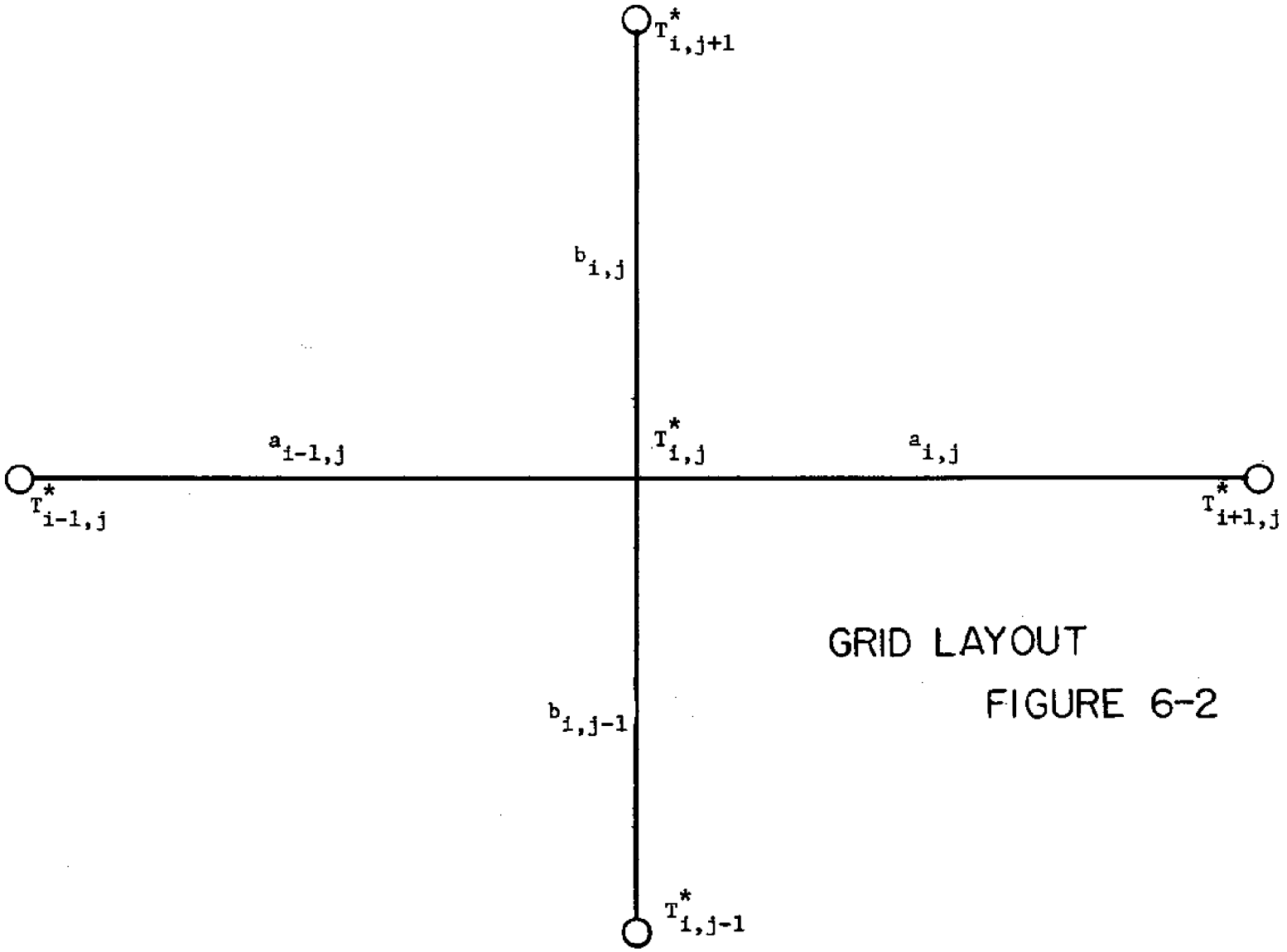

GRID LAYOUT

FIGURE 6-2

on grid setup, origin location, and iterative procedure see Pavelec (ref. 14).

6.1 Program Changes

The problems encountered and changes made in Pavelec's program included the following:

1. Boundary conditions
2. Incorporating the new boiling models
3. Accounting for bubble phenomena

Each of these will be discussed in detail.

6.11 Boundary Conditions

In order to solve the finite difference equation it was necessary to establish inner and outer bounds on the plate conduction. Pool blow-out data was gathered and correlated. The resulting maximum dimension equations for each process were then incorporated into the computer model. To specify a specific process its corresponding number was read in as program input:

Process number 1 - GMA
Process number 2 - 6013S
Process number 3 - 6013R
Process number 4 - 7014S
Process number 5 - 7014R

This change was straight-forward and proved satisfactory.

The external boundary conditions proved to be more difficult to specify. Pavelec's model was for dry-welding, and he assumed that far away from the weld the temperature distribution would converge to that derived by point source theory. This assumption is not valid underwater, so another method had to be determined. To extend the size of the computational block so that ambient temperature might be specified would have increased execution time by at least a factor of 10. Such a method had to be ruled out. The non-linear aspect of the boiling model made the development of an underwater point source theory nearly impossible.

It was observed in the experimental temperature measurements that the rapid cooling during boiling was followed by a period of relatively slow cooling, that is all the temperature distributions were asymptotic to a temperature just above boiling ($T^* = .07$). It was further noticed that a computational block size of one inch in front of the arc, three inches in back, and one-half inch to either side was sufficient to satisfy this condition. This size was left as input, however, to allow flexibility for adapting to other processes. This external

boundary model proved adequate.

6.12 The Boiling Models

Except for the dynamic bubble model all the actual heat transfer information is incorporated into subroutine COEF. The heat transfer equation for surface welding does not change with various temperature ranges, but the numerous boiling regimes underwater required that the proper heat transfer relations be chosen for a given temperature. This was done using a series of if-statements. Furthermore it was necessary to set boiling heat transfer within the bubble (RMAX) to zero. As the spread heat was already set to zero outside RMAX, values for boiling heat transfer were assigned only to points in this region, using the zero spread heat value as a test of location.

Three separate COEF subroutines were made, one for each of the three boiling models to be tested:

1. Sub-cooled
2. Modified
3. Saturated

The result of interchanging these is quite evident and consistent.

6.13 The Dynamic Bubble Models

As discussed in Chapter V a dynamic bubble model was derived for each of the processes. From this information values for RMAX, the effective radius of the dynamic bubbles were chosen. During the temperature initialization stage of Pavelec's program he used the radius to the origin and computed spread heat. Modifying this for underwater welding simply required that the value of this radius be compared to RMAX. Points within RMAX were assigned a spread heat value which is later used in the finite difference equation. Those points outside were assigned spread heats of zero.

6.2 Program Input

The program was found to be extremely data sensitive. Many of the inputs to Pavelec's program were eliminated to simplify program use. However, this was done selectively so as to maintain sufficient generality. Even with these changes convergence and other problems may still arise when varying various parameters. The following is a description of the input used in this thesis. Runs were accepted when they provided "sensible" results.

1. RRED, BIORD, BIlRD, BKORD, BKlRD are a list of Bessel functions and their arguments (x, $I_o(x)$, $I_1(x)$, $B_o(x)$, $B_1(x)$) These values should remain unchanged for all inputs considered.

2. TRED, TKRD, TDRD, NPRP are conductivity and diffusivity for corresponding temperature arguments. (T, K, α) These will change with material. The presented listing is for mild steel. NOPRP is the number of these values to be read in.

3. SPDCOR is the normalizing factor for convergence. For SMA a value of 4 was used. For GMA a value of 8.

4. V, I are voltage and amperage.

5. TMELT, THIKRD, SPD are melting temperature (^oK), plate thickness (in.), welding speed (in./min.)

6. TAMB, CRAD are ambient temperature (^oK) and the radiation coefficient.

7. RHO, ABAR, C are metal density, average conductivity and specific heat.

8. XLONG, YLONG, XLONGF describe the computational block (in.)

9. GRX12, GRX34, YMULT1, YMULT2 These values refer to grid size in front and behind the arc and are in N-D units. A value of .5 for all was found suitable.

10. ITCHK maximum number of iterations behind the arc.

11. ITFRNT maximum number of iterations in front of the arc.

12. NEVIS1, NEVIS2, NEVLSI; Print columns NEVIS1 to NEVIS2 in increments of NEISI.

13. NPROC is the process designation number.

14. CONVG is the convergence tolerance in N-D units (.01-.03)

15. NGO equal to zero will print point-source distribution.

16. NTCPL, TCPL are number and location of thermocouples.

17. FACTOR, RHOTSP, RMAX are welding efficiency, radius of hot spot (in.) and effective bubble radius (in.) Values for these are listed in Table 6-1

Once the program had been de-bugged, an object deck was made to eliminate compilation.

Table 6-1

WELDING PARAMETERS

PROCESS	FACTOR (%)	RHOTSP (in.)	RMAX (in.)
6013S	50	.2	.32
6013R	40	.2	.32
7014S	48	.2	.35
7014R	40	.2	.35
GMA	40	.2	.27

CHAPTER VII

RESULTS AND CONCLUSIONS

In the course of this thesis many different mechanisms involved in underwater welding processes have been studied. Understanding all or part of these mechanisms makes the development of new processes more feasible. The observation of "above the plate" phenomena and its relation to heat transfer and spread heat has probably been the most successful and revealing aspect of this thesis. This phenomena distinguishes one process from another and ultimately determines their success. Boiling, as it applies to underwater welding, has been studied in depth and the immense complexity of subcooled, transient boiling can now be appreciated. Both "above the plate" phenomena and the boiling model warrant a final discussion here.

7.1 The Boiling Model

Inspection of the predicted temperature distributions (figures 7-1 through 7-10) reveals that reservations concerning the boiling models derived in Chapter III were certainly well founded. The existing knowledge

FIGURE 7-1
U.W.W. TEMPERATURE DISTRIBUTION

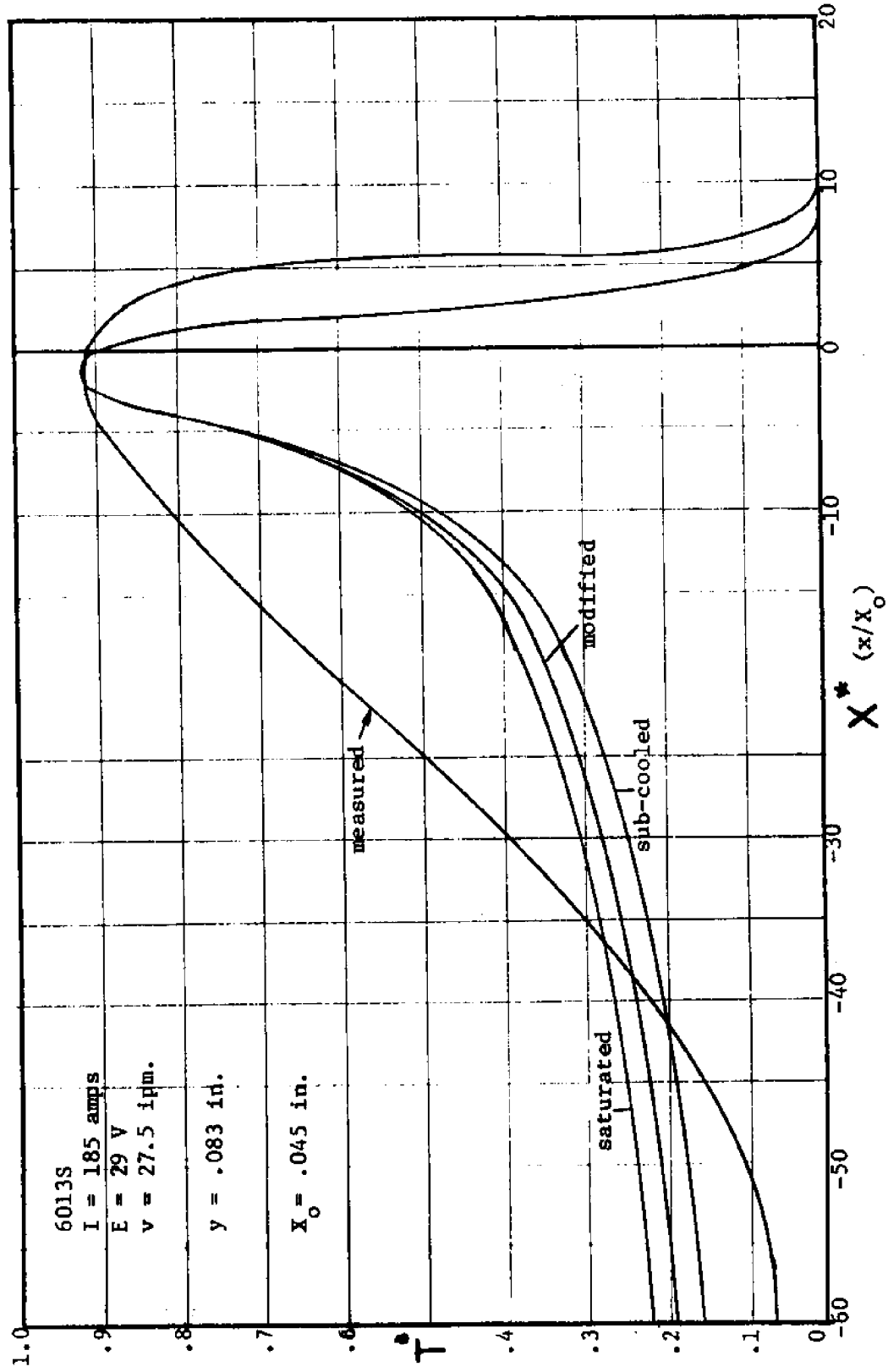

FIGURE 7-2
U.W.W. TEMPERATURE DISTRIBUTION

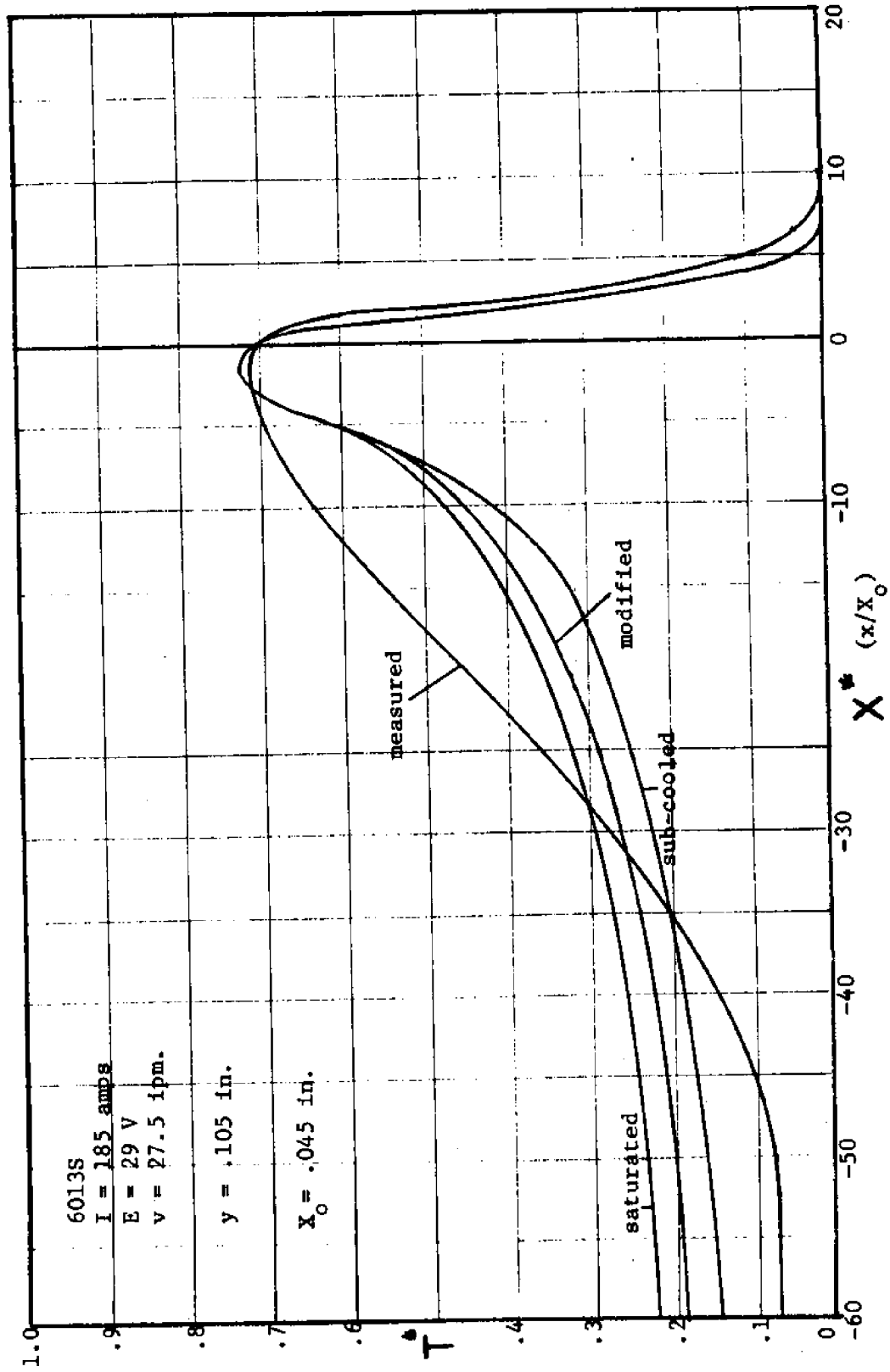

FIGURE 7-3
U.W.W. TEMPERATURE DISTRIBUTION

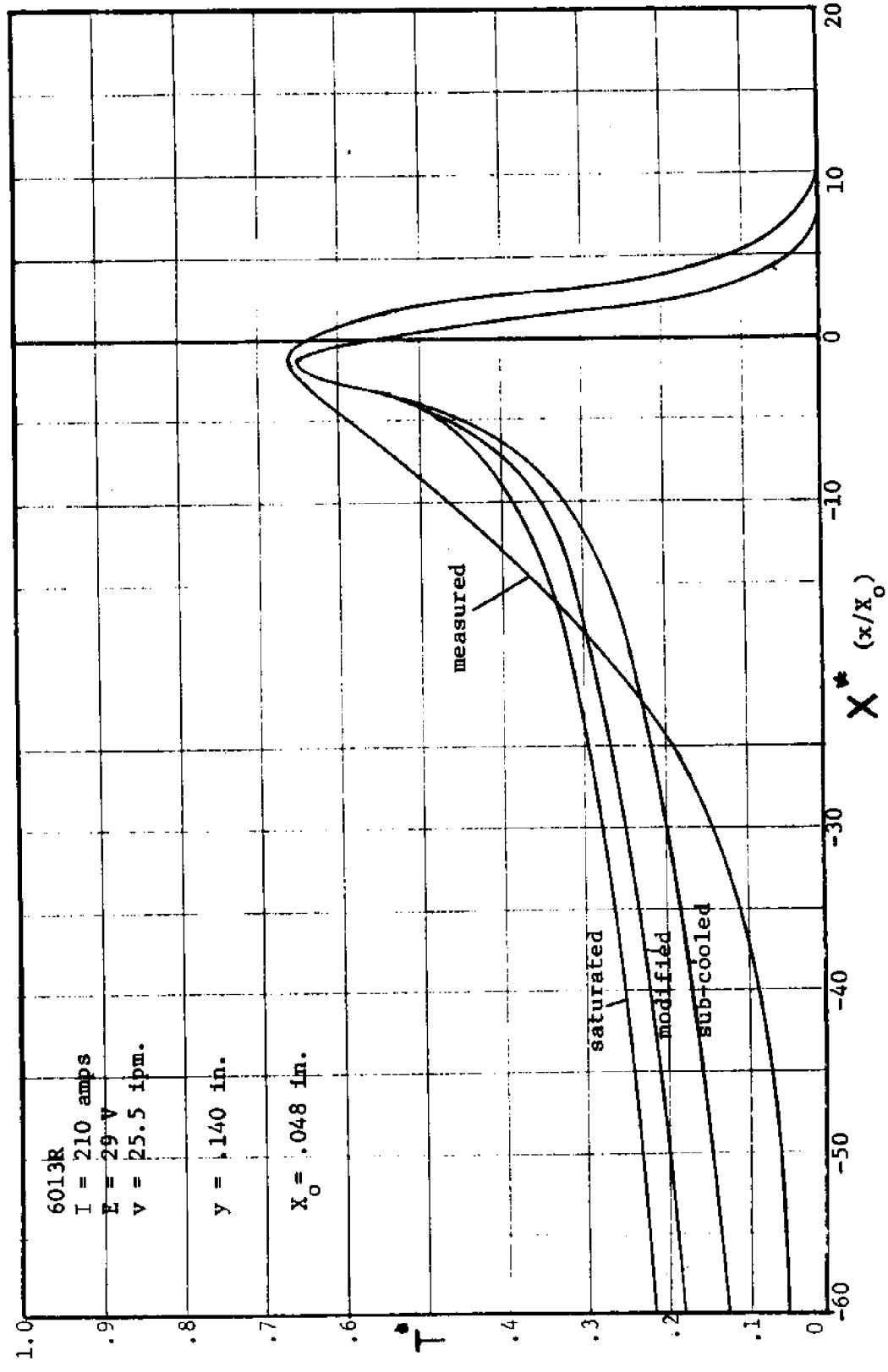

FIGURE 7-4
U.W.W. TEMPERATURE DISTRIBUTION

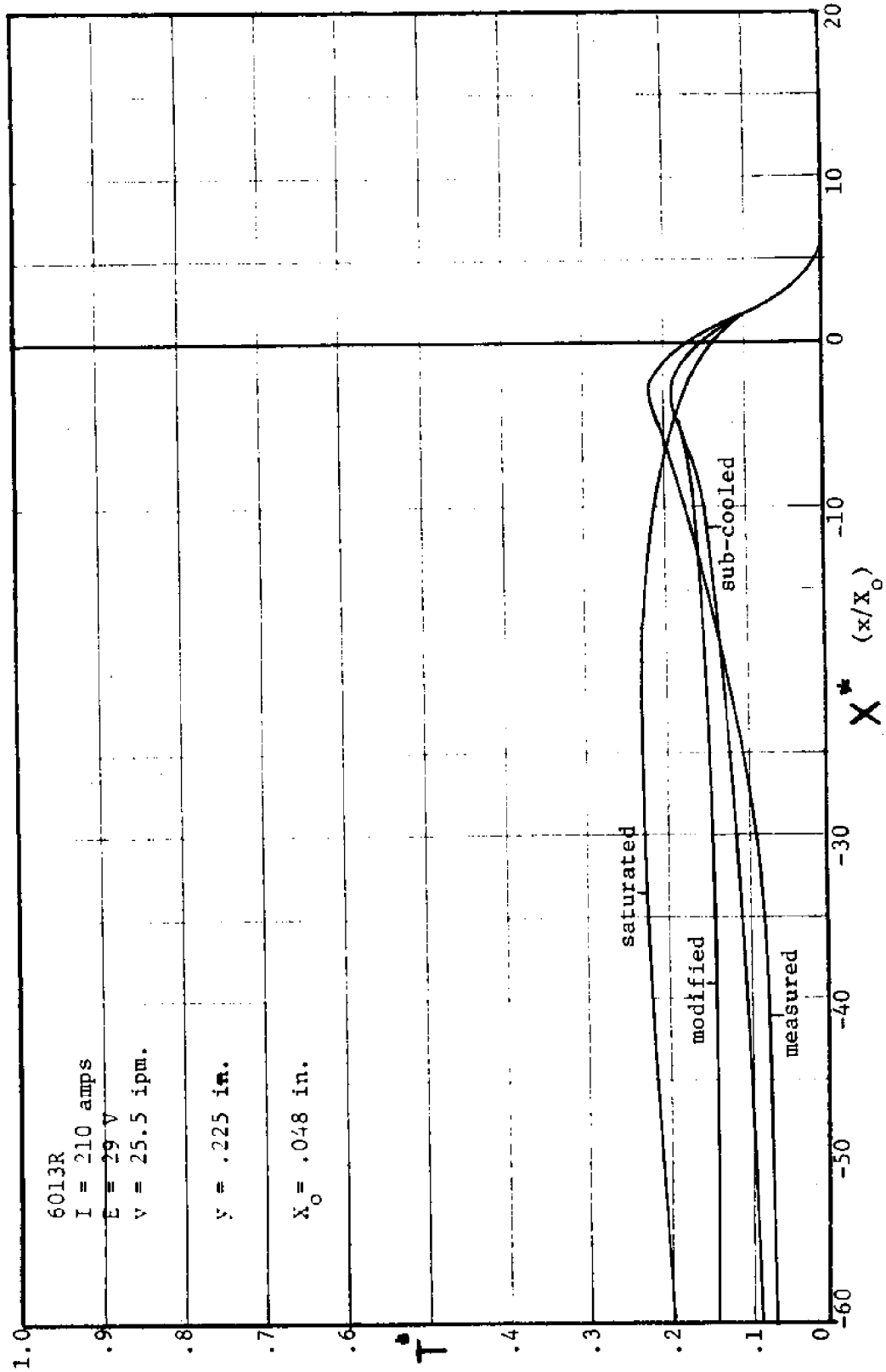

FIGURE 7-5
U.W.W. TEMPERATURE DISTRIBUTION

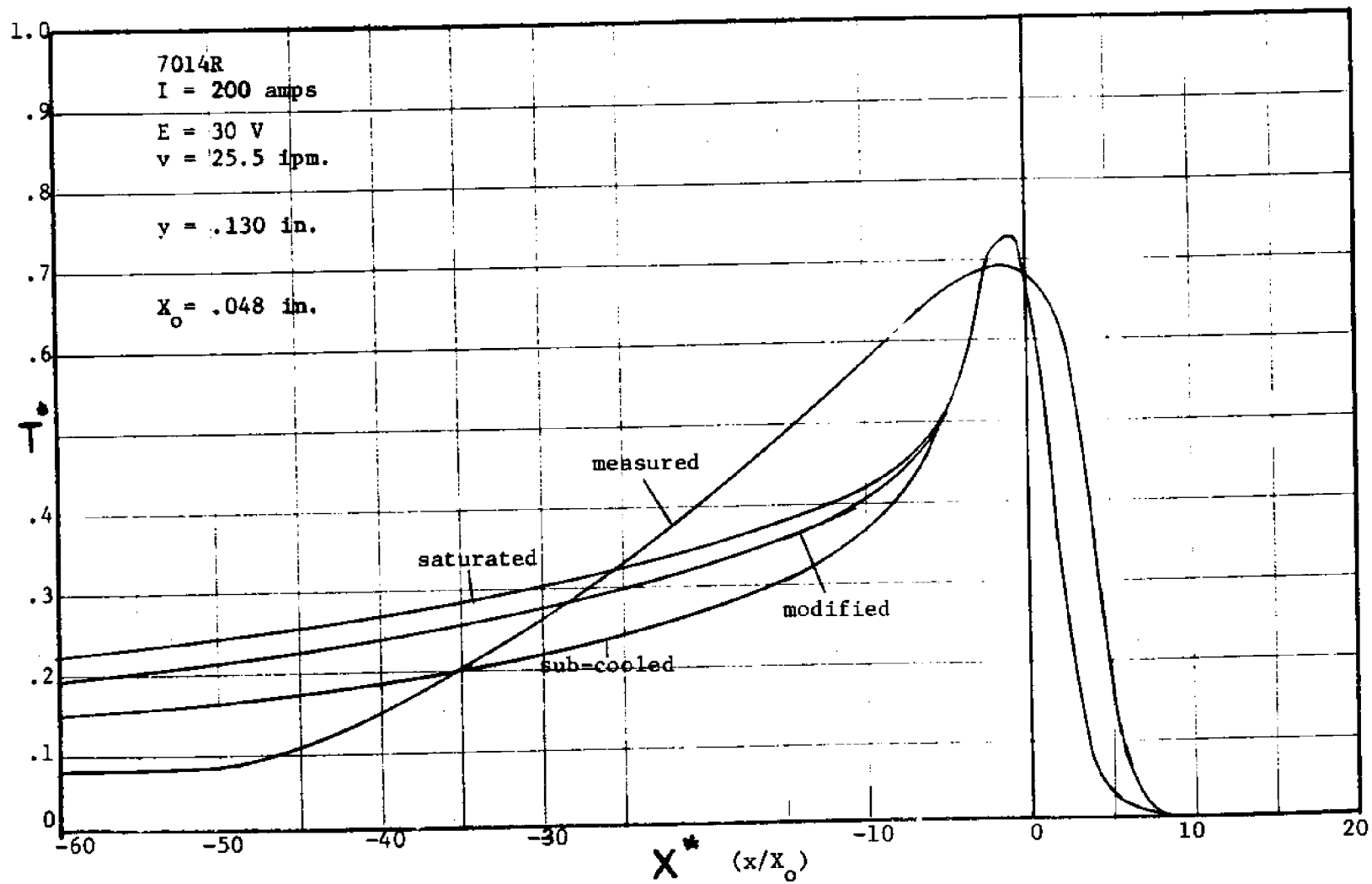

FIGURE 7-6
U.W.W. TEMPERATURE DISTRIBUTION

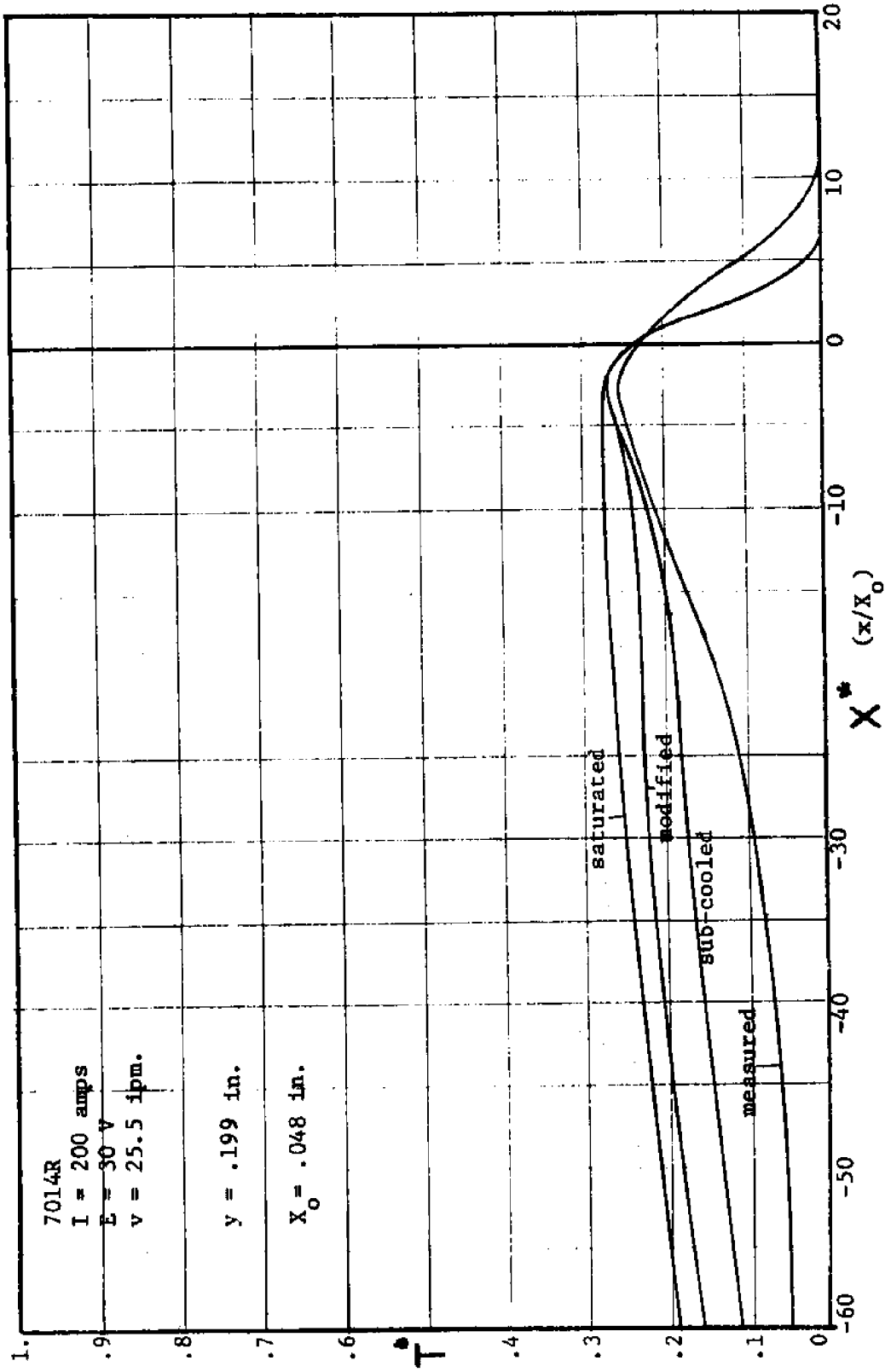

FIGURE 7–7

U.W.W. TEMPERATURE DISTRIBUTION

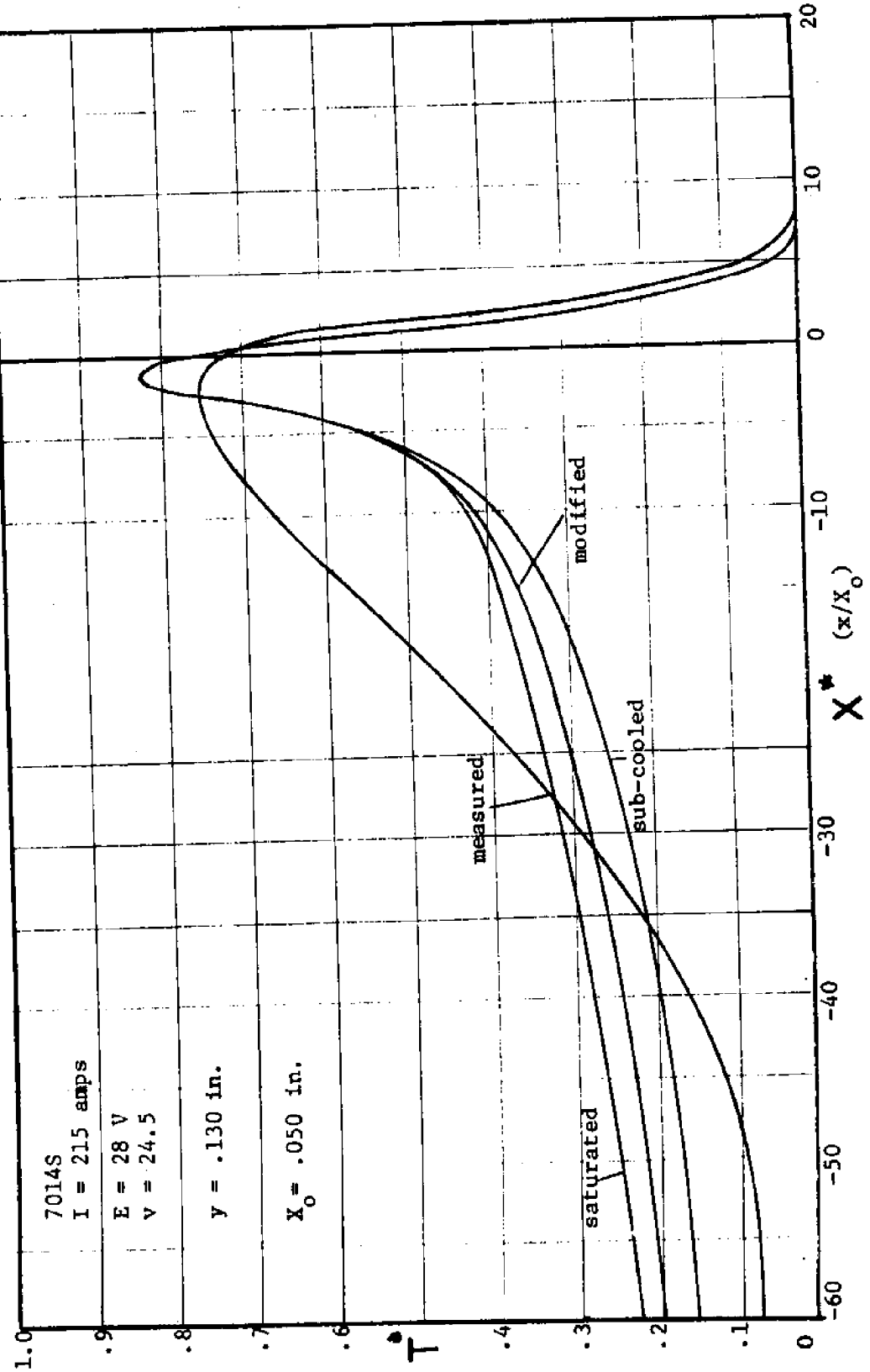

FIGURE 7-8
U.W.W. TEMPERATURE DISTRIBUTION

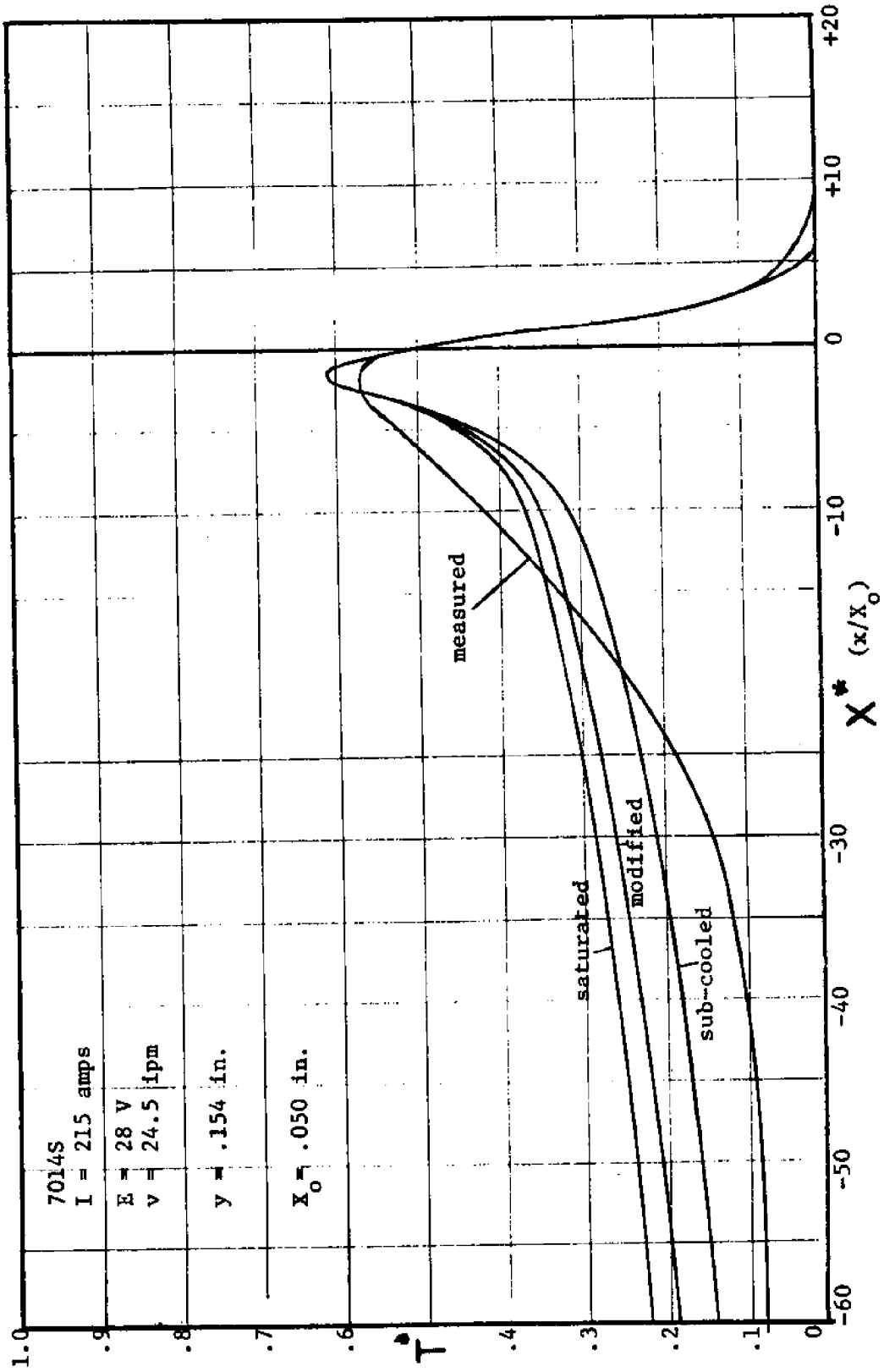

FIGURE 7-9
U.W.W. TEMPERATURE DISTRIBUTION

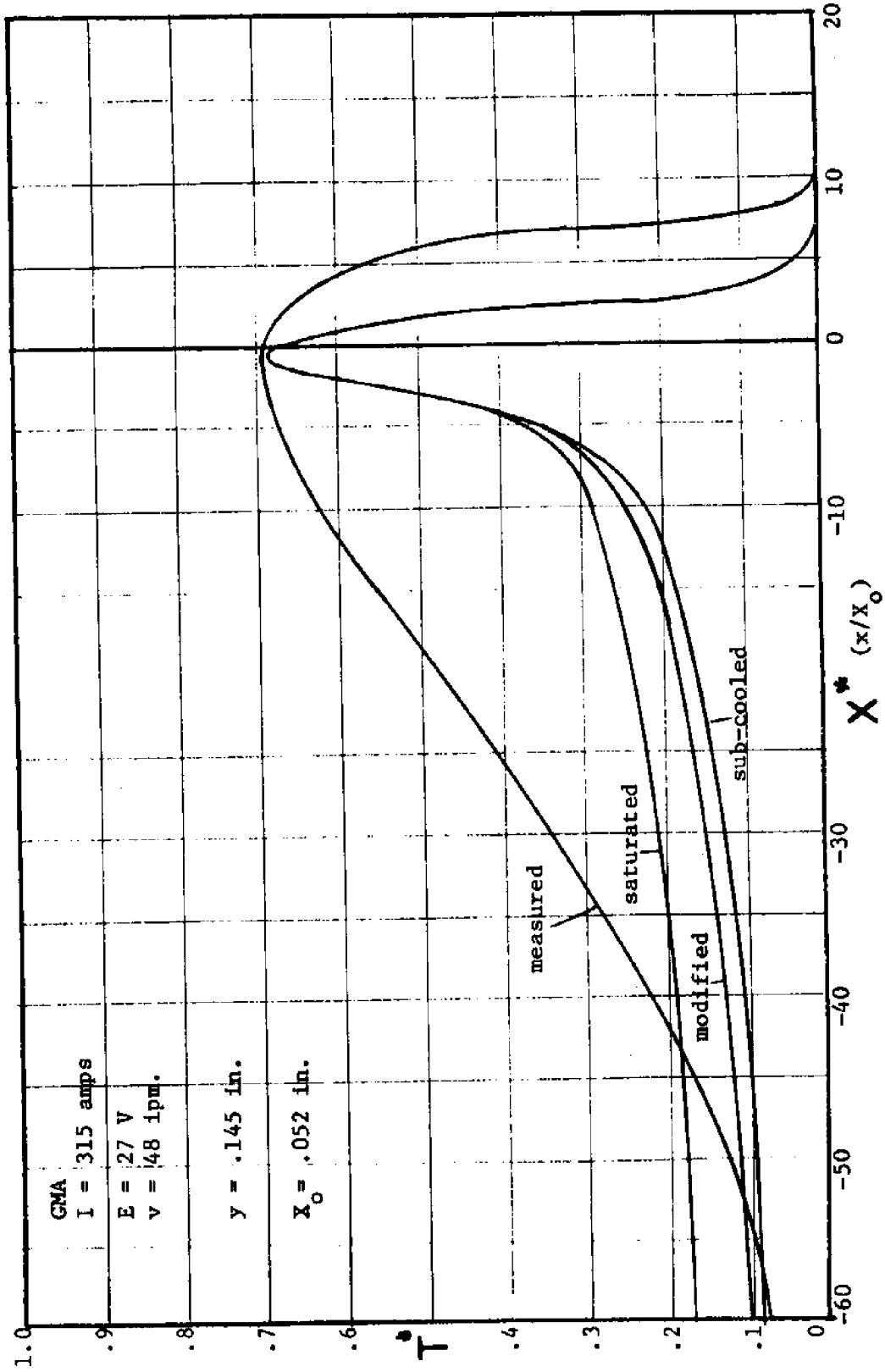

FIGURE 7-10
U.W.W. TEMPERATURE DISTRIBUTION

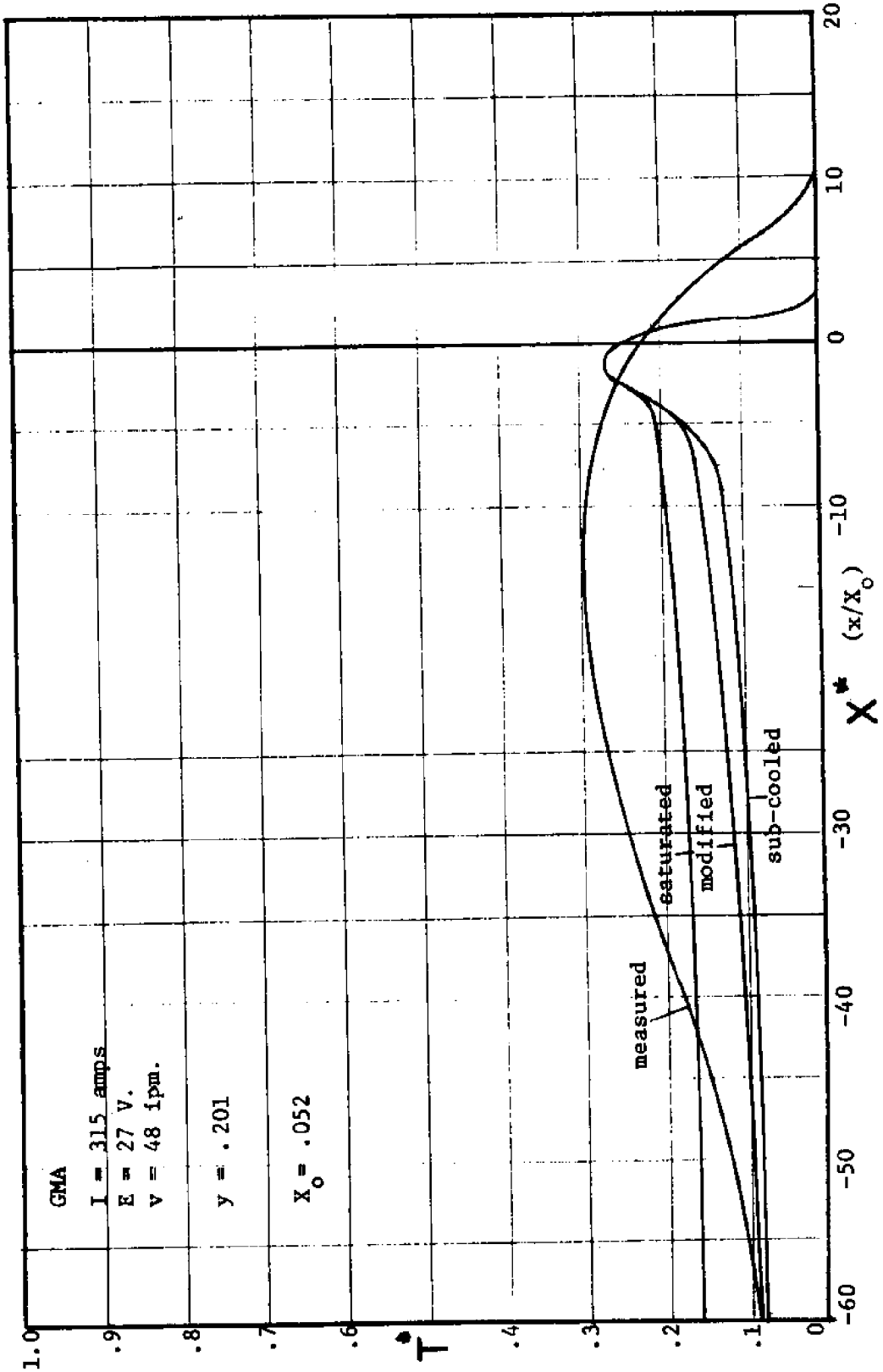

of boiling heat transfer was exhausted. Not one, but three models were tried. However, the one over-riding factor limiting their applicability was the extremely steep temperature gradients encountered in any underwater welding process.

Reference to figure 3-2 (predicted heat transfer rates) helps explain the consistent error encountered in the predicted temperature distribution. Variations in heat flux and boiling regimes cannot physically occur one upon the other as existing temperature gradients necessitate. Each regime is a physical phenomena which requires a certain amount of room, be it bubble radius or film wave length. Thus this side-by-side phenomena must result in a smoothed out compromise of the heat fluxes predicted in figure 3-2. Such a compromise would extend the effect of peak heat flux over a range of temperatures. Regions at temperatures even below T_{SAT} might then be cooled by near-by boiling.

This theory for boiling with a temperature gradient explains many of the problems in the derived distributions. Traditional models predict relatively little cooling below peak heat flux, thus in order to meet boundary conditions the computer model predicted immediate

rapid cooling followed by a slow approach to the boundary value which is below the peak temperature. This problem was compounded in the saturated model where the minimum heat flux region has so little heat flux that cooling beyond this could often not occur. The modified model seemed to be a compromise between subcooled and saturated.

Thus many aspects of such a boiling situation have been observed. Unfortunately existing knowledge prevents any further analysis here. It should be noted, however, that predicted and actual boiling heat flux are both exceedingly large and further advancement depends most heavily on eliminating this heat flux all-together.

7.2 Above the Plate Phenomena and Future Recommendations

Probably the most useful information uncovered in this thesis pertains to "above the plate" phenomena. Analysis of the various processes has pinpointed their problems and revealed a number of possible methods for overcoming these problems.

1. The SMA process is not an effective process as is. This is due to the limited shielding offered by its dynamic bubble. Using multi-pass methods could

increase the reliability of this process, and thus take advantage of its relatively simple and unencumbered application.

2. The shroud process is limited by the gas production at the arc, and the sliding shroud does not provide a positive, stable barrier. A larger shroud with an external gas supply could make this a very efficient process.

3. Probably most unexpected of all was the poor performance observed using the GMA process. The shielding gas was not impinging to the plate, but was just bubbling up ineffectively. Higher flow rates or combination with a shroud-type device could greatly improve the process.

In closing. Although the inadequacy of the boiling model limited the accuracy of the predicted temperature distributions, a greater understanding of the interactions between the boiling, spread heat, and "above the plate" phenomena has been derived.

Most important, the knowledge obtained using high speed cinematography to study "above the plate"

phenomena has suggested a number of alternatives for future development.

APPENDIX A

DERIVATION AND CONVERGENCE OF THE BASIC EQUATION

1. Derivation

The two dimensional energy equation for unsteady heat transfer is simply

$$\nabla\cdot(K\nabla T) + w_i = \rho c \frac{DT}{Dt}$$

where w_i is a source or loss term with units Btu/ft^3-hr. Evaluating this expression yields the following partial differential equation

$$\frac{\partial^2 T}{\partial x^2} + \frac{\partial^2 T}{\partial y^2} + \frac{1}{K}\frac{\partial K}{\partial T}\left[\left(\frac{\partial T}{\partial x}\right)^2 + \left(\frac{\partial T}{\partial y}\right)^2\right] + \frac{w_i}{K} = \frac{\rho c}{K}\frac{\partial T}{\partial t}$$

Note that:

$$\frac{1}{K}\frac{\partial K}{\partial T} = \frac{\partial}{\partial T}(\log K)$$

$$\frac{\rho c}{K} = \frac{1}{\alpha} \qquad w_i = \frac{\dot{q}}{L}$$

and when considering a coordinate system moving with the

arc at velocity V(ft./hr.) parallel to the X-axis:

$$w = x - Vt \qquad t = t \qquad y = y$$

yields the following equation:

$$\frac{\partial^2 T}{\partial w^2} + \frac{\partial^2 T}{\partial y^2} + \frac{\partial \log K}{\partial T}\left[\left(\frac{\partial T}{\partial w}\right)^2 + \left(\frac{\partial T}{\partial y}\right)^2\right] + \frac{\dot{q}}{KL} = -\frac{V}{\alpha}\frac{\partial T}{\partial w} \qquad \text{(A-5)}$$

This equation may then be made dimensionless using the following expressions

$$T^* = \frac{T - T_o}{T_M - T_o}$$

$$w^* = \frac{w}{X_o} \qquad y^* = \frac{y}{X_o} \qquad X_o = \frac{N\alpha_{MIN}}{V}$$

The normalizing factor, X_o, is chosen to best simplify the right hand side of A-5, with the integer value N being chosen to insure convergence.

Substitution of these yields finally,

$$\frac{\partial^2 T^*}{\partial w^{*2}} + \frac{\partial^2 T^*}{\partial y^{*2}} + \frac{\partial \log K}{\partial T^*}\left[\left(\frac{\partial T^*}{\partial w^*}\right)^2 + \left(\frac{\partial T^*}{\partial y^*}\right)^2\right] + \frac{\dot{q} X_o^2}{KL(T_M - T_o)} = \frac{-VX_o}{\alpha}\frac{\partial T^*}{\partial w^*}$$

2. Convergence

The partial differential equation above is an extremely non-linear one. For this reason when solving numerically extreme care must be taken to insure convergence of the solution. Greenspan (ref. 31) states as a criteria for convergence that:

$$h < \frac{2\alpha(T^*)}{X_o V}$$

where h is the grid spacing. To obtain maximum grid spacings and always insure convergence necessitates that:

$$h_{max} = \frac{2\alpha_{MIN}}{X_o V}$$

Staub in general followed Tanbakuchi's reasoning and set $h_{max} = 1$ or:

$$X_o = \frac{2\alpha_{MIN}}{V}$$

This proved very efficient at the slow welding speeds used with stick electrodes, however, at the higher speeds used for underwater GMA values of X_o became too small for effi-

cient use by the computer. This necessitated a re-definition of X_o:

$$X_o = \frac{N\alpha_{MIN}}{V} \qquad h_{MAX} = \frac{2}{N}$$

h_{max} should be as large as possible to insure efficient computer solution.

It should be noted that even with strict adherence to these rules the highly non-linear nature of this equation may still cause the solution to diverge.

APPENDIX B

WELD POOL CORRELATION

Starting with Rosenthal's point source temperature equation:

$$T-T_\infty = \frac{\dot{Q}}{L}\,\frac{1}{2\pi\bar{K}}\,e^{-(\bar{\lambda}Vw)}K_o(\bar{\lambda}Vr)$$

$$r=\sqrt{w^2+y^2}$$

$$\dot{Q}=3.415\,\eta EI$$

And assuming the total heat content of the plate to be

$$H_m=\bar{c}\bar{\rho}\,(T_M-T_\infty)\ \frac{Btu}{ft^3}$$

results in:

$$T-T_\infty=\eta\,\frac{3.415EI}{L}\,\frac{1}{2\pi}\,\frac{\bar{\rho}\bar{c}(T_M-T_o)}{\bar{K}\,\bar{\rho}\bar{c}(T_M-T_o)}e^{-\bar{\lambda}Vw}K_o(\bar{\lambda}Vr)$$

or:

$$T^*=\frac{T-T_\infty}{T_M-T_\infty}=\eta\frac{3.415EI}{\alpha 2\pi LH_m}e^{-w^*}K_o(r^*)$$

By defining a lumped welding parameter:

$$N^* = \frac{3.415\,EI}{2\pi L H_m \bar{\alpha}}$$

this reduces to:

$$T^* = \eta\, N^* e^{-w^*} K_o(r^*)$$

which is the basic equation for what follows.

If the shape of the molten pool is assumed to be tear-drop, then at the point of maximum pool width:

$$\frac{\partial T^*}{\partial w^*} = 0$$

or:

$$N^* \eta e^{-w_m^*}\left[K_o(r_m^*) - K_1(r_m^*)\frac{w^*}{r_m^*}\right] = 0$$

which reduces to:

$$w_m^* = r_m^* \frac{K_o(r_m^*)}{K_1(r_m^*)}$$

Since this contour is also at the melting temperature

$$T^* = 1 = N^* \eta e^{-w_m^*} K_o(r_m^*)$$

or finally:

$$N^* = \frac{\exp\left[-r_m^* K_0(r_m^*)/K_1(r_m^*)\right]}{\eta K_0(r_m^*)}$$

The width at this maximum point is simply:

$$Y_m^* = \sqrt{r_m^{*2} + W_m^{*2}} = r_m^* \left[1 - \left(\frac{K_0(r_m^*)}{K_1(r_m^*)}\right)^2\right]^{1/2}$$

or the maximum width is:

$$B_m^* = \frac{B_m}{X_0} = 2r_m^* \left[1 - \left(\frac{K_0(r_m^*)}{K_1(r_m^*)}\right)^2\right]^{1/2}$$

The maximum length is simply

$$X_{MAX} = L_b - L_f$$

Since y* = 0 and T* = 1 at these points:

$$\eta N^* e^{-L_f} K_o(r_m^*) = 1$$

$$\eta N^* e^{L_b} K_o(r_m^*) = 1$$

or

$$L_f = \ln\left[N^* K_o(r_m^*)\right]$$

$$L_b = -\ln\left[N^* K_o(r_m^*)\right]$$

Finally:

$$X^*_{MAX} = \frac{X_{MAX}}{X_o} = L_b - L_f = 2r_m^* \frac{K_o(r_m^*)}{K_1(r_m^*)}$$

APPENDIX D

VAPOR VELOCITY IN FILM BOILING

Heat conducted through the vapor film has two possible outlets:

1. Conduction into the liquid
2. Steam production which results in a vapor flow to the bubble

These two processes must be looked at separately.

The empirical results used in the following analysis are (all apply to water):

1. $(D_b)_{max} = .75$ (from Westwater analysis, ref.30)
2. $\tau_{av} = .20$ sec (observed by Westwater to be fixed by hydrodynamic considerations)
3. Film thicknesses are on the order of 10^{-4} ft.
4. Bubbles generally appear in a close-packed lattice with 4 bubbles per λ^2, two growing simultaneously.

Each time a bubble grows and departs, new liquid comes in contact with the vapor film. This situation may be treated as transient conduction in a slab initially at T_∞, then exposed at one surface to the vapor film which is constantly at T_{SAT}.

The differential equation for one-dimensional transient conduction is

$$\frac{\partial T}{\partial t} = \alpha \frac{\partial^2 T}{\partial z^2}$$

Solving for the instanteous heat transfer yields:

$$\dot{q}_2(t) = \frac{K_L(T_{SAT} - T_\infty)}{\sqrt{\pi \alpha t}}$$

Averaging over the bubble period and substituting for τ yields:

$$\dot{q}_2 = \int_0^\tau \frac{\dot{q}_2(t)}{\tau} dt \quad \frac{2(60) K_L(T_{SAT} - T_\infty)}{\sqrt{.2\pi\alpha}} \quad \frac{Btu}{hr\text{-}ft^2}$$

$$\dot{q}_2 = \frac{269\, K_L\, \Delta T_{SUB}}{\sqrt{\pi \alpha}}$$

The heat resulting in vaporization can be derived from latent heat:

$$\dot{q}_1 = \dot{w} h_{fg} = 2\pi r a \rho_v V_v h_{fg}$$

The total conducted heat is then:

$$\dot{q}_T = \frac{K_v}{a}(\pi r_2^2 - \pi r^2)\, \Delta T_{SAT}$$

Since there are 2 bubbles per λ^2 , the area from which each bubble draws liquid is: (see figure 3-4)

$$\pi r_2^2 = \frac{\lambda^2}{2}$$

or:

$$\dot{q}_T = \frac{K_v}{a}\left(\frac{\lambda^2}{2} - \pi r^2\right)\Delta T_{SAT}$$

Finally equating these:

$$\dot{q}_T = \dot{q}_1 + \dot{q}_2$$

$$\frac{K_v}{a}\left(\frac{\lambda^2}{2} - \pi r^2\right)\Delta T_{SAT} = 2\pi r a \rho_v V_v h_{fg} + \frac{269 K_L \Delta T_{SUB}}{\sqrt{\pi \alpha}}$$

The vapor velocity can then be determined:

$$V_v = \frac{\frac{K_v}{a}\left(\frac{\lambda^2}{2} - \pi r^2\right)\Delta T_{SAT} - \frac{269 K_L}{\sqrt{\pi \alpha}}\Delta T_{SUB}}{2\pi r a \rho_v h_{fg}} \frac{ft}{hr.}$$

It can be seen in this equation that no vapor flow can

occur until the total heat transfer exceeds that required to support transient conduction. This will of course occur at a much higher temperature. Assuming that once this threshold is reached the process will proceed in a manner similar to film boiling in saturated liquids, the equations derived by Berensen may be used. Using empirical observations and various hydrodynamic and thermodynamic considerations, he derived the minimum heat flux ($\dot{q}_1$) necessary to support a vapor film.

$$(\dot{q}_1)_{MIN} = .09 \rho_{vf} h_{fg} \left[\frac{g(\rho_L - \rho_v)}{\rho_L + \rho_v}\right]^{\frac{1}{2}} \left[\frac{g_o \sigma}{g(\rho_L - \rho_v)}\right]^{1/4}$$

$$(q_1)_{MIN} = 5980 \ \frac{Btu.}{hr.\text{-}ft^2}$$

The heat necessary to support transient conduction during film boiling is then

$$\dot{q}_2 = 692.6 \ \Delta T_{SUB}$$

or finally:

$$\dot{q}_{MIN} = 5980 + 692.6 \ \Delta T_{SUB}$$

This heat must all be conducted through the vapor film where Berensen calculates the heat transfer coefficient to be

$$h = .425 \frac{K_{vf}^3 h_{fg} \rho_v g(\rho_L - \rho_v)}{\mu_f (\Delta T_{MIN})_{SAT}} \sqrt{\frac{g_o \sigma}{g(\rho_L - \rho_v)}}$$

The $(\Delta T_{min})_{SAT}$ comes from the calculation of film thickness which is assumed to be the same as that in a saturated liquid, thus the $(\Delta T_{min})_{SAT}$ is the temperature difference required for film boiling in a saturated liquid. This equation yields:

$$h = \frac{\dot{q}_{MIN}}{\Delta T_{MIN}} = 20.25$$

or finally

$$\dot{q}_{MIN} = 20.25 \, \Delta T_{min}$$

$$\Delta T_{min} = .0494 \, \dot{q}_{MIN}$$

Part 3 is a revised edition of the M. S. Thesis by Alan Brown to be submitted to M.I.T. in June, 1973. This edition does not include Appendixes C and E and three photographs. A copy of the thesis can be purchased through the Engineering Library of M.I.T.

→ MISSING PAGES 168-211

REFERENCES

1. Vagi, J. J., Mishler, Randall, "Report on Underwater Welding and Cutting--State of the Art," Battelle Memorial Institute.

2. Masubuchi, K., Materials for Ocean Engineering, M.I.T. Press, M.I.T., 1970.

3. Silva, E. A., An Investigation of Fusion Controlled Metallurgical Bonding in a Marine Environment, Ph.D., University of California at Berkeley, 1971.

4. Madatov, "U.W.W. Electrodes-Iron Powder Coatings," Welding Production, Vol. 10, No. 8, 1962.

5. Madatov, "Special Features of Underwater Touch Welding," Automatic Welding, Vol. 15, No. 9, 1962.

6. Madatov, "Energy Characteristics of the U.W.W. Arc," Welding Production, Vol. 13, No. 3, 1966.

7. Madatov, "Shape Relations for U.W.W.," Welding Production, Vol. 16, No. 3, 1969.

8. Avilov, T. I., "Electrodes for U.W. Welding and Cutting Steel," Welding Production, Vol. 3, No. 6, 1955.

9. Madatov, N. M., "The Properties of the Bubble of Steam and Gas Around the Arc in U.W.W.," Automatic Welding, Vol. 18, No. 12, 1965.

10. Silva, E. A., "Shielded Metal Arc Welding Underwater with Iron Powder Electrodes," Welding Journal, pp. 406-415, June, 1971.

11. Silva, E. A., "Gas Production and Turbidity During Underwater Shielded Metal Arc Welding with Iron Powder Electrodes," Naval Engineer's Journal, pp. 59-63, December, 1971.

12. Silva, E. A., "Welding Processes in the Deep Ocean," Naval Engineer's Journal, Vol. 80, No. 4, pp. 561-568, August, 1968.

13. Tanbakuchi, R., "Metal Temperatures During Arc Welding," Ph.D. Thesis, University of Wisconsin, 1967.

14. Pavelec, V., "Temperature Histories in Thin Steel Plate Welded with TIG," Ph.D. Thesis, University of Wisconsin, 1968.

15. Liphert, R., "Temperature Distribution in Thin Steel Plate During Gas Metal Arc Welding," Ocean Engineer Thesis, M.I.T., 1972.

16. Staub, J., "Temperature Distribution in Thin Plates Welded Underwater," Naval Engineer's Thesis, M.I.T., 1971.

17. Forster, K. E., Grief, R., "Heat Transfer to a Boiling Liquid-Mechanism and Correlations," Journal of Heat Transfer, February, 1959.

18. Rohsenow and Choi, Heat, Mass, and Momentum Transfer, Prentice-Hall, Inc., Englewood Cliffs, New Jersey, 1961.

19. Zuber, T., "The Hydrodynamic Crisis in Pool Boiling of Saturated and Sub-Cooled Liquids," International Developments in Heat Transfer, Part II, ASME, p. 230, 1961.

20. Freith, F., "Principles of Heat Transfer," International Textbook Company, 1969.

21. Jacob, M., "Heat Transfer," John Wiley and Sons, New York, 1949.

22. Lamb, H., Hydrodynamics, 6th Edition, Cambridge University Press.

23. Berensen, PL J., "Film Boiling Heat Transfer from a Horizontal Surface," Ph.D. Thesis, M.I.T., 1960.

24. Nestor, O. H., "Heat Intensity and Current Density Distribution at the Anode of High Current, Inert Gas Arcs," Physics of the Welding Arc, British Institute of Welding, 1966.

25. Rykalin, N. N., "Berechnungder Warmevorgange beim Schweissen," Veb Verlag Technik, Berlin, 1957.

26. Brown, A., "Methods of Research in Underwater Welding," B.S. Thesis, M.I.T., 1971.

27. Davidson, J. F., "Bubble Formation at an Orifice in an Inviscid Liquid," Institute of Chemical Engineers, Vol. 38, 1960.

28. Milne-Thomson, L. N., Theoretical Hydrodynamics, 3rd Edition, 1955.

29. McAdams, W., Heat Transmission, McGraw-Hill Book Co., New York, 1954.

30. Westwater, "Photographic Study of Boiling," Industruial and Engineering Chemistry, Vol. 47, 1955.

31. Greenspan, D., "Introductory Numerical Analysis of Elliptic Boundary Value Problem," Harper and Row, 1965.